7-1-1972

Some effects of temporal coherence of the Fourier transform holographic system

Ronald Antos

SOME EFFECTS OF TEMPORAL COHERENCE OF THE FOURIER TRANSFORM HOLOGRAPHIC SYSTEM

A THESIS

SUBMITTED TO THE SCHOOL OF PHOTOGRAPHIC ARTS AND SCIENCES AND THE COUNCIL ON GRADUATE STUDIES IN PHOTOGRAPHIC SCIENCE AND INSTRUMENTATION OF THE ROCHESTER INSTITUTE OF TECHNOLOGY IN PARTIAL FULFILLMENT OF THE REQUIREMENTS FOR THE DEGREE OF MASTER OF SCIENCE

Accepted Aug. 4, 1972
John F. Carson, Thesis Advisor
G. W. Schumann
Mohamed F. Abouelata

By

Ronald L. Antos

July 1972

ABSTRACT

The objective of this investigation was to evaluate experimentally the effects of slight changes in the temporal coherence of a quasi-monochromatic source on the real images of Fourier transform holograms. The method of investigation included: (1) A review of some of the theoretical aspects of Fourier transform holography, (2) some approximations for experimental system limitations due to the coherence length and size of the quasi-monochromatic source, (3) sensitometric experimentation to obtain an adequate photographic reversal process, (4) temporal coherence measurements using a Michelson interferometer, (5) formation and reconstruction of Fourier transform holograms, and (6) analysis of experimental data. The results have shown that decreases in the coherence length of the source are accompanied by increases in the spectral width and can cause progressive blurring of edges and geometrical shape distortion for a rectangular-shaped object.

CONTENTS

CONTENTS (cont'd.)

APPENDIXES

APPENDIXES (cont'd.)

ILLUSTRATIONS

ILLUSTRATIONS (cont'd.)

ACKNOWLEDGMENT

The author respectively acknowledges the guidance and encouragement of Professor John F. Carson throughout the period of research and publication. His questions, critical comments and advice stimulated the author's interest in both holography and the overall field of optics. Also, the author wishes to thank Dr. Burt H. Carroll, Professor Albert D. Rickmers and Professor Hollis N. Todd for their interest and suggestions during the initial phase of this research and Professor Abou El Ata for the reading and criticism of the manuscript.

Appreciation is also expressed to Mr. Edward R. Thomas of Data Corporation for the support provided in both time and materials to complete the experimental investigation and its documentation.

CHAPTER I

STATEMENT OF OBJECTIVES

1.1 DEFINITION OF THE PROBLEM

Due to the potential application of coherent optical systems, an increasing amount of emphasis has been placed on scientific investigations in the areas of coherence theory and utilization of coherent sources, such as in optical processing and holography. At first, much of this emphasis was placed on the effects of coherence on images of generalized optical communication systems. This included predictions of image sizes and locations and some experimental verifications of these predictions.

More recently, the effects of coherence on images of specific systems, such as Fresnel and Fraunhofer holographic systems, have been investigated. These investigations, however, have considered only system resolution as an image quality measure, even though both temporal and spatial coherence variations have been addressed.

Based upon these considerations, this investigation considered coherence effects on a Fourier transform holographic system using image quality measures that are more readily definable, such as geometrical shape and density profile. The coherence variable was limited to changes in temporal coherence for a relatively constant spatial coherence and all image quality measures considered only those that are photographically recorded.

1.2 PURPOSE OF INVESTIGATION

The purpose of this investigation was to determine experimentally the relative effects of slight changes in temporal coherence on Fourier transform holograms and their respective real images.

The experimental procedures utilized show the effects of variations in the spectral width of a quasi-monochromatic source on:

1. The density level and contrast of the fringe patterns recorded on Fourier transform holograms;

2. The density level of photographed real images of the Fourier transform holograms;

3. The geometrical shapes of the reconstructed real images of the Fourier transform holograms.

1.3 METHOD OF INVESTIGATION

The primary experimental stages utilized to meet the objectives of this investigation are outlined as follows.

1. Calculations were made to approximate the physical limitations placed on the experimental design of the Fourier transform holographic system due to the coherence length and size of the quasi-monochromatic source. This included an estimation of: (a) The approximately uniform, spatially coherent area of illumination at the object plane; (b) the anticipated spatial frequency at the hologram plane; and (c) the allowable path differences between the object and reference beams of the Fourier transform holographic arrangement.

2. Separate sensitometric experiments were performed to determine the procedure to be utilized in the photographic reversal processing of the Fourier transform holograms.

3. Temporal coherence measurements were made on the quasi-monochromatic source using a Michelson interferometer and a PMT detector. A high-pressure mercury arc filtered by four narrow-band interference filters was used for the quasi-monochromatic source. The intensity data obtained were used to calculate the visibility curve, coherence length, and spectral width for each source/filter combination.

4. Fourier transform holograms were formed and their respective images reconstructed using the filtered high-pressure mercury arc source and an object target consisting of a transmissive pinhole and a rectangular bar surrounded by opaque regions. Photographs were taken of the reconstructed real images.

5. The reconstructed holograms and their photographed real images were analyzed using a microdensitometer for density measurements and a comparator for geometrical shape measurements.

CHAPTER II

INTRODUCTION TO HOLOGRAPHY

2.1 GENERAL BACKGROUND

Holography is a two-step imaging process discovered by Gabor[1,2*] in 1948. It involves the simultaneous recording of the Fresnel or Fraunhofer diffraction pattern of an object field and an interfering reference field. The recorded diffraction pattern, called a hologram, is used to reconstruct an image of the original object.[3]

The first step of holography is called the formation or recording step and utilizes a square law sensitive medium. In this step, a reference wave (plane or spherical) is allowed to interfere with an object wave which is essentially the Fresnel or Fraunhofer diffraction pattern of the object. The photosensitive medium (usually photographic film or plates) records this interference pattern so that the entire wave can later be regenerated from this record.[4,5]

The second step, or reconstruction, consists of placing the recorded interference pattern, or hologram, into the path of a wave similar to the reference wave. As a result, two images of the original object will appear. One image, the real image, will appear on the side of the hologram which is opposite the source (except in the case of Fourier transform holography, as will be shown later). Another image, the virtual image, will appear on the same side of the hologram as the source (again with exception of Fourier transform holography). Mathematically, the virtual image is the complex conjugate of the real image. Also, the images may be simultaneously or independently photographed and/or viewed, depending upon the geometry of the formation and reconstruction steps.[4,5,6]

2.2 HOLOGRAPHY AND CONVENTIONAL PHOTOGRAPHY

Although a basic description of holography is easily followed and understood, the rigorous theories of diffraction and coherence are essential to any mathematical treatment of the subject. Also, experimental work in the area of holography is very

*All references are contained in the bibliography at the end of this document.

expensive and time-consuming when consideration is given to the cost of equipment and the planning time involved in constructive experimentation. Thus, to overcome these basic disadvantages, holography must be able to offer some real advantages over the quick and inexpensive methods of conventional photography.

Essentially, holography has three distinct advantages[7] over conventional photography. The first is that, in holography, either the positive or negative version of the hologram will generate an identical scene or object. This is due to the similarity between holography and Fresnel zone plates.

Secondly, the image of a conventional photograph is not subjectively representative of an original scene. The two-dimensional image of photography does not yield the three-dimensional information contained in the original scene without the aid of further instrumentation such as stereo viewers. The holographic image, however, is capable of retaining this three-dimensional information which can be viewed or photographed from various viewing planes.

Lastly, due to its extremely large information storage capacity, a holographic image of an original scene may be reconstructed using only part of the original hologram, providing the required components of the diffraction pattern are not destroyed. Also, many images can be stored "on top" of one another in holography, depending on the geometry of the formation and reconstruction steps.

All three of the above advantages are the direct result of the ability of the hologram to store both phase and amplitude information as compared to conventional photography which can store only the amplitude information.[8]

2.3 FOURIER TRANSFORM HOLOGRAPHY

Basically, there are three main types of holograms that can be formed. These are the Fresnel, Fraunhofer, and Fourier transform holograms. All other holographic systems are slight modifications of these and all are produced by making slight changes in the geometry of the formation step.[4]

However, for two very important reasons, the present work concerns itself with only the Fourier transform holographic system. First, since the point under investi-

gation considers differences in image shape corresponding to slight changes in an already low level of coherence and illumination, it was necessary to choose a holographic technique whose geometrical considerations did not limit the quality of the reconstructed image. Secondly, it has been shown[4] that the Fourier transform holographic system is capable of producing a greater maximum resolution for planar objects than the Fraunhofer hologram due to the absence of the quadratic phase factor or zone-lens term in the coordinates of the hologram plane.

Of the two possible Fourier transform holographic systems, as described by DeVelis and Reynolds,[4] only the point-reference method utilizing a lens is discussed and experimentally proven to overcome the illumination and coherence constraints. This method consists of formation and reconstruction steps as shown in the diagrams of Figures 2-1 and 2-2. In each case, the lens is used to effect the Fourier transform of the object plane (or holograph plane) amplitude distribution. The hologram then becomes the photographic record of the interference pattern created between the transformed object distribution and the transformed background reference wave from the on-axis point reference.

The object plane consists of a planar object off-axis by a distance and a point reference on-axis. The optical disturbance, ψ_f , in the hologram plane created by the object and the point reference consists of the sum of a constant from the Fourier transform of the reference point and the Fourier transform of the object with a linear phase factor:

$$\psi_f = \psi_1 + \psi_2 = A_1 + \hat{A}_2 e^{i\phi_2} \qquad 2.201$$

where A_1 = complex constant

$\hat{A}_2 = \hat{D}(x)$ = Fourier transform of object amplitude distribution, $D(\xi)$.

$\phi_2 = k\xi_o x / f$ where $k = 2\pi/\lambda$, f is the focal length of the lens, and ξ_o is the off-axis distance of the object.

Since intensity can be defined as the product of the optical disturbance and its complex conjugate, we obtain:

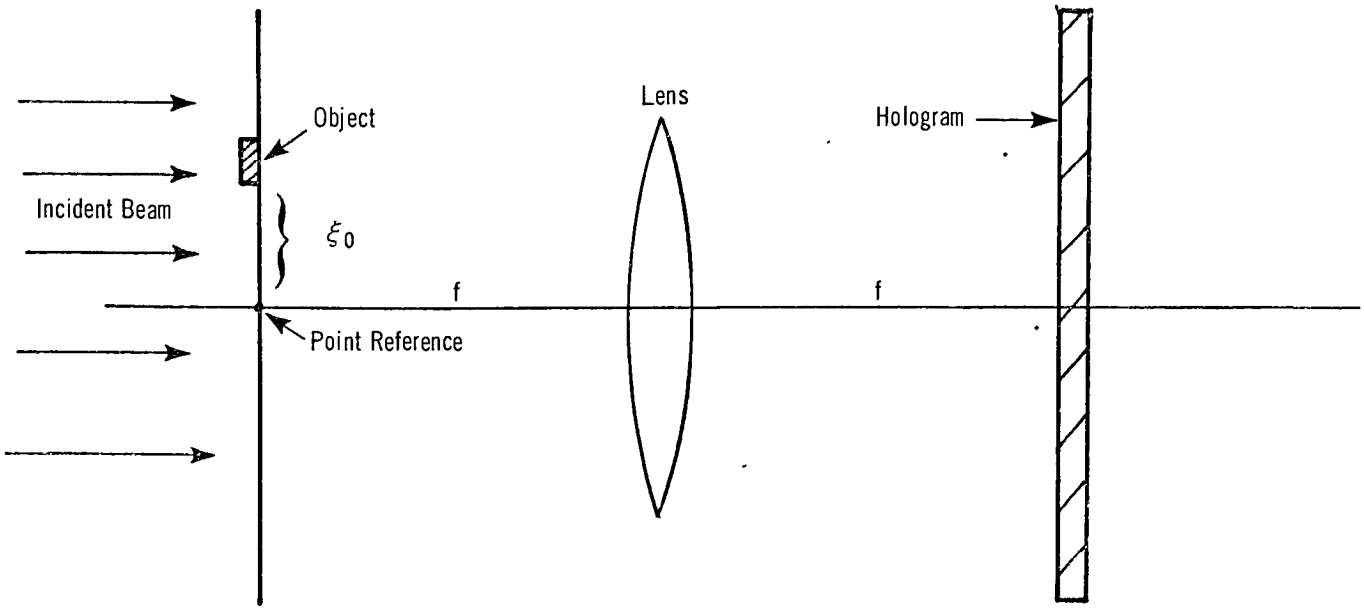

Figure 2-1. Schematic Diagram of Formation Step

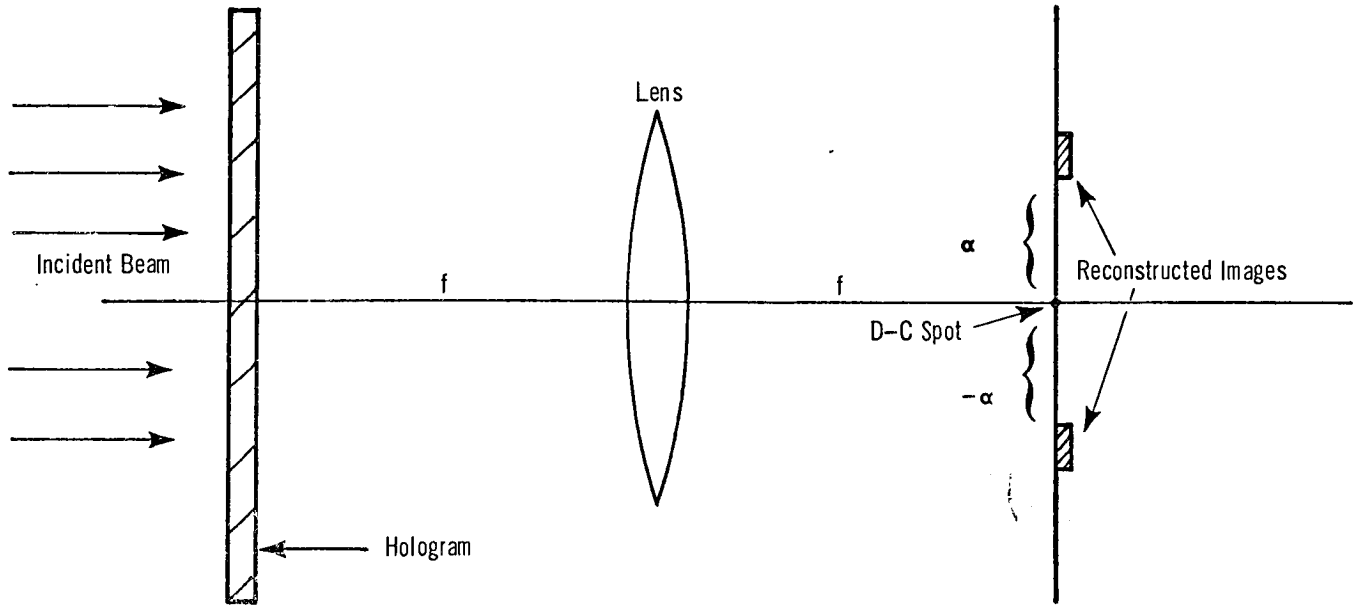

Figure 2-2. Schematic Diagram of Reconstruction Step

$$I = \psi_f \cdot \psi_f^* \qquad 2.202$$

$$I = (A_1 + A_2 e^{i\phi_2})(A_1^* + \hat{A}_2^* e^{-i\phi_2}) \qquad 2.203$$

$$I = |A_1|^2 + |A_2|^2 + A_1 A_2 e^{-i\phi_2} + A_1^* \hat{A}_2 e^{i\phi_2} \qquad 2.204$$

where ψ_f^* is the complex conjugate of ψ_f, the optical disturbance.

When the holographic exposure is made on the linear portion of the photographic sensitometric curve, the complex amplitude, ψ_3 of the field transmitted through the hologram can be represented by[9,10,11]

$$\psi_3 = K [I]^{-\gamma/2} \cdot A_1 \qquad 2.205$$

where ψ_3 represents the optical disturbance of the reconstructed field at the image plane and K is a constant to account for exposure time.

Processing the hologram to a predescribed gamma and reinserting it in the front focal plane of the lens, as shown in Figure 2-2, the amplitude distrubution, $A(\alpha)$, in the image plane becomes:[4]

$$A(\alpha) = \delta(\alpha) + A_2 \circledast A_2^* + A_1^* A_2(\alpha - \xi_o) + A_1 A_2(\alpha + \xi_o) \qquad 2.206$$

where $\circledast$ denotes a convolution operation. Examining the terms in 2.206, it follows that the first two terms represent the original pinhole with spreading due to the off-axis object. The last two terms represent the original object distribution at two off-axis locations.

It will be noted that both of the reconstructed images are real, since the two images are reconstructed in the same plane through a common lens of a given focal length, in contrast to obtaining a real and a virtual image as in other holographic systems.[4,12]

CHAPTER III

THEORY OF PARTIAL COHERENCE

3.1 INTRODUCTION

In measurements involving electromagnetic waves governed by Maxwell's equations, it is usually assumed that the electric field $\overline{E}$ and magnetic field $\overline{H}$ are measurable as functions of position and time.[13] However, for optical fields, existing equipment does not have the response time sufficient to measure radiation amplitudes.[4] Thus, an average quantity must be selected which is, first, representative of the electromagnetic field, and second, is experimentally related to physical phenomena. This average quantity is expressed in optics as being a stationary ergodic ensemble. "Stationary implies that all the ensemble averages are independent of the origin of time, whilst ergodicity implies that each ensemble average is equal to the corresponding time average involving a particular member of the ensemble."[14]

This criterion is readily fulfilled by the theory of partial coherence, which is the theory of an average quantity of the electromagnetic field.[15] From this theory, a second-order moment, $\Gamma(x_1, x_2, \tau)$, termed the mutual coherence function, was introduced by Wolf[14] to specify the correlation that exists between the vibrations at two arbitrary points in a wave field, the field being emitted from a finite source of finite spectral width.

3.2 THE MUTUAL COHERENCE FUNCTION AND THE COMPLEX DEGREE OF COHERENCE

The basic quantity in the theory of partial coherence that is experimentally measurable is called the mutual coherence function[14]

$$\Gamma_{1,2}(\tau) \equiv \Gamma(P_1, P_2, \tau) = \langle V_1(P_1, t+\tau)\, V_2^*(P_2, t) \rangle \qquad 3.201$$

defined as the complex cross-correlation of the optical disturbance at two typical field points, P_1 and P_2, in S_1, as shown in Figure 3-1, where

V_1 = optical disturbance at P_1

V_2 = optical disturbance at P_2

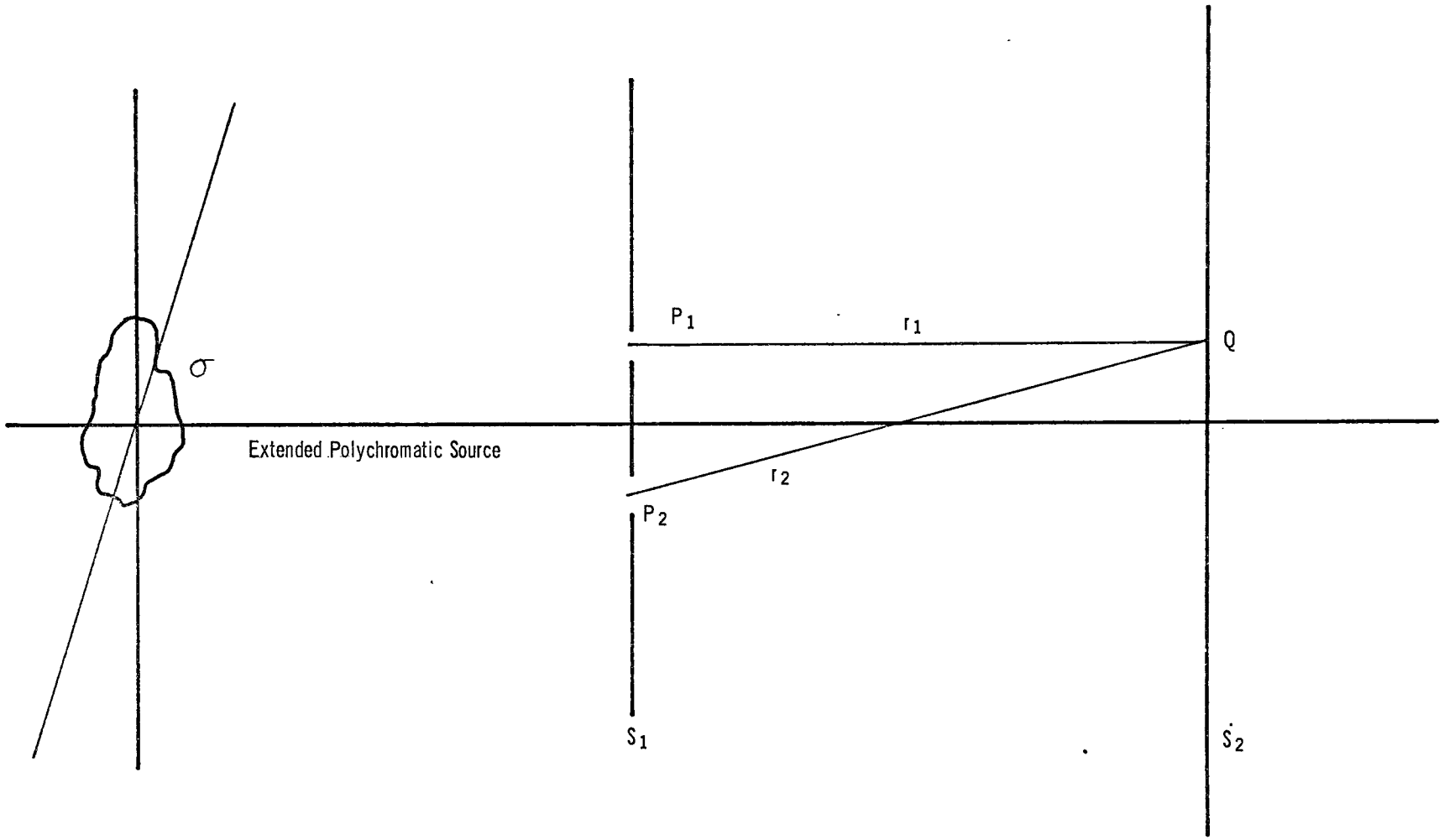

Figure 3-1. Interference Experiment with Extended Polychromatic Source

$\tau = t_2 - t_1$ is given by $\Delta L/C$ where ΔL is the path difference between the two beams and C is the velocity of light in the medium.

$\langle\ \rangle$, denotes a long time average, i. e.,

$$\langle f(t)\rangle = \lim_{T\to\infty} \frac{1}{2T}\int_{-T}^{T} f(t)\,dt$$

$*$ denotes complex conjugate.

When the two points coincide ($P_1 = P_2$) the mutual coherence function becomes the self-coherence function of the light vibrations at either P_1,

$$\Gamma_{11}(\tau) \equiv \Gamma(P_1,\tau) = \langle V_1(P_1, t+\tau)V_1^*(P_1,t)\rangle \qquad 3.202$$

or P_2,

$$\Gamma_{22}(\tau) \equiv \Gamma(P_2,\tau) = \langle V_2(P_2, t+\tau)V_2^*(P_2,t)\rangle \qquad 3.203$$

At zero time delay, $\tau = t_2 - t_1 = 0$, the self-coherence function reduces to:

$$\Gamma_{11}(0) = I_1 \qquad \Gamma_{22}(0) = I_2 \qquad 3.204$$

which is equal to the intensity, or the time average of the product of each optical disturbance with its complex conjugate, of the first and second beams, respectively.

Using the above autocorrelation functions to normalize the mutual coherence function, or the complex cross-correlation, we obtain $\gamma_{12}(\tau)$;

$$\gamma_{12}(\tau) = \frac{\Gamma_{12}(\tau)}{\sqrt{\Gamma_{11}(0)}\sqrt{\Gamma_{22}(0)}} \qquad 3.205$$

which will be called the complex degree of coherence of the light vibrations.[14,15]

The value of the complex degree of coherence is specified within the boundaries, $0 \leq |\gamma_{12}(\tau)| \leq 1$. For an incoherent source, the value of $|\gamma_{12}(\tau)| = 0$, while for a highly coherent source, $|\gamma_{12}(\tau)| = 1$.[14,15]

3.3 QUASI-MONOCHROMATIC APPROXIMATION

When the value of the complex degree of coherence is equivalent to unity, $|\gamma_{12}(\tau)| = 1$, it is implied that the field is strictly monochromatic.[15] Since all fields in nature have some spectral width, a perfectly monochromatic source does not exist. There are fields, however, that have a spectral width, $\Delta\nu$, which is very small compared to $\bar{\nu}$, the mean frequency of the radiation. Such fields are called quasi-monochromatic fields.[14,15,16]

It must be noted that the quasi-monochromatic quality of a field does not imply that it is a coherent field or that its value of the complex degree of coherence even approaches unity. This has been pointed out by both Beran and Parrent[15], as well as by Skinner[16], for extended sources. Thus, a quasi-monochromatic field can be either coherent, partially coherent, or completely incoherent, depending upon the value of the complex degree of coherence rather than the spectral width of the source.

Thus, quasi-monochromatic fields are characterized by the condition that the spectral width of the source ($\Delta\nu$) must be very small compared to the mean frequency($\bar{\nu}$):

$$\Delta\nu \ll \bar{\nu} \qquad 3.301$$

Additionally, however, when we assume that all the path differences satisfy the condition

$$\Delta l \ll C/\Delta\nu \qquad 3.302$$

then the quasi-monochromatic field is a close approximation to a strictly monochromatic field. Most of the following discussion is based on a field of radiation that meets these conditions as stated in equations 3.301 and 3.302, known as the quasi-monochromatic approximation.

3.4 INTERFERENCE WITH PARTIALLY COHERENT LIGHT

The intensity distribution of a partially coherent source can be derived through the use of the interference experiment, shown in Figure 3-1. For the extended polychromatic source, σ, the light disturbance at S_2 can be expressed as a real scalar

function of position and time, $V^r(P,t)$ with which we associate an analytical signal $V(P,t)$. Since detectors can record only time averages of actual signal variations with time, the measurable quantity becomes the time averaged modulus of the signal amplitude sum. In the incoherent limit, this becomes the intensity $I(P)$ which is proportional to the mean value of $[V^r(P,t)]^2$ given by[14]

$$I(P) = 2\langle V^r(P,t)\rangle = \langle V(P,t)V^*(P,t)\rangle \qquad 3.401$$

Now, inserting a screen, S_1, into the wave field, we obtain an intensity distribution $I(P_1)$ and $I(P_2)$ at S_2 due to the pinhole P_1 and P_2, respectively. From this we can measure not only the individual intensities $I(P_1)$ and $I(P_2)$, but also the interference between them.

Let r_1 and r_2 represent the distance from some point Q on the screen S_2 to points P_1 and P_2 on screen S_1, respectively. Then the points P_1 and P_2 become secondary sources yielding a complex disturbance at Q given by

$$V(Q,t) = k_1 V(P_1, t-t_1) + k_2 V(P_2, t-t_2) \qquad 3.402$$

where t_1 and t_2 are the times necessary for the disturbance to travel from P_1 to Q and P_2 to Q, respectively; i.e.,

$$t_1 = r_1/C \quad ; \quad t_2 = r_2/C$$

with C the velocity of light in a vacuum.

Now, with the factors k_1 and k_2 being the complex propogation factors independent of time, it can be shown by combining equations 3.401 and 3.402 that the intensity distribution at Q is given by

$$I(Q) = |k_1|^2 I_1 + |k_2|^2 I_2 + 2|k_1||k_2|\,\Gamma_{12}^r\left(\frac{r_2-r_1}{C}\right) \qquad 3.403$$

where $\Gamma_{12}^r(\tau)$ is the real part of the mutual coherence function.[11,12] The terms $|k_1|^2 I_1$ and $|k_2|^2 I_2$ represent the intensities at Q due to independent illumination of P_1 and P_2 respectively. Utilizing this in conjunction with the definition of the complex degree of coherence, as given by equation 3.205, the relationship for $I(Q)$, equation 3.403, becomes

$$I(Q) = I_1(Q) + I_2(Q) + 2\sqrt{I_1(Q)}\sqrt{I_2(Q)}\,\gamma_{12}^{r}\left(\frac{r_2 - r_1}{c}\right) \qquad 3.404$$

which represents the general interference law for stationary optical fields. It is readily shown that the intensity distribution of two superimposed beams is a function of the intensities of the individual beams and the real part of the complex degree of coherence.[14,15]

By expressing $\gamma_{12}(\tau)$ in a different form, its importance becomes more descriptive. Let $\bar{\nu}$ be the mean frequency of the field such that

$$\gamma_{12}(\tau) = |\gamma_{12}(\tau)|\, e^{i[\alpha_{12}(\tau) - 2\pi\bar{\nu}\tau]} \qquad 3.405$$

where

$$\alpha_{12}(\tau) = 2\pi\bar{\nu}\tau + \arg\,\gamma_{12}(\tau) \qquad 3.406$$

Now equation 3.404 becomes

$$I(Q) = I_1(Q) + I_2(Q) + 2\sqrt{I_1(Q)}\sqrt{I_2(Q)}\,|\gamma_{12}(\tau)|\cos(\alpha_{12}(\tau) - \delta) \qquad 3.407$$

with the values of τ and δ being

$$\tau = \frac{r_2 - r_1}{c} \quad ; \quad \delta = 2\pi\bar{\nu}\tau = \frac{2\pi}{\bar{\lambda}}(r_2 - r_1) \qquad 3.408$$

and $\bar{\lambda}$ is the mean wavelength. When $\gamma_{12}(\tau) = 0$, the last term disappears and the intensity distribution is dependent only upon the sum of the individual intensities. Thus, the interference term is missing and the field is incoherent. When $\gamma_{12}(\tau) = 1$, the intensity $I(Q)$ is dependent upon the individual intensities as well as the phase term. In this case, the field acts as a strictly monochromatic field of wavelength $\bar{\lambda}$ and the vibrations are coherent. Intermediate values of $\gamma_{12}(\tau)$ create a partially coherent field.

3.5 INTERFERENCE WITH QUASI-MONOCHROMATIC LIGHT

The intensity distribution at point Q, of Figure 3-1, for a polychromatic source was found to be given by equation 3.407.

Now, since $\Delta\nu \ll \bar{\nu}$, it follows from equation 3.405 and considerations given to the trigonometric function expressing the difference of two angles, that $|\gamma_{12}(\tau)|$ and $\alpha_{12}(\tau)$ will change much more slowly than the $\cos 2\pi\bar{\nu}\tau$ and $\sin 2\pi\bar{\nu}\tau$. Also, if P_1 and P_2 are small, the intensities $I_1(Q)$ and $I_2(Q)$ from each opening will remain essentially constant over the region of the field at Q, while the $\cos 2\pi\bar{\nu}\tau$ and $\sin 2\pi\bar{\nu}\tau$ terms will change many times in sign over this same region. Thus, $I(Q)$ appears as a constant intensity distribution of $I_1(Q) + I_2(Q)$ with a sinusoidal intensity distribution superimposed on it with an amplitude of approximately $2\sqrt{I_1(Q)}\sqrt{I_2(Q)}|\gamma_{12}(\tau)|$. Therefore, the maximum and minimum intensities near Q are approximately given by

$$I_{max.} = I_1(Q) + I_2(Q) + 2\sqrt{I_1(Q)}\sqrt{I_2(Q)}|\gamma_{12}(\tau)| \qquad 3.501$$

$$I_{min.} = I_1(Q) + I_2(Q) - 2\sqrt{I_1(Q)}\sqrt{I_2(Q)}|\gamma_{12}(\tau)| \qquad 3.502$$

Utilizing these equations and the definition of fringe visibility[14,15]:

$$V = \frac{I_{max.} - I_{min.}}{I_{max.} + I_{min.}} \qquad 3.503$$

The visibility of the fringes for a quasi-monochromatic source becomes

$$V(Q) = \frac{2\sqrt{I_1(Q)}\sqrt{I_2(Q)}}{I_1(Q) + I_2(Q)}|\gamma_{12}(\tau)| \qquad 3.504$$

When the two beams are of equal intensity, the visibility reduces to

$$V(Q) = |\gamma_{12}(\tau)| \qquad 3.505$$

Or, the visibility is a direct measure of the complex degree of coherence.[14,15,18]

3.6 SPATIAL COHERENCE CONSIDERATIONS

Although spatial coherence is not the immediate subject of this paper, it must be given some consideration in reference to determining the radius within which

the experimental source will have an approximately uniform, spatially coherent beam.

As previous literature has shown[4, 14, 15], the spatial coherence of a beam determines the contributions placed on the degree of coherence by the finite spatial extent of the source. Determination of these contributions is accomplished through the use of the Van Cittert-Zernike theorem[14] which provides the mathematical relationships between extended quasi-monochromatic sources and the degree of coherence for the experimental arrangement shown in Figure 3-2. In making this measurement, it is important to vary only the radius of the source[19] or the distance between the pinholes P_1 and P_2 [20], assuming that the spectral width of the source remains constant.

More important to this paper, however, are the results of the Van Cittert-Zernike theorem, which yields the diameter of the circular area illuminated by an approximately uniform, spatially coherent beam[14]. For a uniform circular source of radius ρ, as shown in Figure 3-3, the degree of coherence $|\mu_{12}|$ is given by:

$$|\mu_{12}| = \frac{2 J_1\left(\frac{2\pi\rho d}{\bar{\lambda} R}\right)}{\left(\frac{2\pi\rho d}{\bar{\lambda} R}\right)} \qquad 3.601$$

where J_1 is a first-order Bessel function and its argument $\nu = 2\pi\rho d / \bar{\lambda} R$. The value of $|2 J_1(\nu)/\nu|$ continuously decreases from a value of unity at $\nu = 0$ to a value of zero when $\nu = 3.83$. For a departure of 12 percent from the ideal value unity as an acceptable variation the value of $|2 J_1(\nu)/\nu|$ becomes 0.88 for $\nu = 1$.

The diameter of the circular area that is illuminated by this approximately* uniform, spatially coherent beam is then given by:

$$\nu = \frac{2\pi\rho d}{\bar{\lambda} R} = 1$$

$$d = \frac{\bar{\lambda} R}{2\pi\rho} = \frac{0.16\ \bar{\lambda} R}{\rho} \qquad 3.602$$

*The diameter of the approximately uniform, spatially coherent beam is based on the value of the degree of coherence to vary from 0.88 to 1.00 for a uniformly illuminated circular source. Thus, it tolerates a 12% variation in coherence.

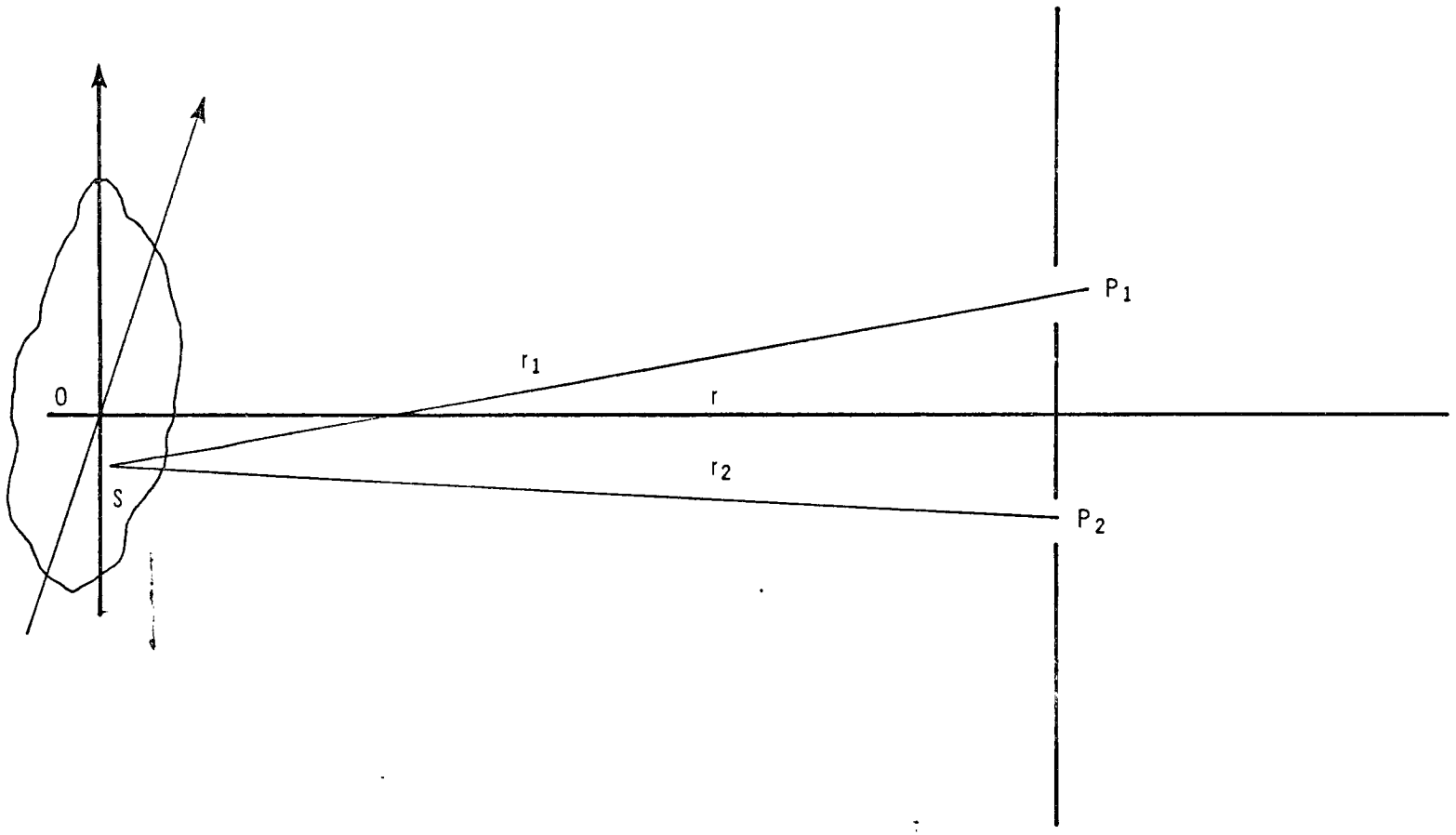

Figure 3-2. Experimental Arrangement for the Van Cittert-Zernike Theorem

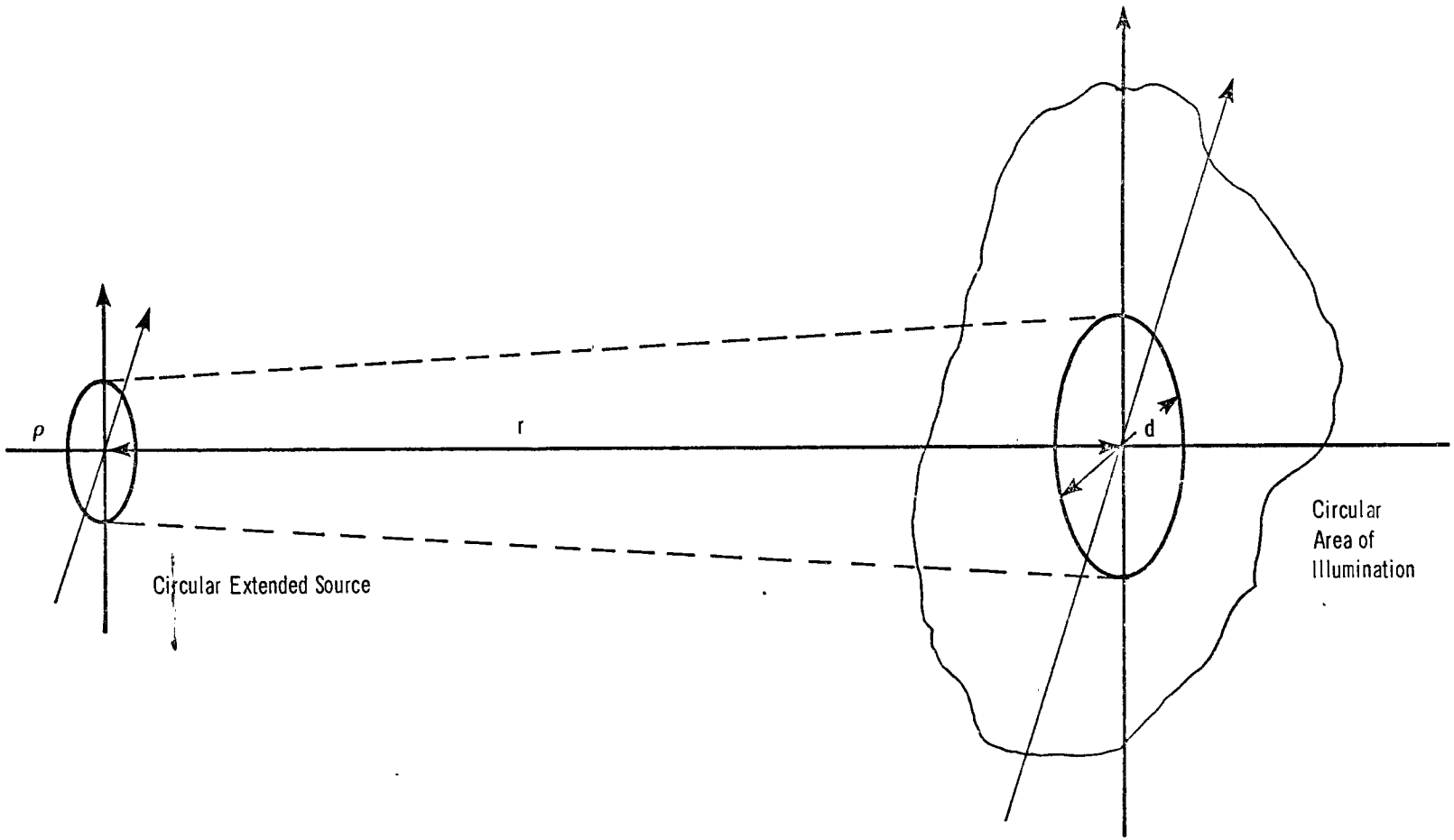

Figure 3-3. Illustration Showing Diameter of Circular Illumination of Uniform, Spatially Coherent Source

where d = diameter of circular area which is uniformly illuminated by a source of circular aperture.

R = perpendicular distance from source to illuminated circular area.

$\bar{\lambda}$ = mean wavelength of illumination.

ρ = radius of uniform circular source.

This result will be used to estimate the actual area of approximately uniform, spatially coherent light available in the experimental holographic object plane for a circular source of given diameter.

3.7 SIGNIFICANCE OF TEMPORAL COHERENCE

Temporal coherence is a measure of the contributions made on the complex degree of coherence, $\gamma_{12}(\tau)$, by the spectral width of the beam. It is, essentially, a measure of the amount of path difference allowed in spatially coherent beams before the superposition of the beams approaches the addition of their intensities rather than the square modulus of the sum of the optical fields.[21]

This can be shown by again considering the mutual coherence functions, $\Gamma_{12}(\tau)$, as given by equation 3.201. For a point source of given spectral width, the mutual coherence function becomes the self-coherence function, $\Gamma_{11}(\tau)$, as given by equation 3.202. By definition, a measure of $\Gamma_{11}(\tau)$ is a measure of the autocovariance of the disturbances emitted by the source. Thus, its Fourier transform, $\hat{\Gamma}_{11}(\nu)$, becomes the energy emitted by the source as a function of frequency, or the power spectral density of the source.[14,15,22] Since the complex degree of coherence is defined as the normalized mutual coherence function, then the degree of coherence, as measured by $\gamma_{11}(\tau)$, is equal to the Fourier transform of the normalized power spectral density of the source.[14] The function $\gamma_{11}(\tau)$ is defined as the measure of the temporal coherence effects.

An illustration of this measurement has been shown by Wolf[14] through the use of a Michelson interferometer adjusted to give interference fringes for an emission line spectrum. It was found that the fringe visibility was a maximum for nearly equal optical paths and that it decreased for increasing optical path differences. Also, the visibility

eventually disappears due to the optical path difference exceeding the finite length of an individual wave train for a stationary field emitted by the source. In addition, the period of a wave train is directly related to the frequency so that we can expect that the longer the wave trains, the narrower the frequency range of the Fourier spectrum

$$\Delta \nu \approx \frac{1}{\Delta t} \qquad 3.701$$

where Δt is the coherence time of the light. Assuming the source has a mean wavelength, $\overline{\lambda}_o$, the coherence length, $\Delta \zeta$, then becomes

$$\Delta \zeta = C \Delta t \approx C/\Delta \nu = (\overline{\lambda}_o)^2/\Delta \lambda_o \qquad 3.702$$

which implies that the path difference between the quasi-monochromatic beams must be small compared to the coherence length.

Again, we find that a measure of the interference fringes, or visibility pattern, is a measure of the coherence. Now, however, it is a measure of the coherence length which determines the coherence time (apart from the constant factor of the velocity of light in the medium).

CHAPTER IV

TEMPORAL COHERENCE EFFECTS ON FOURIER TRANSFORM HOLOGRAPHY UTILIZING QUASI-MONOCHROMATIC, PARTIALLY COHERENT LIGHT

4.1 RAYLEIGH-SOMMERFELD-GREEN'S FUNCTION

To investigate the effects of temporal coherence in the Fourier transform holographic process, it is necessary to investigate the propogation of the optical disturbance from the object, through the lens system, and onto the holographic plane, in the formation process. It is then necessary to repeat this process through the reconstruction step.

In order to do this, use must be made of the Rayleigh-Sommerfeld-Green's function[4,11,15,23] solutions

$$\hat{\Gamma}(X_1, X_2, \nu) = \iint \hat{\Gamma}(S_1, S_2, \nu) \frac{\partial G_1(S_1, X_1, \nu)}{\partial n} \frac{\partial G_2(S_2, X_2, \nu)}{\partial n} dS_1 dS_2 \quad 4.101$$

to the coupled wave equations

$$\nabla_n^2 \Gamma(X_1, X_2, \tau) = \frac{1}{C^2} \frac{\partial^2 \Gamma(X_1, X_2, \tau)}{\partial \tau^2} \qquad n = 1, 2 \quad 4.102$$

where C is the speed of light in air, ∇_n^2 is the Laplacian operator, S_1 and S_2 are the coordinates of the boundary surface, X_1 and X_2 are observation coordinates, and $\hat{\Gamma}(X_1, X_2, \nu)$ is the temporal Fourier transform of $\Gamma(X_1, X_2 \tau)$ represented by

$$\hat{\Gamma}(X_1, X_2, \nu) = \int \Gamma(X_1, X_2, \tau) e^{2\pi i \nu \tau} \, d\tau \quad 4.103$$

By application of the appropriate boundary conditions to these solutions, an expression for the temporal coherence effects will be obtained.

4.2 EFFECTS OF TEMPORAL COHERENCE ON FORMATION OF FOURIER TRANSFORM HOLOGRAMS

Utilizing a similar geometry to that used in Chapter II, the formation step of Figure 4-1 is obtained. The analysis of this system will assume that $Z_1 = Z_2 = f$, the focal length of the lens, and that f is much greater than any length in the region of interest in the object, lens, hologram, or image planes. Also, for simplicity, only

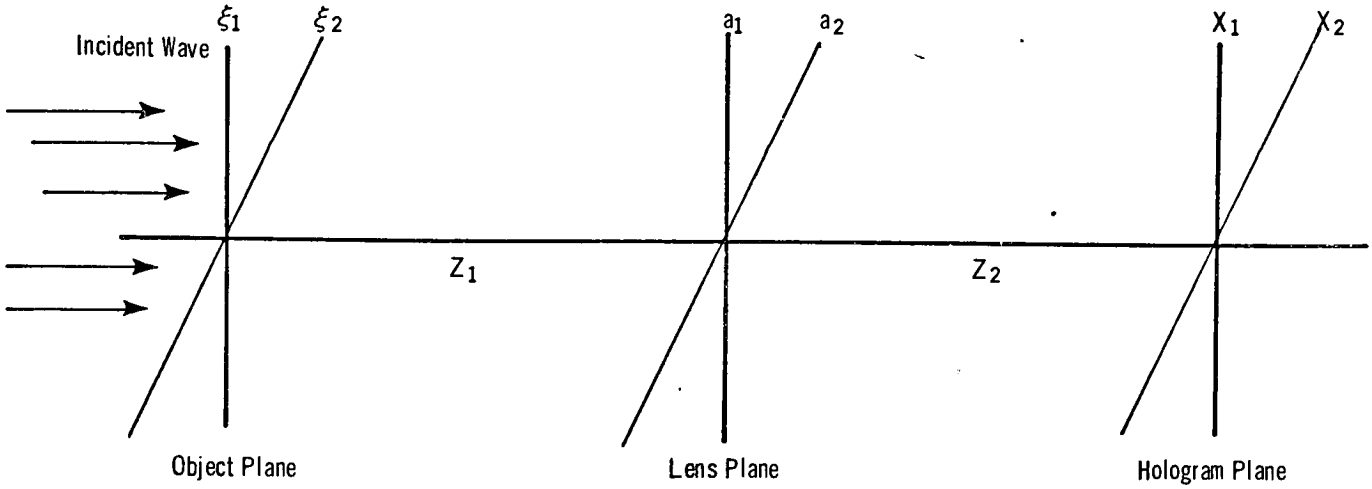

Figure 4-1. Schematic Diagram of Formation Step

the one-dimensional case will be considered, assuming that the results are equivalent to the two-dimensional case by lens symmetry.

Given the mutual intensity function in the object plane at zero time delay, $\Gamma_{ob}(\xi_1,\xi_2,0)$, the mutual intensity function in the hologram plane will be determined.

Applying the Rayleigh-Sommerfeld-Green's solution, equation 4.101, and the appropriate Green's function[4,11,23],

$$G = \frac{e^{ikr_1}}{r_1} - \frac{e^{ikr_2}}{r_2} \qquad 4.201$$

we obtain the mutual intensity function in a plane at an infinitesimal distance to the right of the lens

$$\Gamma(a_1,a_2,0) \approx \iint \Gamma_{ob}(\xi_1,\xi_2,0)\cdot \exp\left\{(ik/2f)\left[(a_1-\xi_1)^2-(a_2-\xi_2)^2\right]\right\} \cdot \exp\left\{(-ik/2f)(a_1-a_2)^2\right\} d\xi_1\, d\xi_2 \qquad 4.202$$

which yields

$$\Gamma(a_1,a_2,0) \approx \iint \Gamma_{ob}(\xi_1,\xi_2,0)\cdot \exp\left\{(ik/2f)\left[-2a_1\xi_1+2a_2\xi_2+\xi_1^2-\xi_2^2\right]\right\} \qquad 4.203$$

where $k = 2\pi/\lambda$.

For the mutual intensity function in the hologram plane, we multiply by the propogation factor to obtain

$$\Gamma(X_1,X_2,0) \approx \iiiint \Gamma_{ob}(\xi_1,\xi_2,0)\cdot \exp\left\{(ik/2f)\left[-2a_1\xi_1+2a_2\xi_2+\xi_1^2-\xi_2^2\right]\right\} \cdot \exp\left\{(ik/2f)\left[(a_1-X_1)^2-(a_2-X_2)^2\right]\right\} d\xi_1\, d\xi_2\, da_1\, da_2 \qquad 4.204$$

Making a linear transformation of the variables

$$a_1 + a_2 = 2P_1 \quad ; \quad a_1 - a_2 = 2P_2$$

equation 4.204 becomes

$$\Gamma(X_1,X_2,0) \approx \iiiint \Gamma_{ob}(\xi_1,\xi_2,0)\cdot \exp\left\{(ik/2f)\left[-2\xi_1P_1-2\xi_1P_2+2\xi_2P_1-2\xi_2P_2 + \xi_1^2-\xi_2^2+4P_1P_2+X_1^2-2X_1P_1-2X_1P_2-X_2^2+2X_2P_1 - 2X_2P_2\right]\right\} dP_1\, dP_2\, d\xi_1\, d\xi_2 \qquad 4.205$$

and remembering the definition for the Dirac delta function[4,11] as

$$\int_{-\infty}^{\infty} e^{-i\omega x}\, d\omega = \delta(x) \qquad 4.206$$

and integrating equation 4.205 for P_2 , we obtain:

$$\Gamma(X_1,X_2,0) \approx \iiint \Gamma_{ob}(\xi_1,\xi_2,0)\cdot \exp\left\{(ik/2f)\left[-2\xi_1P_1+2\xi_2P_1+\xi_1^2-\xi_2^2 + X_1^2-2X_1P_1-X_2^2+2X_1P_1\right]\right\} \cdot \delta(-2\xi_1-2\xi_2-2X_1-2X_2+4P_1) \qquad 4.207$$
$$d\xi_1\, d\xi_2\, dP_1$$

Integrating for P_1 and remembering the convolution theorem[4,11]

$$\int_{-\infty}^{\infty} f(x)\cdot\delta(\gamma-a)\, dx = f(a) \qquad 4.208$$

the mutual intensity function becomes:

$$\Gamma(X_1,X_2,0) \approx \iint \Gamma_{ob}(\xi_1,\xi_2,0)\cdot \exp\left\{(ik/2f)\left[\xi_1^2-\xi_2^2+X_1^2-X_2^2\right]\right\} \cdot \exp\left\{(ik/2f)\left[-\xi_1+\xi_2-X_1+X_2\right]\left[\xi_1+\xi_2+X_1+X_2\right]\right\} d\xi_1\, d\xi_2 \qquad 4.209$$

which reduces to

$$\Gamma(X_1,X_2,0) \approx \iint \Gamma_{oc}(\xi_1,\xi_2,0) \cdot \exp\left\{(-ik/2f)\left[X_1\xi_1 - X_2\xi_2\right]\right\} d\xi_1\, d\xi_2 \qquad 4.210$$

or

$$\Gamma(X_1,X_2,0) \approx \hat{\Gamma}_{oc}\left(\frac{X_1}{\lambda f}, -\frac{X_2}{\lambda f}, 0\right). \qquad 4.211$$

Thus, a spatial Fourier transform exists between the mutual intensity function in the object plane and the mutual intensity function in the hologram plane.

4.3 TEMPORAL COHERENCE EFFECTS ON THE RECONSTRUCTION OF FOURIER TRANSFORM HOLOGRAMS

The mutual coherence function in the hologram plane can be related to exposure on the photographic hologram through the use of the self-coherence function.

Reducing equation 4.211 to the self-coherence function and using the relationship $I(X_1) = \Gamma(X_1,X_1,0)$ [4,14,15] we obtain

$$I(X_1) = \Gamma(X_1,X_1,0) \approx \hat{\Gamma}_{ob}\left(\frac{X_1}{\lambda f}, -\frac{X_2}{\lambda f}, 0\right) \qquad 4.301$$

which is the intensity at point X_1 in the hologram plane.

As previously shown in equation 2.205, the intensity can be related to the transmittance of the film. Thus, the self-coherence at the hologram plane is related to the transmittance of the photographic hologram when it is properly aligned, as shown in Figure 4-2, for the reconstruction step. This transmittance becomes

$$T(X_1) \approx \hat{\Gamma}_{ob}\left(\frac{X_1}{\lambda f}, -\frac{X_2}{\lambda f}, 0\right) \qquad 4.302$$

which then propogates to an infinitesimal distance to the right of the lens to yield:

$$\Gamma(a_1,a_2,0) \approx \int \Gamma(\xi_1,\xi_1,0) \cdot T(X_1) \cdot \exp\left\{(ik/2)\left[(a_1-\xi_1)^2 - (a_2-\xi_1)^2\right]\right\} \cdot \exp\left\{(-ik/2f)\left[a_1^2 - a_2^2\right]\right\} d\xi_1 \qquad 4.303$$

This may be simplified to:

$$\Gamma(a_1,a_2,0) \approx \int \Gamma(\xi_1,\xi_1,0) \cdot T(X_1) \cdot \exp\left\{(ik/2f)\left[-2a_1\xi_1 + 2a_2\xi_1\right]\right\} d\xi_1 \qquad 4.304$$

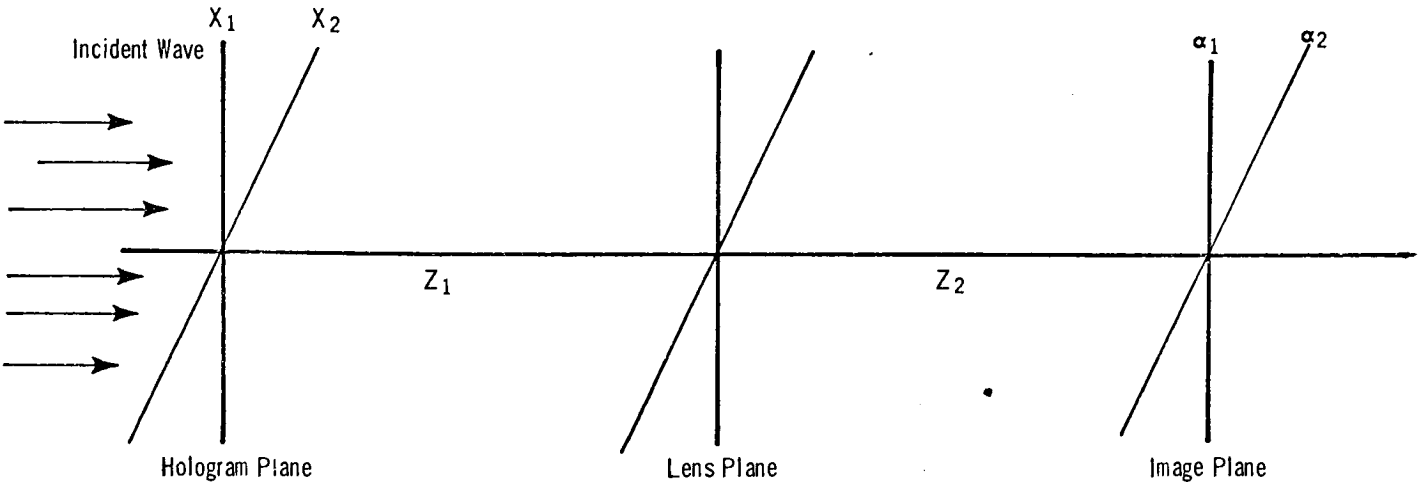

Figure 4-2. Schematic Diagram of Reconstruction Step

which then propogates to the image plane to become:

$$\Gamma(\alpha_1,\alpha_2,0) \approx \iiint \Gamma(\xi_1,\xi_1,0)\cdot T(X_1)\cdot \exp\left\{(ik/2f)\left[-2\alpha_1\xi + 2\alpha_2\xi_1\right]\right\} \cdot \exp\left\{(ik/2f)\left[(\alpha_1-\alpha_1)^2 - (\alpha_2-\alpha_2)^2\right]\right\} d\xi_1\, d\alpha_1\, d\alpha_2 \qquad 4.305$$

Transforming the variables

$$\alpha_1 + \alpha_2 = 2P_1 \quad ; \quad \alpha_1 - \alpha_2 = 2P_2$$

we obtain

$$\Gamma(\alpha_1,\alpha_2,0) \approx \iiint \Gamma(\xi_1,\xi_1,0)\cdot T(X_1)\cdot \exp\left\{(ik/2f)\left[-2\xi_1P_1 - 2\xi_1P_2 + 2\xi_1P_1 - 2\xi_1P_2 - 2\alpha_1P_1 - 2\alpha_1P_2 + 4P_1P_2 + \alpha_1^2 + 2\alpha_2P_1 - 2\alpha_2P_2 - \alpha_2^2\right]\right\} d\xi_1\, dP_1\, dP_2 \qquad 4.306$$

which, when integrated with respect to P_2, becomes

$$\Gamma(\alpha_1,\alpha_2,0) \approx \iiint \Gamma(\xi_1,\xi_1,0)\cdot T(X_1)\cdot \exp\left\{(ik/2f)\left[-2\xi_1P_1 + 2\xi_1P_1 - 2\alpha_1P_1 + \alpha_1^2 + 2\alpha_2P_1 - \alpha_2^2\right]\right\} \cdot \delta(-4\xi_1 - 2\alpha_1 - 2\alpha_2 + 4P_1)\, d\xi_1\, dP_1 \qquad 4.307$$

This is now integrated with respect to P_1 :

$$\Gamma(\alpha_1,\alpha_2,0) \approx \iiint \Gamma(\xi_1,\xi_1,0)\cdot T(X_1)\cdot \exp\{(ik/2f)[\alpha_1^2-\alpha_2^2]\} \cdot \exp\{(ik/2f)[(-\alpha_1+\alpha_2)(2\xi_1+\alpha_1+\alpha_2)]\}\, d\xi_1 \qquad 4.308$$

and simplified to:

$$\Gamma(\alpha_1,\alpha_2,0) \approx \iiint \Gamma(\xi_1,\xi_1,0)\cdot T(X_1)\cdot \exp\{(ik/2f)[2\xi_1\alpha_2-2\xi_1\alpha_1]\, d\xi_1 \qquad 4.309$$

Remembering that the transmittance is simply the Fourier transform of the self-coherence of the object, equation 4.309 reduces to

$$\Gamma(\alpha_1,\alpha_2,0) \approx \hat{\Gamma}\left(\frac{2\alpha_1}{\lambda f},-\frac{2\alpha_2}{\lambda f},0\right)\cdot T(X_1) \quad . \qquad 4.310$$

or

$$\Gamma(\alpha_1,\alpha_2,0) \approx \hat{\Gamma}\left(\frac{2\alpha_1}{\lambda f},-\frac{2\alpha_2}{\lambda f},0\right)\cdot \hat{\Gamma}_{ob}\left(\frac{X_1}{\lambda f},-\frac{X_2}{\lambda f},0\right) \qquad 4.311$$

Thus, the mutual intensity function in the image plane is simply the product of the Fourier transform of the self-coherence function in the reconstructively illuminated hologram plane and the Fourier transform of the self-coherence of the object plane. Assuming that the illumination for the formation and reconstruction steps is identical, it becomes obvious that the mutual intensity function of the image plane closely resembles the mutual intensity function of the object plane. Thus, for a given object, the image plane should yield, with the exception of some phase factors, an accurate reproduction.

Also, and most important to this paper, the coherence properties of the light are "carried through" the holographic system and thus become an important factor when considering the reproduction of objects.

CHAPTER V

CONSIDERATION OF SYSTEM LIMITATIONS

5.1 INTRODUCTION

In this investigation, there were three important factors or limitations to be placed on the design of the experimental program before actual experimentation could take place. Also, in the evaluation of each of these factors, it had to be kept in mind that certain system components are selected because of their availability and previous use as given in a wide range of references. An example of such a component is the high-pressure mercury arc source which is available and has been suggested for use in previous literature.[4]

The first factor for consideration was the area of the partially coherent beam which is spatially coherent. The measurement of temporal coherence with a Michelson interferometer and the construction of Fourier transform holograms require that the light source have some degree of partial coherence. Since a partially coherent beam is both temporally and spatially coherent[14,15] and the measurement of temporal coherence was of prime importance in this investigation, it was necessary that the spatial coherence remain constant and that an estimate be obtained of the area of illumination which had a constant or approximately constant degree of spatial coherence.

The second factor to be considered was the resolution or frequency limitations required by the overall system. Since the main components of the holographic system consist of optical lenses and photographic film, it was necessary to evaluate the maximum frequency response that would be required by each.

The last factor to be considered was the required path differences (between the object and reference beams of the holographic system) necessary to yield the coherence characteristics set by the experimental objectives.

5.2 SPATIAL COHERENCE CONSIDERATIONS

The spatial coherence theory of an extended quasi-monochromatic source was discussed in Chapter III. The results of the discussion yielded the relationship 3.602, which will be repeated here for convenience:

$$d = \frac{0.16\,R\bar{\lambda}}{\rho}$$

The diameter, d, will determine the constraints placed on the holographic object or target. Thus, the choice of parameters R, $\bar{\lambda}$, and ρ is critical to the entire experiment.

The selection of these parameters was based primarily on the energy problems involved in constructing and reconstructing the holograms. First, a high-energy, partially coherent source is necessary for the temporal coherence measurements on the Michelson interferometer, as well as to allow for reasonable exposure times in the holographic formation step.

Secondly, a compromise must be made in selecting the values of source diameter, ρ, and source distance, R, since their effect on the uniform area of illumination, as given in equation 3.602, is inversely related to their effect on the amount of energy transmitted by ρ over the distance R.[24,25]

With these considerations in mind, the following values were given to the parameters of wavelength, source diameter, and source distance.

Mean wavelength = $\bar{\lambda}$ = 0.546 micron
Source diameter = ρ = 100 microns
Source distance = R = 1 meter (collimator lens with focal length of 1 meter)

Inserting these values into equation 3.602 yields:

$$d = \frac{0.16 \times 1 \times 5.46 \times 10^{-7}}{10^{-4}}$$

$$d = 0.875 \text{ millimeter}$$

for the diameter of the approximately uniform, spatially coherent area of illumination.

Strict adherence to this diameter would require that the actual holographic target used in the experimental portion of this investigation be confined to a circular area of diameter less than 0.875 millimeter and centered on the optical axis.

However, for this particular investigation, the strict interpretation of allowing only a 12% variation[14] in spatial coherence places critical dimensional requirements

on the construction of the target that are not really required. The experimental methods utilized in this investigation, as described in Chapter VIII, required: (1) Approximately equivalent mean wavelengths for the spectra of the interference filters utilized to change the coherence interval of the source, and (2) no change in the object target position between individual holographic exposures. In addition, all methods utilized in the analysis of the experimental data obtained from the holograms and their respective reconstructed images emphasized relative changes that had occurred rather than absolute magnitudes of the hologram densities and their respective image intensities. This means that even though there is a degradation of spatial coherence across the illuminated target area, the degradation will have minimal effect on the results of this investigation. This assumes, of course, that the lower value of spatial coherence degradation is maintained well above the incoherent level.

Therefore, for this experimental investigation, the strict 12% variation of spatial coherence was not followed, but rather a 50% variation was considered as a lower limit of allowable spatial coherence degradation. The relation between this 50% variation and the maximum allowable target diameter is found by considering the mathematical form of the degree of coherence that exists for the Van Cittert-Zernike theorem discussed previously in paragraph 3.6. The constant 0.16 is based upon a value of 0.88 for the degree of coherence where the spatial coherence is represented by a first-order Bessel function. A plot of a first-order Bessel function, as shown in Figure 5-1, yields a value of $\nu = 1$ for $|2J_1(\nu)/\nu| = 0.88$, which is equivalent to a constant of 0.16, i.e.,

$$\text{Constant} = \nu/2\pi = 1/2\pi = 0.16$$

When the spatial coherence variation is allowed to decrease by 50%, the value of ν becomes 2.175, which yields:

$$\text{Constant} = \nu/2\pi = 2.175/2\pi = 0.346$$

Inserting this constant in equation 3.602, the allowable diameter of uniform spatial coherence becomes:

$$d = \frac{0.346 \times 1 \times 5.46 \times 10^{-7}}{10^{-4}}$$

$$d = 1.88 \text{ mm}$$

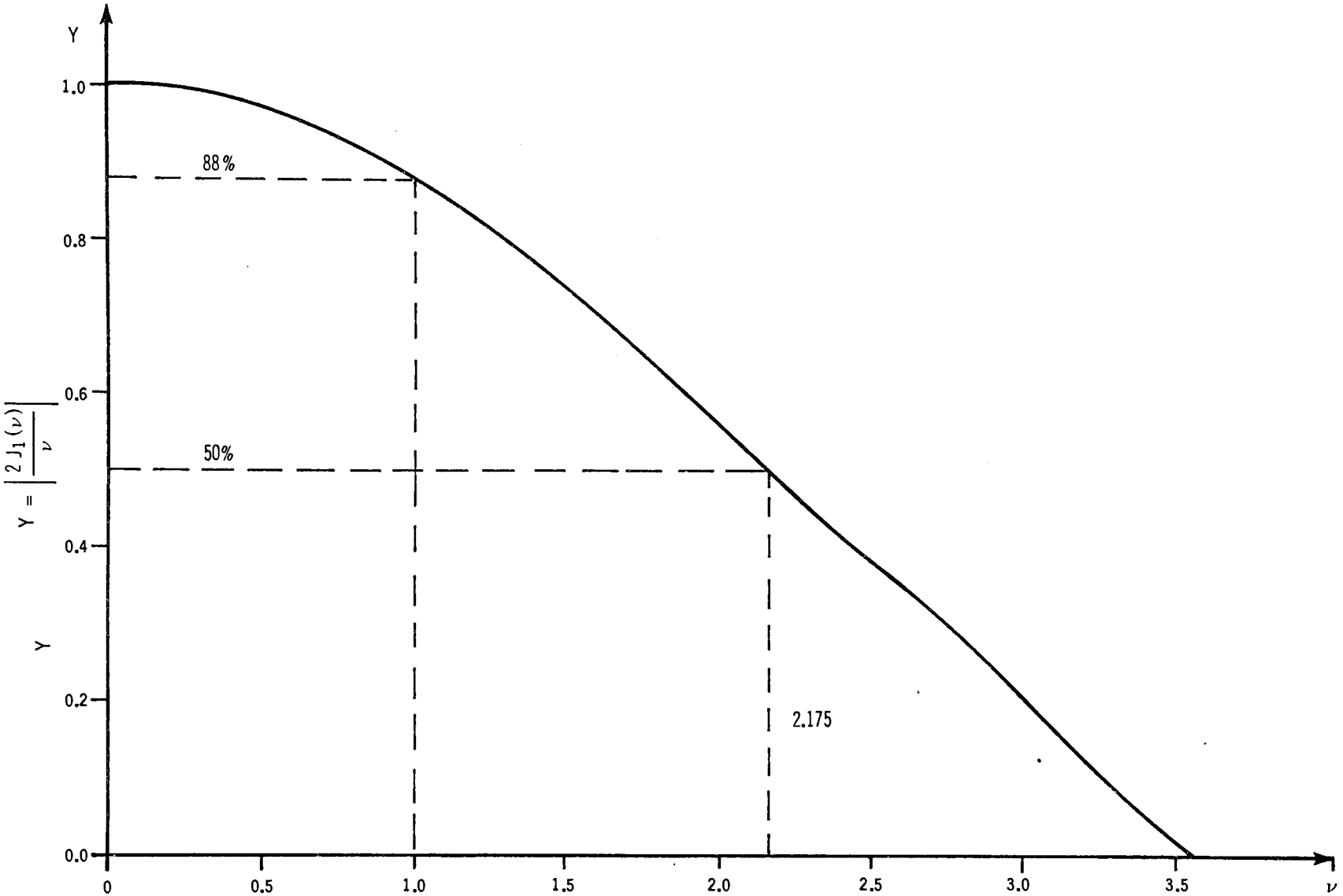

Figure 5-1. First-Order Bessel Function

Since this was an estimation, the actual holographic target was confined to an area of less than 1.88 mm.

5.3 FREQUENCY RESPONSE OF THE HOLOGRAPHIC SYSTEM

Consideration will be given to the frequency response of each of the two steps in the holographic imaging process. In the formation step, an estimate is given for the highest spatial frequency that will be recorded in the hologram plane when the object and reference are separated by a distance equal to the diameter of the circle of uniform spatial coherence as given in paragraph 5.2. In the reconstruction step, confirmation is made that the highest frequency recorded in the hologram plane is passed through the system in forming the reconstructed image.

First, consider the Fourier transform hologram formation step as shown in Figure 5-2.

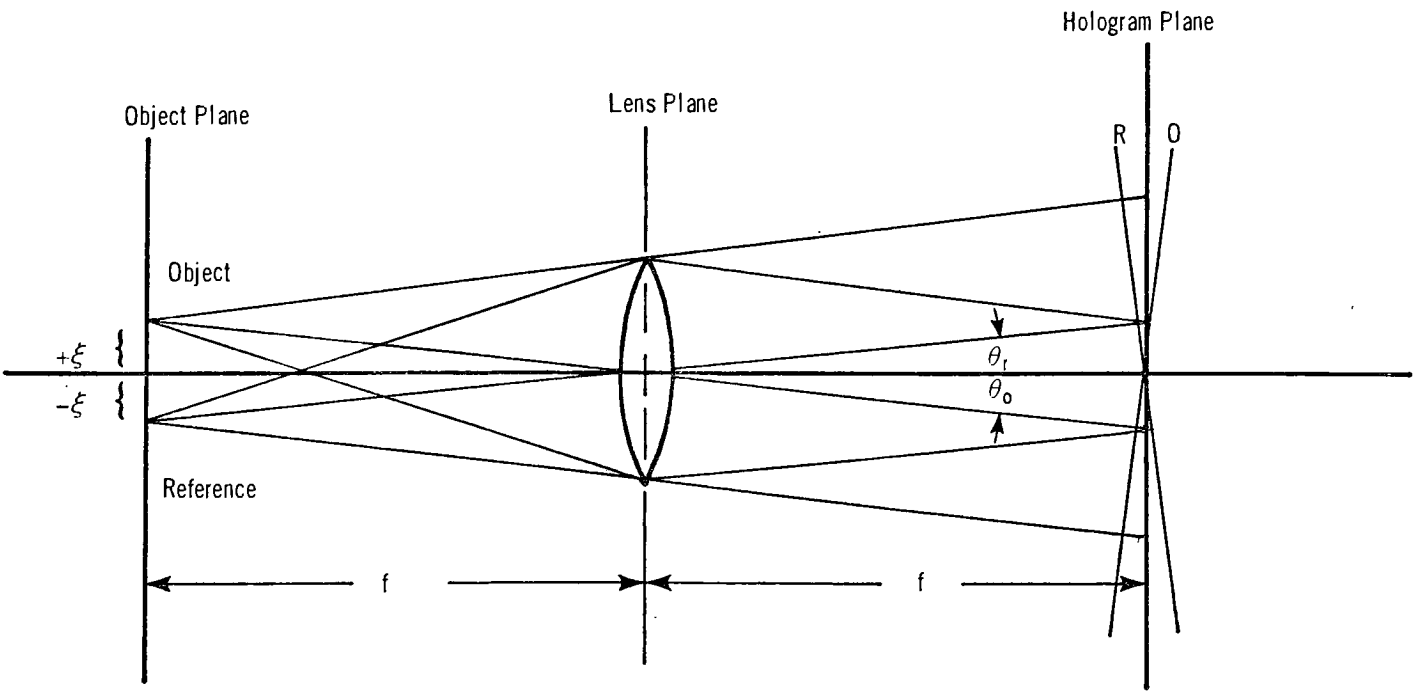

Figure 5-2. Fourier Transform Hologram Formation Step

This represents the experimental arrangement utilized during the formation step to be discussed in Chapter VIII. The object plane consists of a planar object and a point reference positioned equidistant from the optical axis by an amount ξ. Thus, the hologram plane is approximately representative of two plane waves incident at angles θ_o for the object wave, and θ_r for the reference wave. From the geometry of Figure 5-2, it is clear that

$$\begin{aligned} \theta_r &= -\tan^{-1}(\xi/f) \\ \theta_o &= \tan^{-1}(\xi/f) \end{aligned} \qquad 5.301$$

and $\theta_r = -\theta_o$ for the symmetrical object.

Also, the plane waves may be written $Ae^{i\bar{k}\cdot\bar{r}}$ where $\bar{k}=\frac{2\pi}{\lambda}(\alpha_x\bar{a}_x+\alpha_y\bar{a}_y+\alpha_z\bar{a}_z)$ and $\bar{r} = X\bar{a}_x + Y\bar{a}_y + Z\bar{a}_z$. The values $\alpha_X, \alpha_Y, \alpha_Z$ are the direction cosines of $\bar{k}$, and a_x, a_y, a_z are unit vectors along X, Y, Z. For the geometry of the holographic recording plane, shown in Figure 5-3, the values for $\bar{k}$ and $\bar{r}$ become:

$$\left.\begin{aligned} \bar{k}_1 &= \frac{2\pi}{\lambda}(\cos\theta\cdot\bar{a}_z - \sin\theta\cdot\bar{a}_y) \\ \bar{k}_1\cdot\bar{r} &= \frac{2\pi}{\lambda}(Z\cdot\cos\theta - Y\cdot\sin\theta) \\ \bar{k}_2 &= \frac{2\pi}{\lambda}(\cos\theta\cdot\bar{a}_z + \sin\theta\cdot\bar{a}_y) \\ \bar{k}_2\cdot\bar{r} &= \frac{2\pi}{\lambda}(Z\cdot\cos\theta + Y\cdot\sin\theta) \end{aligned}\right\} \qquad 5.302$$

The amplitude of the sum of the two waves becomes

$$\begin{aligned} &A_1\cdot\exp\{(2\pi i/\lambda)[Z\cdot\cos\theta - Y\cdot\sin\theta]\} \\ &+ A_2\cdot\exp\{(2\pi i/\lambda)[Z\cdot\cos\theta + Y\cdot\sin\theta]\} \end{aligned} \qquad 5.303$$

and the modulus squared yields the intensity:

$$(A_1^2+A_2^2)\left[1+\frac{2A_1A_2}{A_1^2+A_2^2}\cos\left(\frac{2\pi}{\lambda}\cdot 2Y\cdot\sin\theta\right)\right] \qquad 5.304$$

This represents the super position of two intensity beams, one constant and one modulated by the cosine function. The cosine function is equivalent to $\cos(2\pi\nu\lambda)$, which represents the fringe pattern, periodic in the Y-direction with frequency

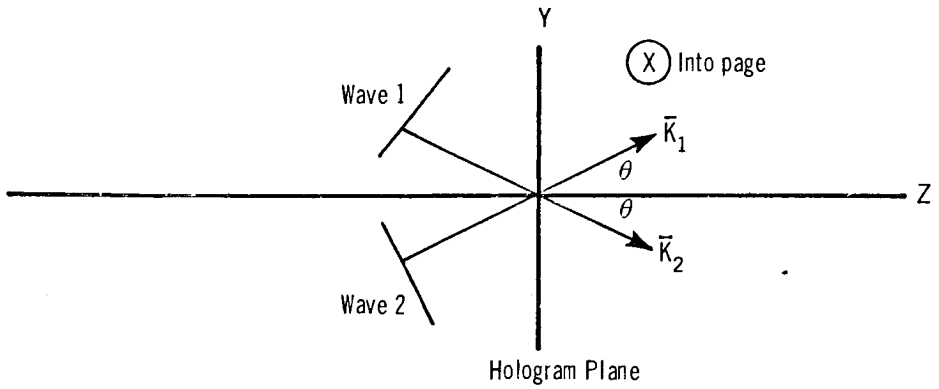

Figure 5-3. Two Plane Waves Incident on Holographic Recording Plane

$$\nu = \frac{2 \sin\theta}{\lambda} \qquad 5.305$$

Combining equations 5.305 and 5.301 yields

$$\nu = \frac{2 \sin(\tan^{-1} \xi/f)}{\lambda} \qquad 5.306$$

which, for very small angles, becomes

$$\nu = 2\xi/f\lambda \qquad 5.307$$

which is the highest spatial frequency recorded by the hologram.

For the values utilized in the experimental arrangement, i.e.,

$\overline{\lambda}$ = 0.546 micrometer

ξ = d/2 = 0.94 millimeter

f = 25.4 centimeters

This spatial frequency becomes

$$\nu = 2\xi/f\bar{\lambda} = 13.5 \text{ cycles/mm} \qquad 5.308$$

This value will be compared to the actual experimental value obtained for the holographic system in Chapter VIII.

Now, considering the hologram in terms of a diffraction grating, the cutoff frequency of the reconstruction step becomes equivalent to the limiting frequency predicted by the grating period. This is illustrated in Figure 5-4, where the limiting spatial frequency, ν_{lim}, is related to the grating period, d, by

$$\nu_{lim} \approx \frac{1}{d} = \frac{\sin\theta}{\lambda} \qquad 5.309$$

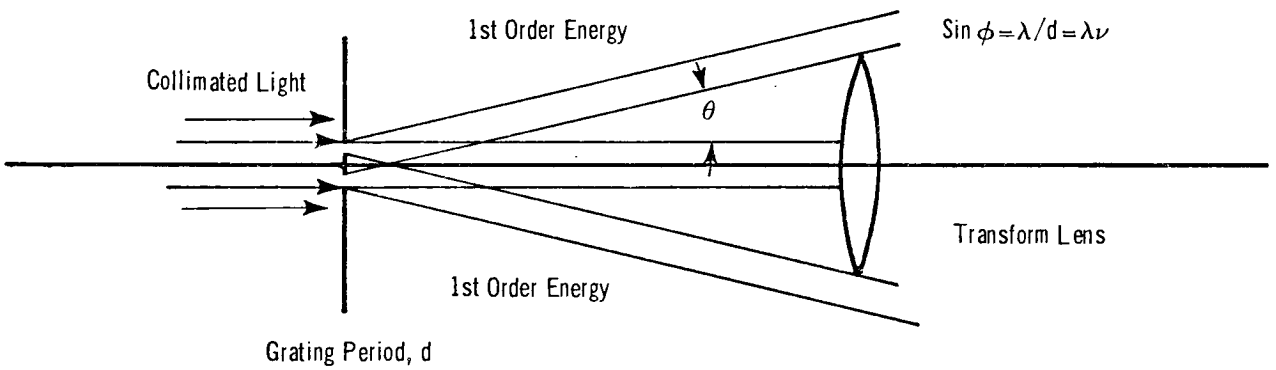

Figure 5-4. Relationship Between Reconstruction Step and Diffraction Grating

Conversely, for the purpose of this investigation, it is important to determine the geometrical constraints placed on the reconstruction step in order to pass the highest frequency recorded by the hologram in the formation step. For the same basic geometrical arrangement utilized in the formation step,

$$\theta = \tan^{-1}(r/f) \qquad 5.310$$

where r is the radius of the transform lens and f is its focal length.

Combining equations 5.310 and 5.309 yields

$$\nu \approx \frac{1}{d} = \frac{\sin(\tan^{-1} r/f)}{\lambda} \qquad 5.311$$

which, assuming very small angles, becomes

$$\nu \approx r/f\lambda \qquad 5.312$$

yielding the lens radius

$$r \approx \nu f \lambda \qquad 5.313$$

For the values previously utilized and determined in the formation step, equation 5.308, the radius of the transform lens must exceed

$$r \approx \nu f \lambda = 1.87 \text{ mm} \qquad 5.314$$

for the reconstruction step to pass the highest frequency recorded by the hologram in the formation step. Since the diameter of the transform lens used in the experimental arrangement was approximately 25 mm, the region of spatial coherence over the object, rather than the system optical components, limits the system frequency response and a reconstructed image of the original object will be obtained.

5.4 ESTIMATION OF ALLOWABLE PATH DIFFERENCES

The interference between the two wavefronts of a holographic system can be compared to the interference between the two beams of a Michelson interferometer. In each case, interference takes place only if the path difference between the two beams is less than the coherence length of the light source as defined by equation 3.702 in Chapter III. This equation is repeated here for convenience:

$$\Delta\ell = C\,\Delta t \approx C/\Delta\nu \approx \bar{\lambda}_o^2/\Delta\lambda$$

where $\Delta\ell$ = coherence length of the source.

Δt = coherence time of the source.

$\Delta\nu$ = frequency range of the Fourier spectrum of the source.

C = velocity of light in a vacuum.

$\bar{\lambda}_o$ = mean wavelength of source.

$\Delta\lambda$ = change in wavelength of source.

Using the right side of equation 3.702, an estimation of the coherence length for the filtered mercury arc source is

$$\Delta\mathcal{L} \approx \bar{\lambda}_o/\Delta\lambda \approx \quad 15 \times 10^{-5} \text{ meters}$$

which yields a coherence length of approximately 150 microns. Thus, the path difference between the object and reference beams should be less than 150 microns for interference and holographic formation to take place.

Referring back to Figure 5-2, the holographic formation step can be represented as shown in Figure 5-5, where the path difference between the interfering object and reference beams can be estimated using the sagittal approximation.

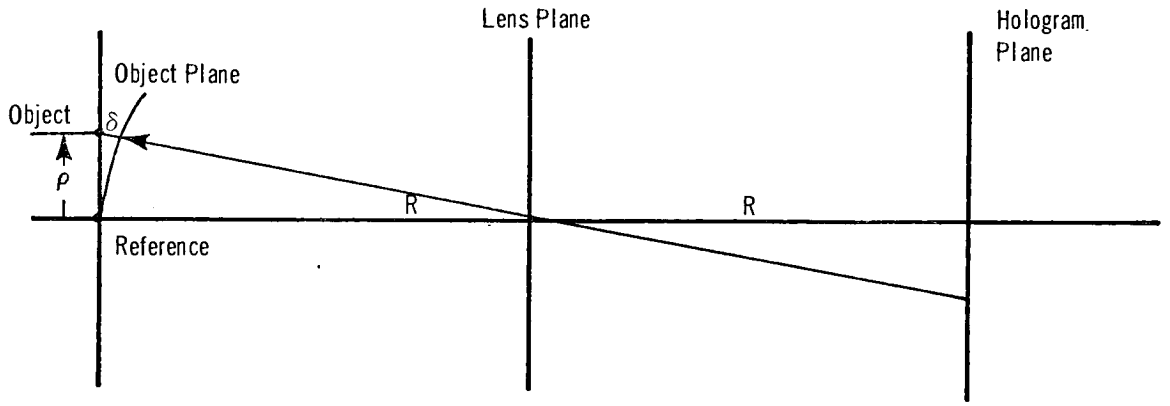

Figure 5-5. Application of Sagittal Approximation to Holographic Formation Step

This yields a path difference of

$$\delta = \rho^2/2r = \frac{(.875)^2}{2 \times 50.8} \times \frac{(10^{-6})}{10^{-2}}$$

$$\delta = .00753 \text{ millimeters}$$

which is significantly less than previously calculated coherence length of the source.

CHAPTER VI

PHOTOGRAPHIC SENSITOMETRY

6.1 SENSITOMETRY OF PHOTOGRAPHIC HOLOGRAMS

It was previously shown (Chapter II, Section 2.2 and Chapter IV, Section 4.3) that the sensitometry of the photographic recording medium is important for two reasons. First, the amplitude transmission of the hologram is dependent upon the shape of the characteristic curve of the photographic material, and secondly, to overcome all of the nonlinearities that may be placed on the Fourier transform hologram by the photographic film, the exposures must be made on the linear portion of this curve, and the value of the slope of the curve must be a negative value of two, $\gamma = -2$.

Experiments were performed, independent of the formation of the holograms, to derive a photographic development process that would fulfill these requirements for Eastman Kodak film type SO-243.

The experiments consisted of replicated exposures through photographic step tablets onto SO-243 film using an EG&G Mark VI Sensitometer. A Kodak Wratten Filter No. 58 was included to simulate the approximate energy distribution of the mercury-arc lamp combined with the interference filters to be utilized in the holographic exposures.

The exposed film strips were developed utilizing a variety of chemical processes and processing times, and all experimental work was accurately controlled and recorded for future replication.

The result of this experimentation is the development process given in Appendix I which yields the characteristic H&D curve shown in Figure 6-1. Note that this is a reversal process so as to attain an optimum negative gamma and that the density values are based on an average of the density values obtained from measurements taken with a Macbeth TD-203 Densitometer for three separate step tablets. The utilization of this characteristic curve with controlled holographic exposures would yield reconstructed images essentially identical to the original object target.

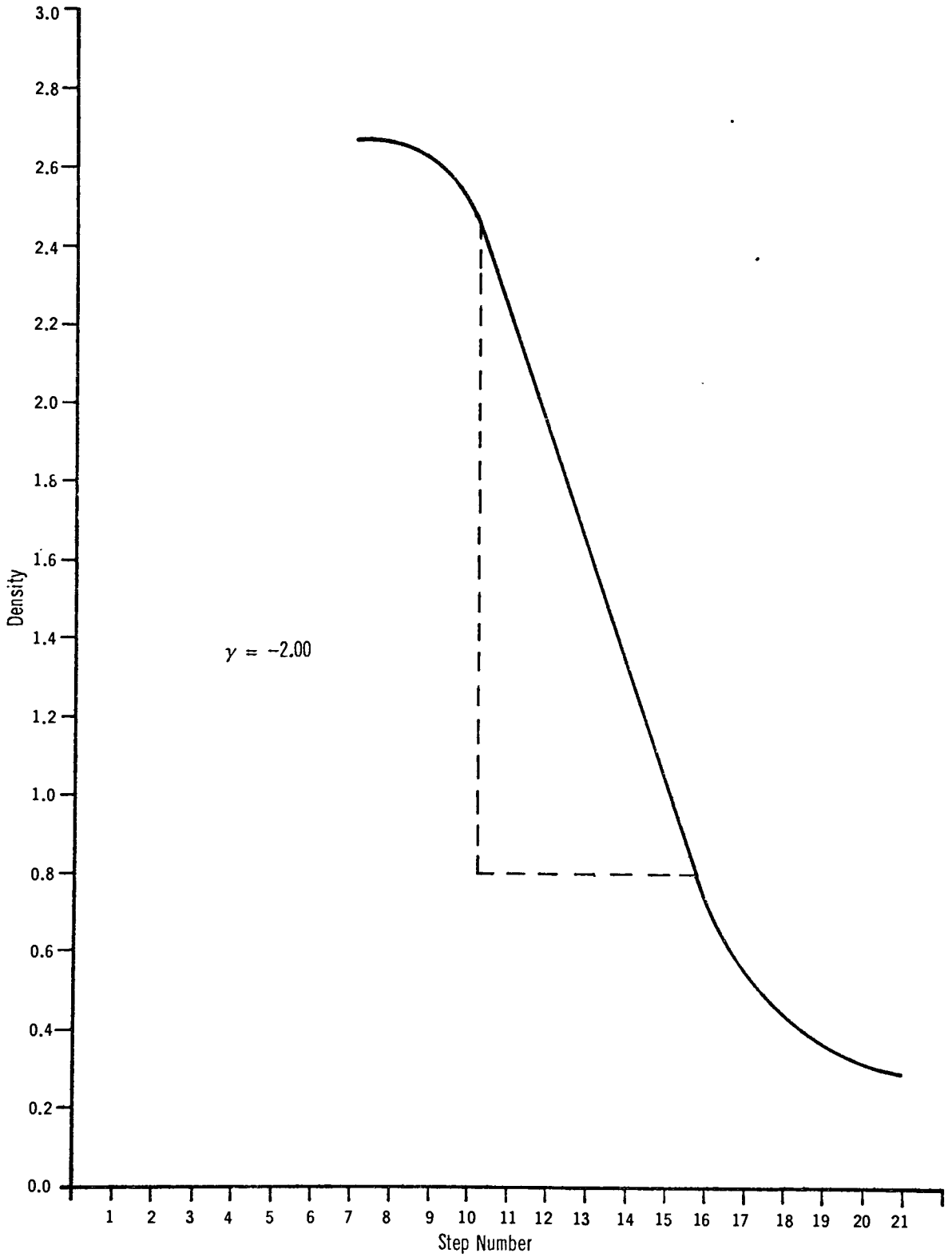

Figure 6-1. Characteristic Curve for Holographic Film

However, further consideration of these experimental sensitometric results indicated that time differences between the sensitometric exposures and the holographic exposures may significantly affect the characteristic curve of Figure 6-1. The sensitometric exposure times were 10^{-2} seconds, while the holograms were exposed, as described in detail in Chapter IX, for a period of one hour. This yields an exposure time ratio of 3.6×10^{5}, which indicates a concern for the failure of the reciprocity law[27,28] for SO-243 and this photographic process.

To clarify the effects of reciprocity, additional sensitometric experiments were performed at each of the exposure times. Neutral density filters were used in the one-hour exposures to limit the total energy transmitted by the step tablets and the Wratten filter. The result of these experiments is given by the characteristic curve shown in Figure 6-2. Note that four significant comparisons must be considered: (1) The slope of the curve has changed from $\gamma = -2$ to $\gamma = -1$, (2) the minimum density level has increased from 0.30 to 0.60, (3) the maximum density has slightly decreased from 2.68 to 2.60, and (4) the overall length of the straight-line portion of the curve has slightly decreased and its only significant change occurs in the lower density levels.

Based upon these comparisons, it was evident that the changes in the lower density levels of the characteristic curve could be considered negligible if all of the holograms were exposed in the upper linear portion of the curve. The generalized effects of the change in the slope of the curve and film nonlinearities on image quality, however, are significant and have been previously investigated for Fresnel, Fraunhofer, and in one case, Fourier transform holograms.[29-33] Because of these investigations, further experimentation into the significance of this particular slope change has been replaced by theoretical predictions based on the results of these investigations.

A review of the literature indicates a variety of approaches to the predication of nonlinear film effects on the reconstructed image. These include the utilization of the characteristic H&D curve[1,2,3,4,10,11,31] or the amplitude versus exposure curve for various film types.[29,30,32,33] In addition, many approximations have been used for these nonlinear effects such as: (1) V th law approximation,[30,32,33] (2) error function limiter[29], and (3) power series approximations.[10,31] Also, some of these approaches include other assumptions in addition to the above approximations, such as:

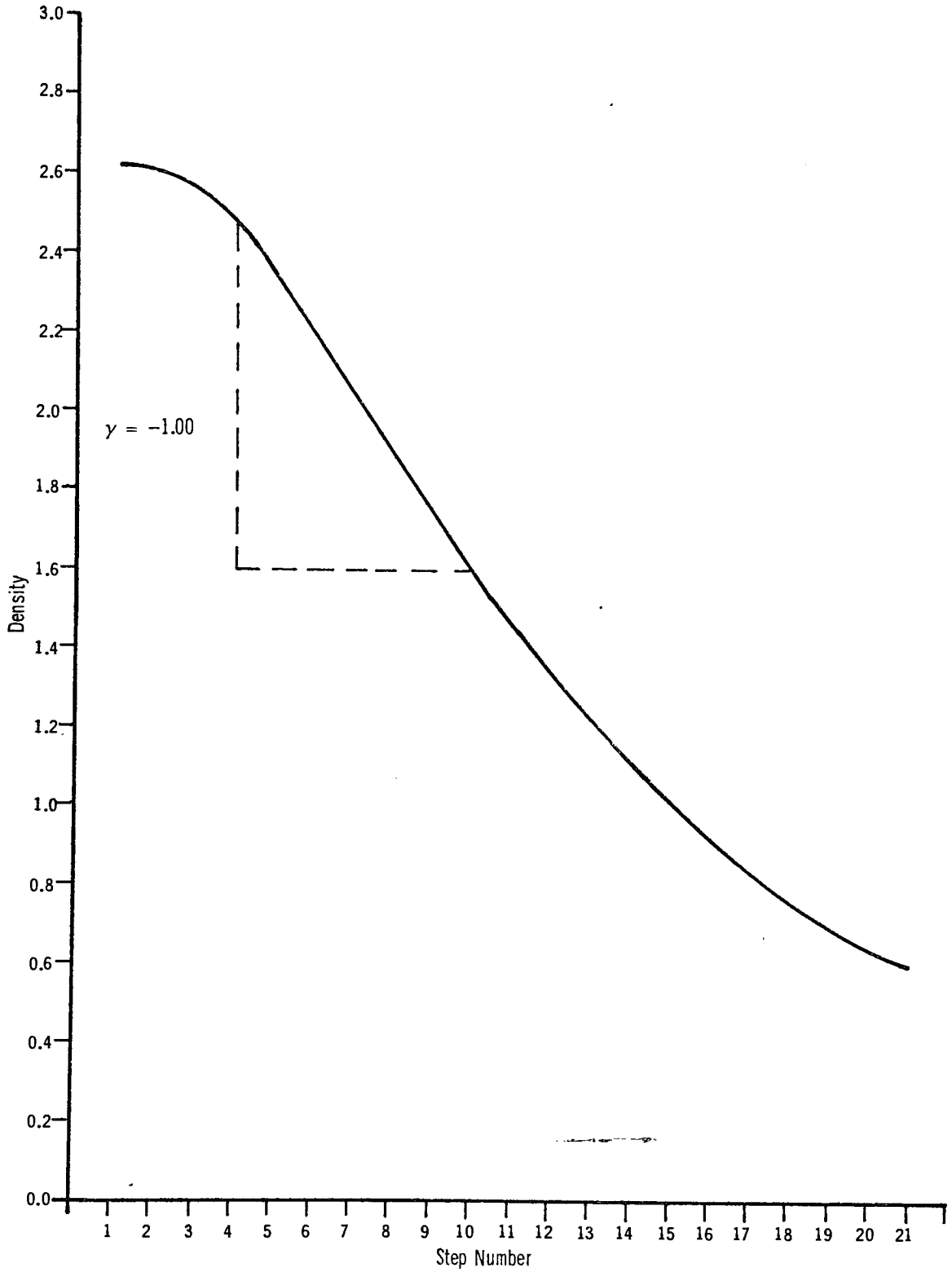

Figure 6-2. Characteristic Curve for Holographic Film

(1) Given ratios of reference beam amplitude to object amplitude,[10] (2) variations in the level of bias imposed by the reference beam, (3) variations in the definition of image quality including sharpness, brightness, contrast, and amount of flare light.[31]

Some of these assumptions and approaches become more significant than others when related to the formation and reconstruction steps of the Fourier transform holograms under investigation.

The significant factors that directly concern this investigation are: (1) The reference beam intensity is approximately equal to the object distribution intensity, (2) the variation of the slope of the characteristic curve has changed from $\gamma = -2$ to $\gamma = -1$, and (3) all holographic formation exposures were made on the linear portion of the characteristic curve.

With full consideration to the significance of these factors, the following evidence has been found in the literature indicating that the photographic sensitometry utilized in the study has eliminated further concern for nonlinear distortion occurring in the Fourier transform holographic images.

Kaspar and Lamberts[31] investigated the quality of Fourier transform holographic images in terms of the amount of light diffracted into the holographic image. In their approach, utilizing the D-log E curve, they derived an expression for the ratio of the flux diffracted into the image to that specularly transmitted; i. e., the ratio of the first-order energy to the zero-order energy. Their results showed that this ratio would produce a maximum value when the holographic exposures were made on the straight-line portion of the characteristic H&D curve. This would yield maximum fringe contrast and maximum energy in the first-order images. Thus, even though the slope of the characteristic curve has changed from its optimum value, Kaspar and Lamberts' investigation indicates that the energy within the first-order image would still remain near maximum because the holograms were made within the straight-line portion of the characteristic curve. However, it is expected that limits must be placed on the allowable slope change, to maintain a near-maximum ratio of this energy.

Information regarding these limits and further supporting evidence for this energy ratio have been given by Wyant and Givens[9]. They investigated the relationship between

the luminance of the reconstructed holographic image and the luminance of the original object for side-band Fresnel holograms. Their results showed that the luminance ratios for holograms of low fringe contrast did not change significantly for values of the slope of the characteristic curve of 5.5, 2.0, and -2.0. That is, the calculated reconstructed luminance ratios were all identical for these values of gamma and were all in very close agreement to measured values of the actual luminance ratios when the hologram exposure ratios were equal to or less than 5:1. Since low holographic fringe contrasts were obtained in this study, as indicated in Chapter X, then it is reasonable to assume that the above investigations eliminate the need for further attention to possible changes in the reconstructed image luminance values from the object luminance values due to the change in the slope of the characteristic curve to the value represented by Figure 6-2.

In addition to this evidence, however, it must be emphasized that all of the exposed holograms were processed in three separate groups. Each group consisted of processing four holograms in one tray, thus eliminating variations due to processing within the group. Thus, even if slight image variations existed due to exposure and subsequent processing of the photographic film, these variations would only be significant among the three film groups. However, as the analysis on the real images of the holograms will show (given in Chapter X), the variations that did exist among groups were not found to be significant. Therefore, it can be concluded that the experimental results presented in this investigation are not significantly different from those that would have been obtained if the slope of the characteristic H&D curve would have been at its optimum value.

6.2 RECORDING OF RECONSTRUCTED IMAGES

The final evaluations of the reconstructed images are made on photographs of these images taken in the image plane of the Fourier transform holographic system. The film type used was Eastman Kodak Tri-X which yields a black-and-white negative image. The film was processed following the directions supplied by the film manufacturer. Three sets of exposures were taken for each of the reconstructed images.

The exposures were determined from the results of an exposure series taken of one of the reconstructed images. An optimum exposure was subjectively selected and

then bracketed one exposure step in each direction to cover an optimum exposure range. Since the holographic experiments yielded 12 reconstructed images, all of the images were photographed on a single roll of Tri-X (36 exposures) to eliminate differences between the images due to film emulsion number and processing.

CHAPTER VII

TEMPORAL COHERENCE MEASUREMENTS

7.1 INTRODUCTION

As shown in Chapter III, the visibility of the fringes obtained from the interference of two beams on a Michelson interferometer is a measure of the temporal coherence of the source from which the beams were emitted.

The following sections in this chapter will describe the apparatus used for such measurements as well as list and discuss the results of such measurements.

7.2 EXPERIMENTAL ARRANGEMENT

The basic experimental arrangement for measuring the temporal coherence of a source is shown in Figure 7-1. The source consists of a high-pressure, mercury arc lamp housing with one of four interference filters* inserted in an internally collimated beam within the lamp housing. This beam is converged to obtain a 300-micron spot external to the housing. A condensing lens, focal length equal to 50 mm, collimates the beam which is then passed through a large metal aperture mounted on the Michelson interferometer. The large metal aperture limits the diameter of the beam to approximately one inch.

The Michelson interferometer, manufactured by Beck, consists of a beamsplitter and two mirrors, one stationary and one with a micrometer adjustment. The entering beam is split into two parts, reflected off each of the mirrors and then recombined to form interference fringes when the path lengths of the two beams are almost equal. The relative intensities of the fringes were measured by moving them, through movement of the variable mirror, across a detector consisting of a small pinhole, a photomultiplier tube, and a multimeter. A complete listing of all the experimental apparatus and manufacturers is given in Appendix III.

*The spectral characteristics of these filters are given in Appendix II.

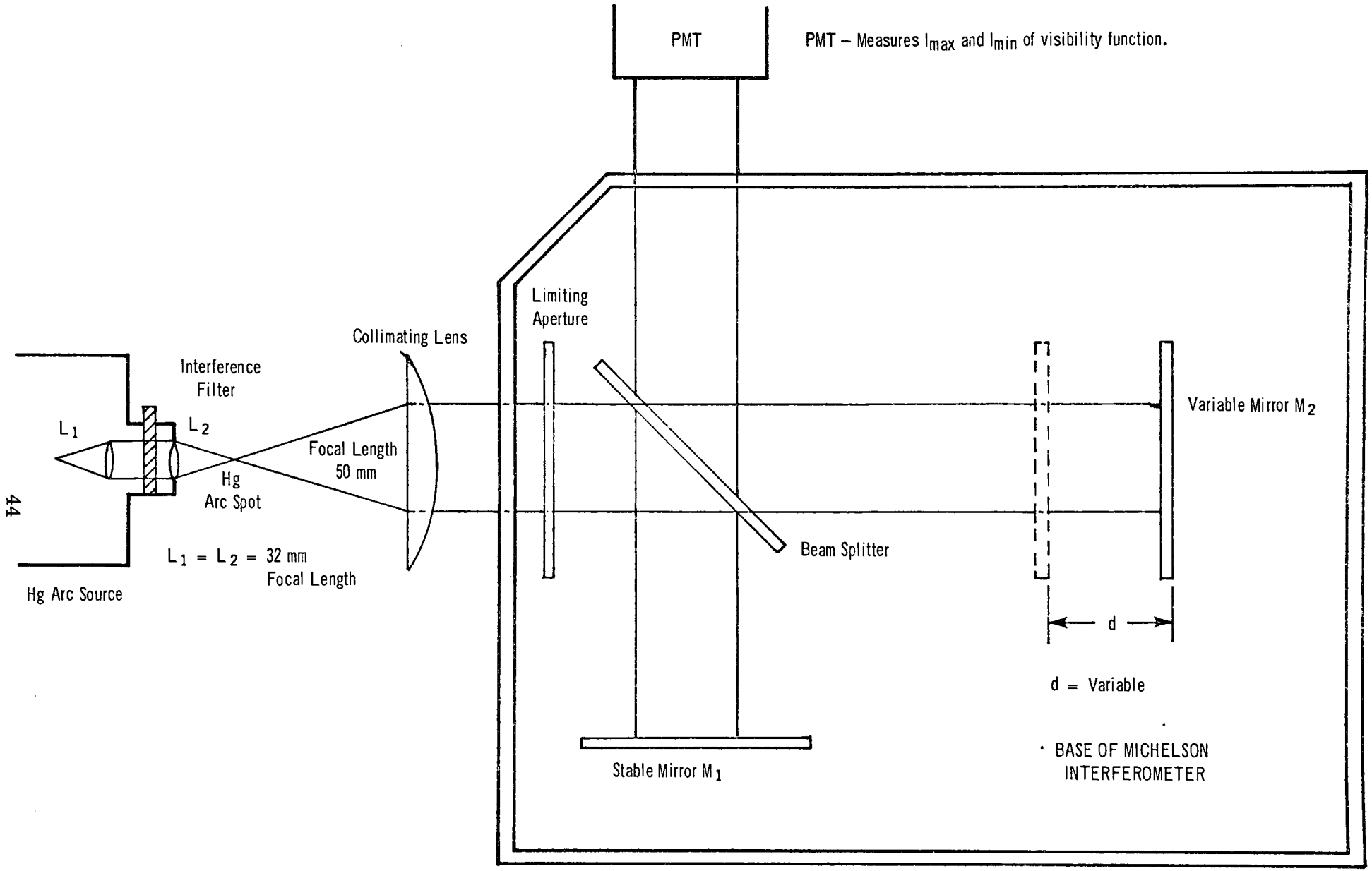

Figure 7-1. Schematic Diagram of Experimental Apparatus for Measurement of the Visibility Function of Hg Arc Source with Various Interference Filters

7.3 STATISTICAL DESIGN

The statistical design of the temporal coherence experiment is concerned with a quantitative measure of the effect of the change in the temporal coherence between each of the four source/filter combinations. The quantitative measure of most interest* in this investigation is that of the visibility of the fringes as a function of the path difference of two interfering beams emitted from the same source.

To ensure the accuracy of the visibility measurements, 10 replicates were performed for each of the four source/filter combinations. Also, to eliminate possible biasing errors, due to either judgment or a change in experimental conditions, the order of the measurements was chosen randomly as shown in Table 7-I.

TABLE 7-I. RANDOM ORDER OF VISIBILITY MEASUREMENTS

Filter Number	Replicate Number	Random Order	Filter Number	Replicate Number	Random Order
33-78-54	1	26	33-78-54	6	19
33-78-55	1	29	33-78-55	6	25
42-47-57	1	23	42-47-57	6	15
4043	1	14	4043	6	21
33-78-54	2	2	33-78-54	7	24
33-78-55	2	27	33-78-55	7	31
42-47-57	2	34	42-47-57	7	16
4043	2	1	4043	7	10
33-78-54	3	11	33-78-54	8	18
33-78-55	3	38	33-78-55	8	6
42-47-57	3	12	42-47-57	8	13
4043	3	36	4043	8	32
33-78-54	4	17	33-78-54	9	20
33-78-55	4	30	33-78-55	9	39
42-47-57	4	40	42-47-57	9	22
4043	4	37	4043	9	8
33-78-54	5	4	33-78-54	10	3
33-78-55	5	35	33-78-55	10	7
42-47-57	5	33	42-47-57	10	9
4043	5	28	4043	10	5

*The measure of the visibility as a function of path length yields information about the spectral intensity distribution of the source.[14] Thus, from the visibility function information can be obtained the spectral width of the source, the coherence time, as well as the coherence length of the source.

7.4 VISIBILITY DATA AND CALCULATIONS

The results of the visibility measurements are best described by the values given in Table 7-II. These values were obtained from the maximum and minimum intensity measurements of the fringe interference pattern for the 40 experimental runs. The values given in Table 7-II correspond to the average of the actual data as given in Appendix IV. The visibility values were calculated from the intensity values utilizing a variation of the visibility equation given in Chapter III (equation 3.505). This variation took the form

$$V = \frac{I_{max.} - I_{min.}}{I_{max.} + I_{min} - 2I_o} \qquad 7.401$$

where $I_{max.}$ = maximum intensity of respective fringe.

$I_{min.}$ = minimum intensity of respective fringe.

I_o = constant minimum background intensity.

This form of the visibility equation can be derived from the original form, equation 3.505, when consideration is given to the fact that the intensities of the individual beams in this experiment were not equal $I_1 \neq I_2$. The actual value of I_o was a constant background intensity equal to the lowest value of the minimum intensity for the zero-order fringes.

TABLE 7-II. AVERAGE VISIBILITY VALUES

Fringe Order	Filter Numbers 33-78-55	33-78-54	42-47-57	4043
0	1.0000	1.0000	1.0000	1.0000
1	0.9706	0.9754	0.9738	0.9704
5	0.8690	0.8968	0.9401	0.9364
10	0.7315	0.7927	0.8665	0.8547
15	0.6156	0.6857	0.7898	0.7819
20	0.4945	0.5810	0.7195	0.7022
25	0.3654	0.4676	0.6396	0.6263
30	0.2681	0.3844	0.5678	0.5555
35		0.3152	0.4954	0.5126
40		0.2715	0.4335	0.4590
45		0.2479	0.3819	0.4061
50		0.2184	0.3205	0.3629
55			0.2658	0.3271
60			0.2288	0.2881

From the average visibility values given in Table 7-II, a plot of visibility versus path difference, or relative fringe number, can be obtained as shown in Figure 7-2. From this figure it is obvious that each filter has its own respective visibility function; however, further analysis of the significance of this point will be delayed until Chapter X. For now it should suffice to state that each of the individual visibility values was found to be within 2.40 standard deviations of the average visibility values as plotted in Figure 7-2. Also, 76% of the individual values were within 2.00 standard deviations of the average values. Each of the standard deviation calculations assumed a 95% confidence level.[28]

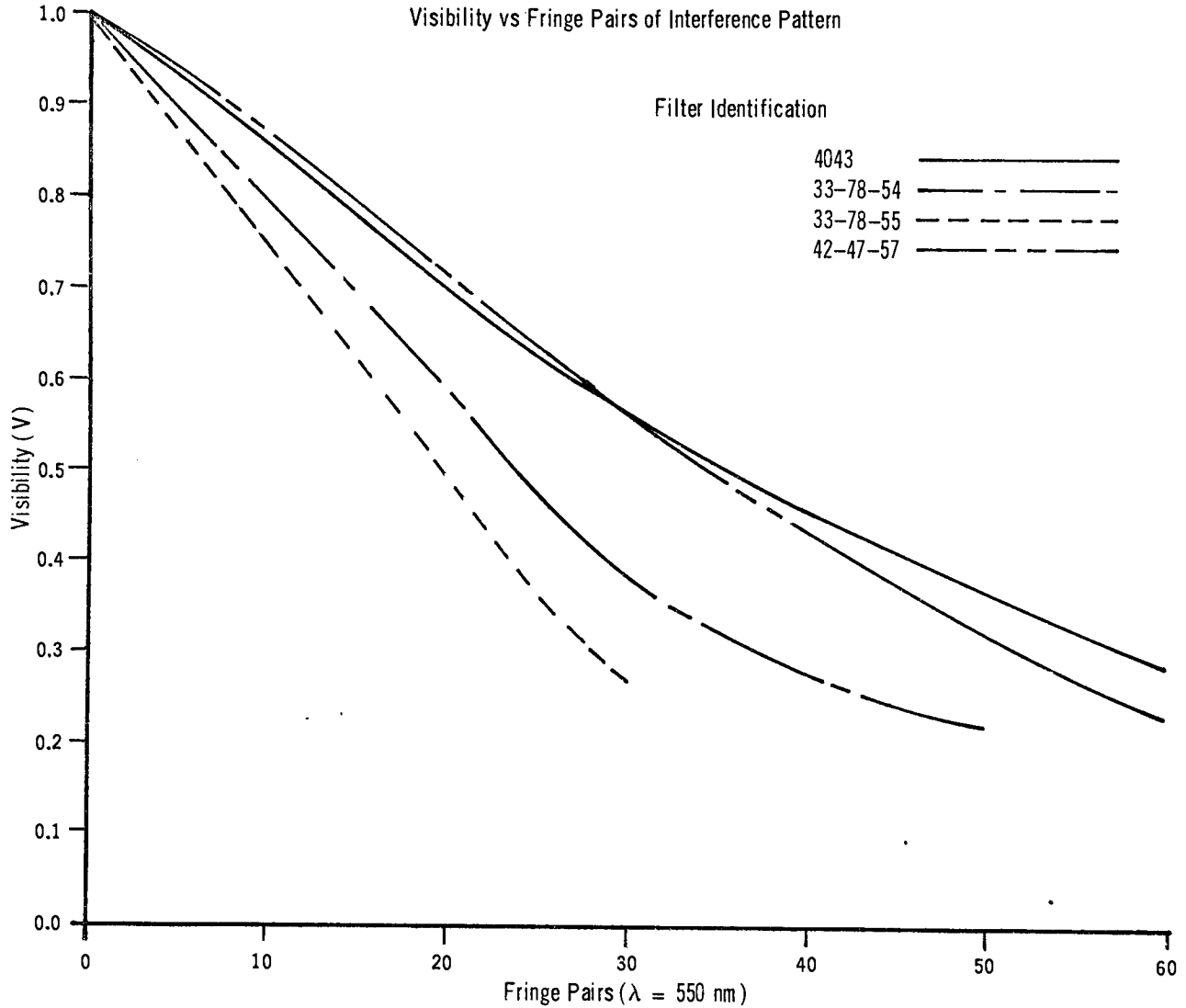

Figure 7-2. Temporal Coherence Measurements

CHAPTER VIII

FOURIER TRANSFORM HOLOGRAPHIC SYSTEM DESIGN

8.1 INTRODUCTION

The purpose of this chapter is to describe briefly the apparatus used for the formation and reconstruction steps of the point reference method of Fourier transform holography. In addition, a comparison will be made between experimental and theoretical system resolution.

8.2 FORMATION STEP

The experimental arrangement used for the formation of Fourier transform holograms is shown in Figure 8-1. A mercury arc lamp and a 100-micron pinhole are the main constituents of the partically coherent source.

From the source, a spherical wave is emitted which is partially coherent and of mean wavelength of 546 nanometers. The wave is collimated by a 1-meter focal length achromatic lens and passed through a limiting aperture which reduces the diameter of the beam to approximately 2 centimeters. This beam is then transmitted through the object plane, which consists of the target shown in Figure 8-2.

The target is positioned perpendicularly to the collimated beam and within the previously calculated 1.88-millimeter diameter of the spatially coherent beam.

The optical disturbance transmitted by the target is focused on the holographic recording film by a 25.4-centimeter focal length lens. The photographic film is held perpendicular to the reference axis by a vacuum back built to meet the specifications of the optical bench and the experimental design. The optical disturbance recorded by the hologram is the interference of the far-field diffraction patterns from the point reference source and the rectangular object.

8.3 RECONSTRUCTION STEP

The reconstruction step, as shown in Figure 8-3, consists of the same basic apparatus used in the formation step. There are, however, two major differences. First, the hologram or photographic film has been developed utilizing the process given

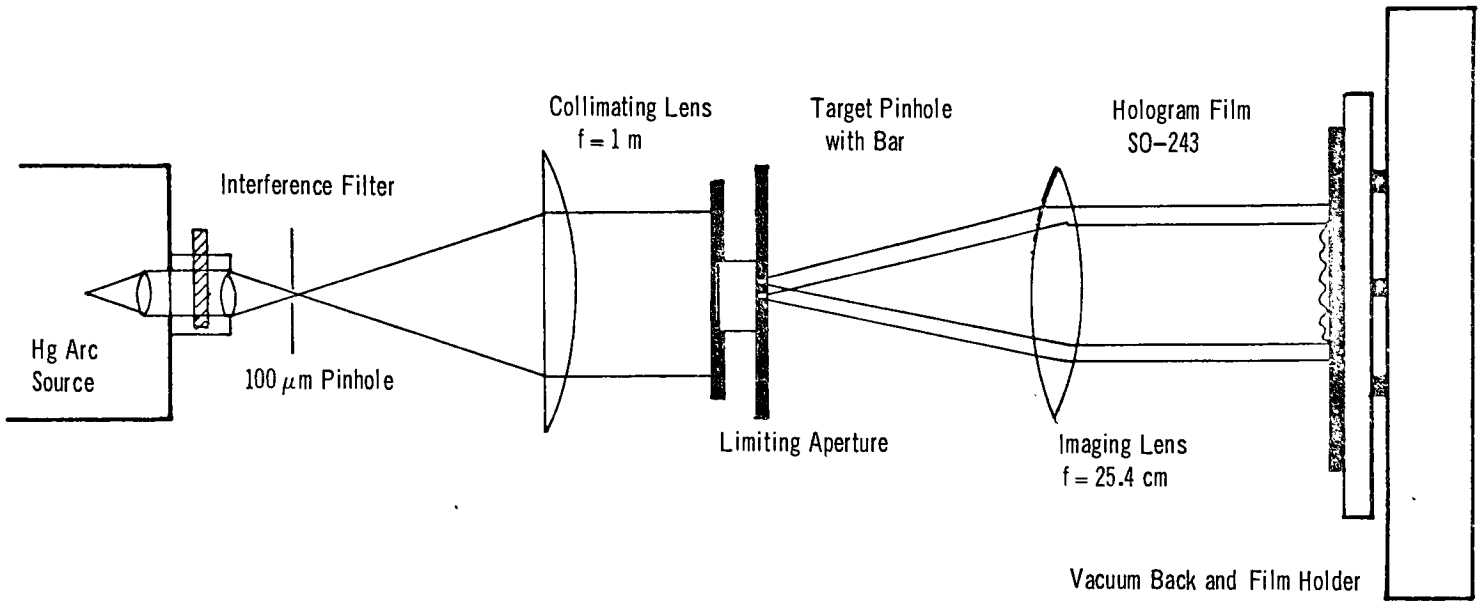

Figure 8-1. Schematic Diagram of Experimental Apparatus for Formation of Fourier Transform Hologram

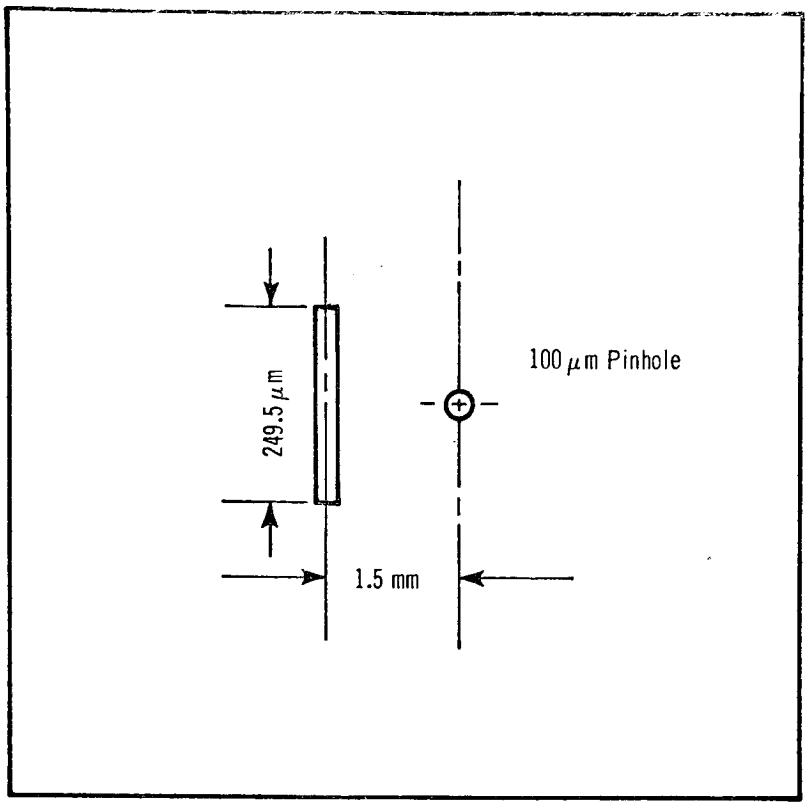

Figure 8-2. Diagram of Object Target

in Appendix I and placed in the object plane. Second, the vacuum back has been removed from the hologram plane and replaced with a Pentax 35-millimeter camera body to record the real images of the reconstruction on 35-millimeter Tri-X film. From this information, the reconstructions were evaluated as described in Chapter X.

8.4 EVALUATION OF EXPERIMENTAL CONDITIONS

Before performing the actual exposures of the Fourier transform holograms, an experimental test was made to evaluate the entire system. The purpose of this test was to verify that the proper assumptions were made in selecting the experimental apparatus.

For this test, a Fourier transform hologram was created using the apparatus shown in Figure 8-1. However, the target as given in Figure 8-2 was altered to obtain that shown in Figure 8-4.

The purpose of using this target was to satisfy some of the practical considerations. First, a target of two pinholes was the easiest to produce. Second, the expected interference pattern of two pinholes was easily determined and tested experimentally.

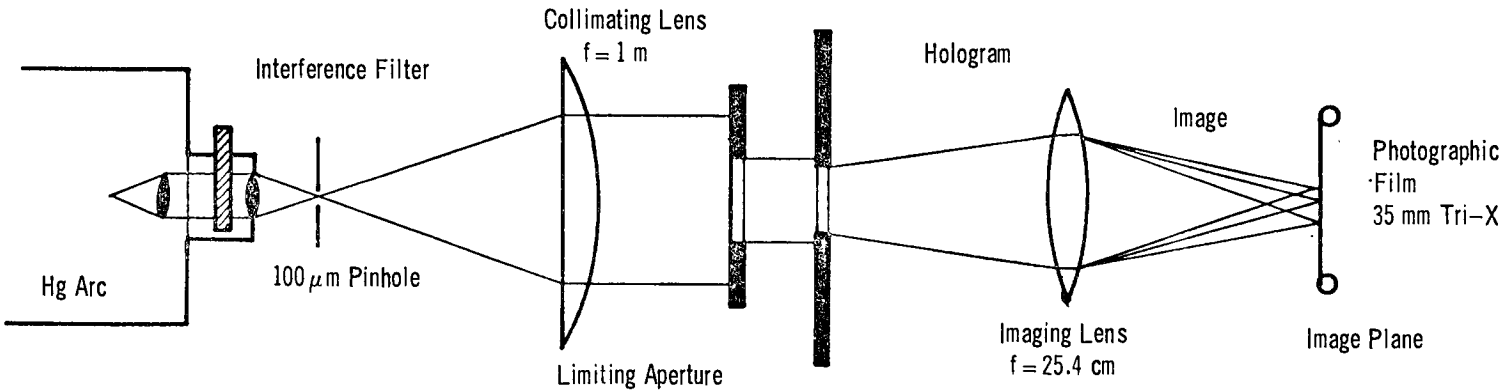

Figure 8-3. Schematic Diagram of Experimental Apparatus for Reconstruction of Fourier Transform Holograms

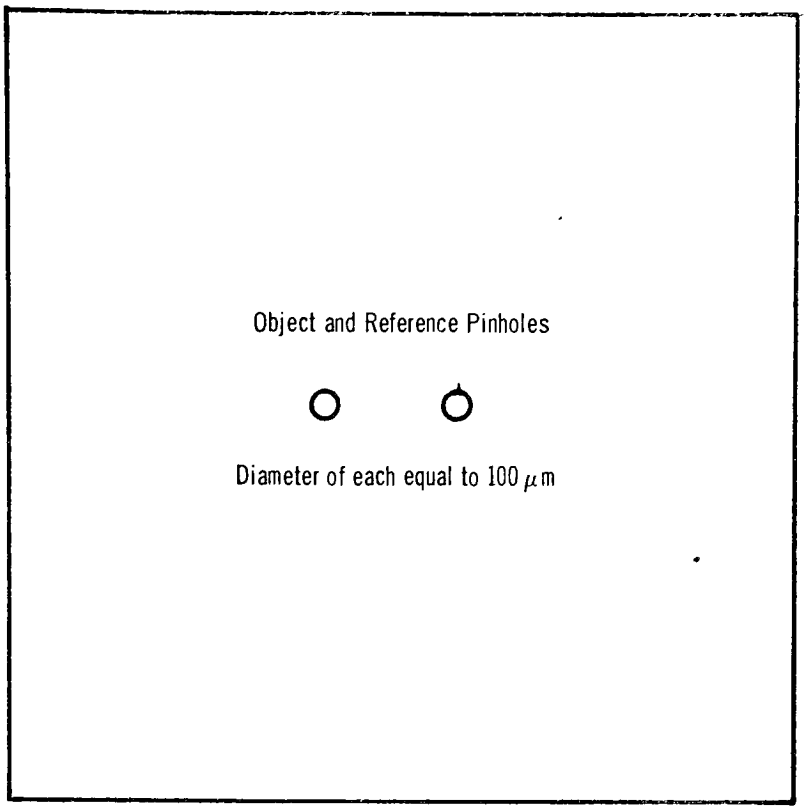

Figure 8-4. Pinhole Test Target

Utilizing this target, eight holographic exposures were attempted, covering a range of exposure times from one to eight minutes with all exposures replicated twice. After development, again using the process outlined in Appendix II, the holograms were examined under a Bausch & Lomb microscope and the following conclusions were reached.

First, due to the low energy of the transmitted partially coherent beams, the only observable fringe patterns occurred on the four- and eight-minute exposures. Also, these patterns were of low contrast in the high-frequency lobes so that future exposures would have to be made at longer exposure times.

Secondly, the interference pattern contained a main interference pattern and a few side lobes consisting of the higher frequency information. As expected, the interference pattern was identical to two interfering Bessel functions.

Lastly, geometrical measurements made on the fringe spacing of the interference pattern of the developed hologram yielded a spatial frequency of 20 lines/mm, which is within the range of the previously predicted 13.5 lines/mm.

Following this, the holograms were reconstructed utilizing the apparatus shown in Figure 8-3 and photographs of the two real images were made as shown by the sample given in Figure 8-4. Upon examination of these photographs, a large d-c spot was found to occur in the center and two real images of the object pinhole appeared around it as conjugates. As predicted in Chapter II, the reconstructed image is that of the original object target.

CHAPTER IX

FOURIER TRANSFORM HOLOGRAPHIC EXPERIMENTS

9.1 INTRODUCTION

It is the purpose of this chapter to describe in detail the procedures followed in both the formation and reconstruction steps of the Fourier transform holographic experiments. The discussion will include a table of random order for the exposures, the environmental conditions surrounding the experimental procedures, and the optimum exposure values used for each of the two steps.

9.2 FORMATION OF FOURIER TRANSFORM HOLOGRAMS

Before proceeding with the formation of the experimental holograms, consideration was given to the following requirements. First, the actual exposure times had to be decided upon, and second, the order of the exposures had to be selected.

The actual exposure times were determined from an exposure series in which holograms were formed at exposure times of 8, 16, 32, and 64 minutes. Subjective evaluation of the reconstructions then set the optimum exposure time at 60 minutes. Although this is a relatively long exposure, it must be remembered that the 100-micrometer pinhole considerably limits the amount of energy passed on to the hologram plane from the mercury arc source and filter combination.

The order of the formation exposures was set up in a random table as shown in Table 9-I. The randomness of the exposure order reduces any systematic effect that uncontrolled factors might contribute to the results. However, note that the randomness is limited within each of the three groups. Thus, the experiment is arranged to block against the variable factor of time and uncontrolled factors that are functions of time.

The purpose in arranging the experimental order to allow for these blocks is primarily due to the fact that variables like absolute temperature, air circulation, and room vibration are rather expensive to control. Thus, the random order within groups was set up to help eliminate their combined effects rather than attempt to set up an

TABLE 9-I. RANDOM ORDER FOR FORMATION OF FOURIER TRANSFORM HOLOGRAMS

Filter Number	Replicate Number	Random Order
4043	1	4
33-78-54	1	3
33-78-55	1	1
42-47-57	1	2
4043	2	2
33-78-54	2	4
33-78-55	2	1
42-47-57	2	3
4043	3	1
33-78-54	3	2
33-78-55	3	3
42-47-57	3	4

experimental environment that would control all of these factors. If unidentified trends or unexplainable results are obtained within groups, the assumption may then be made that the environmental conditions must be given more consideration and that possibly the experimental apparatus might necessitate revision.

Initially, however, every precaution was taken to eliminate these uncontrolled factors as shown by the following.

1. All exposures were performed between the hours of 6 p. m. and 6 a. m. to minimize the effects of:
   a. Building vibration due to occupancy and mechanical equipment.
   b. Air turbulance due to necessary daytime air-conditioning system.
   c. Unexpected interference due to academic or maintenance activity.
2. Special apparatus was used to isolate the optical bench from external sources of vibration.

With these considerations in mind, the Fourier transform holograms were formed. The photographed diffraction patterns were then processed according to the instructions given in Appendix II. The development step in the processing procedure was

used to develop four holograms simultaneously or each group of holograms independently.

9.3 RECONSTRUCTION OF FOURIER TRANSFORM HOLOGRAMS

The apparatus used in the reconstruction step is the same as that shown in Figure 8-3. The individual holograms were placed in the object plane and illuminated with the partially coherent collimated beam. The reconstructions were then photographed using a Pentax camera back and an independently mounted shutter to control the shutter times. The 12 holographic reconstructions were each photographed at three exposure levels to ensure an optimum image. The three exposure levels were selected to bracket a previously determined optimum exposure time of 10 seconds for one of the holograms.

In the photographed reconstructions, the exposure order was selected to change within groups. Thus, in all of the following analysis the main emphasis will be placed on within-group changes rather than between-group changes.

CHAPTER X

ANALYSIS OF RECONSTRUCTED HOLOGRAMS

10.1 INTRODUCTION

This chapter will focus on the relationships that exist between the four source/filter combinations and the results of the reconstructed holograms. In doing this, it is assumed that any significant changes that occur between the reconstructed holograms must be primarily due to two factors: Differences in the general exposure level and differences in the level of temporal coherence of the source/filter combinations. As emphasized throughout this research endeavor, every precaution was taken to assure that the effects of all other factors were negligible.

The significance of the effects of both the exposure level and the temporal coherence level was investigated in reference to the holograms themselves, as well as in reference to the reconstructed real images. Briefly, the investigations were made in the following areas:

1. Significance of the visibility measurements of the source/filter combinations.
2. Source/filter and group effects on the density level and contrast of the holographic fringe patterns.
3. Source/filter and group effects on the density level of the reconstructed real images.
4. Source/filter and group effects on the shapes of the reconstructed bar images.

In each of these steps, consideration was given to differences caused by changes in both the exposure level and temporal coherence level of each of the source/filter combinations.

10.2 ANALYSIS OF VISIBILITY MEASUREMENTS

The visibility data, as discussed in Chapter VII, consisted of 10 replicates of each of four source/filter combinations as measured on a Michelson interferometer arrangement. The average visibility values of each of the 10 replicates were calcu-

lated and are given in Table 7-II. A plot of these average values against the relative fringe number is given in Figure 7-2.

Upon initial investigation of Figure 7-2, it appears that the only change taking place between source/filter combinations is the visibility value. This, however, is not entirely true. Referring to Appendix IV, it becomes evident that the visibility measurements were performed at two different levels of energy, as indicated by the control values of the photomultiplier tube monitoring device.

The higher level of energy was transmitted by source/filter combination numbers 4043 and 42-47-57. In this case, the meter multiplier setting was 0.03, while the sensitivity was set at 40. For the lower energy level, transmitted by source/filter combinations 33-78-54 and 33-78-55, the meter multiplier setting was at 0.01, while the sensitivity was set at a value of 20. Further information regarding the experimental equipment is given in Appendix III.

From the previous information, it is evident that actual comparisons of the visibility values (and thus the coherence values) can only be made between the source/filter combinations within each set. This will be further emphasized later in this chapter when the density values of the holograms are analyzed. For now it is sufficient to analyze the visibility data in hopes of attaining a measure of the difference between the various visibility functions.

The visibility measure can be accomplished utilizing a statistical test based on the least significant difference (to be referred to as the LSD test) of the individual curves.[34,35] The LSD test determines the difference between two means required to conclude that the means originate from two entirely different populations.

The value of the LSD test is given by:

$$LSD = t_{\nu,\alpha/2}\sqrt{\frac{2S_e^2}{N}} \qquad 10.201$$

where α = 0.05 = the risk of stating that a difference in the means exists when, in fact, it does not.

ν = 9 = number of degrees of freedom (associated with the number of replications).

t = the value of the "Student's t" distribution as given in Table A. 2 of Reference 28.

N = the total number of observations.

S_e^2 = the mean square for error term.

The results of the calculations based on the LSD test are given in Tables 10-I. through 10-IV. The values of most importance in each of the tables are found in the last two columns. The LSD value found in the fifth column represents a confidence limit placed on each of the average visibility values. The values given in the sixth column represent the differences between the visibility pairs at each of the two energy levels. In order to state that the average visibility values of each of the visibility curves originate from different populations, it is necessary that the differences between the average values exceed the LSD values. As given in the tables, the visibility curve for each of the pairs yields a different result.

The visibility curves from source/filter combinations 4043 and 42-47-57 appear approximately the same for the first 30 fringe pairs. Then an increasingly significant difference occurs for the last 30 fringe pairs. However, the visibility curves for source/filter combinations 33-78-54 and 33-78-55 are significantly different for all recorded fringe pairs. Thus, it is possible to conclude that each source/filter combination has a different visibility curve and that this difference can be stated in quantitative terms.

In addition, it is also possible to conclude that each source/filter combination has its own independent value of temporal coherence. Since the source size is unchanged, the spatial coherence of each source/filter combination must be constant. Therefore, the changes in the visibility curves must be due to changes in the temporal coherence between sources. This fact was proven in Chapter III and can be quantitatively represented by changes in the coherence lengths of the various source/filter combinations.

Referring to equation 3. 702 and relating the number of fringe pairs to the respective path differences for the visibility curves, it is found that the coherence length can be expressed as

$$\Delta L = \text{Path Difference} = n\bar{\lambda}_o \qquad 10.202$$

where n = number of fringe pairs.

TABLE 10-I. LSD TEST RESULTS: FILTER NO. 4043

Fringe Order	Average Visibility	Std. Dev. S	Variance S^2	LSD	$V_{avg\ 4043} - V_{avg\ 42\text{-}47\text{-}57}$
0	1.0000				
1	0.9704	0.0103	0.0001	0.0032	-0.0034
5	0.9364	0.0192	0.0003	0.0061	-0.0037
10	0.8547	0.0243	0.0005	0.0077	-0.0118
15	0.7819	0.0257	0.0006	0.0082	-0.0079
20	0.7022	0.0266	0.0007	0.0085	-0.0173
25	0.6263	0.0212	0.0004	0.0067	-0.0133
30	0.5555	0.0268	0.0007	0.0085	-0.0123
35	0.5126	0.0215	0.0004	0.0068	+0.0172
40	0.4590	0.0207	0.0004	0.0066	+0.0255
45	0.4061	0.0252	0.0006	0.0080	+0.0242
50	0.3629	0.0214	0.0004	0.0068	+0.0424
55	0.3271	0.0259	0.0006	0.0082	+0.0613
60	0.2881	0.0268	0.0007	0.0085	+0.0615

SAMPLE CALCULATIONS:

$$LSD = t_{\nu,\alpha/2}\sqrt{\frac{2\,S_e^2}{N}}$$

$$S_e^2 = \left(\frac{S}{\sqrt{N}}\right)^2 = \frac{S^2}{N}$$

$$t_{9,0.05/2} = 2.2622$$

$$\therefore LSD = t_{\nu,\alpha/2}\sqrt{\frac{2\,S^2}{N^2}} = t_{\nu,\alpha/2}\sqrt{2}\,\frac{S}{N}$$

$$= \frac{2.2622(1.414)}{10}\,S = \underline{0.3198 \cdot S}$$

TABLE 10-II. LSD TEST RESULTS: FILTER NO. 42-47-57

Fringe Number	Average Visibility	Std. Dev. S	Variance S^2	LSD	$V_{avg\ 42-47-57} - V_{avg\ 4043}$
0	1.0000				
1	0.9738	0.0095		0.0030	+0.0034
5	0.9401	0.0198	0.0003	0.0063	+0.0037
10	0.8665	0.0313	0.0009	0.0100	+0.0118
15	0.7898	0.0224	0.0005	0.0071	+0.0079
20	0.7195	0.0302	0.0009	0.0096	+0.0173
25	0.6396	0.0259	0.0006	0.0082	+0.0133
30	0.5678	0.0205	0.0004	0.0065	+0.0123
35	0.4954	0.0175	0.0003	0.0055	-0.0172
40	0.4335	0.0223	0.0004	0.0071	-0.0255
45	0.3819	0.0188	0.0003	0.0060	-0.0242
50	0.3205	0.0269	0.0007	0.0086	-0.0424
55	0.2658	0.0253	0.0006	0.0080	-0.0613
60	0.2266	0.0270	0.0007	0.0086	-0.0615

TABLE 10-III. LSD TEST RESULTS: FILTER NO. 33-78-54

Fringe Number	Average Visibility	Std. Dev. S	Variance S^2	LSD	$V_{avg\ 33-78-54} - V_{avg\ 33-78-55}$
0	1.0000				
1	0.9754	0.0087		0.0027	+0.0048
5	0.8968	0.0341	0.0011	0.0109	+0.0278
10	0.7927	0.0244	0.0005	0.0078	+0.0612
15	0.6857	0.0244	0.0005	0.0078	+0.0701
20	0.5810	0.0340	0.0011	0.0109	+0.0865
25	0.4676	0.0297	0.0008	0.0094	+0.1022
30	0.3844	0.0216	0.0004	0.0069	+0.1163
35	0.3152	0.0218	0.0004	0.0069	
40	0.2715	0.0127	0.0001	0.0040	
45	0.2479	0.0212	0.0004	0.0067	
50	0.2184	0.0203	0.0004	0.0064	

TABLE 10-IV. LSD TEST RESULTS: FILTER NO. 33-78-55

Fringe Number	Average Visibility	Std. Dev. S	Variance S^2	LSD	$V_{avg\ 33-78-55} - V_{avg\ 33-78-54}$
0	1.0000				
1	0.9706	0.0128	0.0001	0.0040	-0.0048
5	0.8698	0.0542	0.0029	0.0173	-0.0278
10	0.7315	0.0432	0.0018	0.0138	-0.0612
15	0.6156	0.0520	0.0027	0.0166	-0.0701
20	0.4945	0.0630	0.0039	0.0201	-0.0865
25	0.3654	0.0647	0.0041	0.0206	-0.1022
30	0.2681	0.0474	0.0022	0.0157	-0.1163

From this expression, the coherence lengths of the various source/filter combinations were calculated and are represented in Table 10-V. Since each of the visibility curves has its own respective minimum value of visibility, a value of 0.3 was selected as a basis for determining the number of fringe pairs for equation 10.202. This minimum value approached the true minimum for each of the source/filter combinations.

TABLE 10-V. COHERENCE LENGTHS OF SOURCE/FILTER COMBINATIONS

Exposure Level	Source/ Filter	No. of Fringe Pairs	Coherence Lengths
1	4043	58	31.90 μm
1	42-47-57	52	28.60 μm
2	33-78-54	37	20.35 μm
2	33-78-55	28	15.40 μm

In addition to the coherence lengths obtained directly from the fringe measurements, information can also be obtained regarding the spectral intensity distribution of the four source/filter combinations.[14]

First, assume that the intensities of the two interfering beams are equal. Second, assume an optical path difference of $\Delta\mathcal{L}$, which yields a phase difference

$$\delta(k_o, \Delta\mathcal{L}) = k_o \cdot \Delta\mathcal{L} \qquad 10.203$$

where $k_o = 2\pi/\lambda$ is the wave number. Superimposing the individual intensities, the intensity pattern of the components in the wave number range, dk_o becomes

$$i(k_o, \Delta\mathcal{L})dk_o = 2 i_1(k_o)\left\{1 + \cos(k_o \cdot \Delta\mathcal{L})\right\}dk_o$$

where $i_1(k_o)$ is the spectral distribution of either beam. Adding these components, the total intensity of the interference pattern is obtained.

$$I(\Delta\mathcal{L}) = 2\int i_1(k_o)\left\{1 + \cos(k_o \cdot \Delta\mathcal{L})\right\} dk_o \qquad 10.204$$

For a nearly monochromatic source, $i_1(k_o)$ will not exist except over a small range, k_o, about some mean wave number $\bar{k}_o$. Changing the variables, we define

$$\chi = k_o - \bar{k}_o \qquad 10.205$$

and

$$j(\chi) = i(\bar{k}_o + \chi) \qquad 10.206$$

and rewrite the total intensity of the interference pattern as:

$$I(\Delta\zeta) = 2\int j(x)\left\{1 + Cos\left[(\bar{k}_o + x)\cdot\Delta\zeta\right]\right\}dx \qquad 10.207$$

which, through expansion and using the cosine of the sum of two angles, becomes

$$I(\Delta\zeta) = 2\int j(x)\left\{1 + Cos(\bar{k}_o\cdot\Delta\zeta)\cdot Cos(x\cdot\Delta\zeta) - Sin(\bar{k}_o\cdot\Delta\zeta)\cdot Sin(x\cdot\Delta\zeta)\right\}dx \qquad 10.208$$

or

$$I(\Delta\zeta) = P + C(\Delta\zeta)\cdot Cos(\bar{k}_o\cdot\Delta\zeta) - S(\Delta\zeta)\cdot Sin(\bar{k}_o\cdot\Delta\zeta) \qquad 10.209$$

where

$$P = 2\int j(x)\,dx \qquad 10.210$$

$$C(\Delta\zeta) = 2\int j(x)\cdot Cos(x\cdot\Delta\zeta)\,dx \qquad 10.211$$

$$S(\Delta\zeta) = 2\int j(x)\cdot Sin(x\cdot\Delta\zeta)\,dx \qquad 10.212$$

In the particular case of the visibility measurements undertaken in this investigation, the intensity pattern was found to be symmetrical so that $S = 0$. Therefore, the total intensity pattern can be expressed as:

$$I(\Delta\zeta) = P + C(\Delta\zeta)\cdot Cos(\bar{k}_o\cdot\Delta\zeta) \qquad 10.213$$

which is equivalent to an intensity distribution similar to that shown in Figure 10-1.

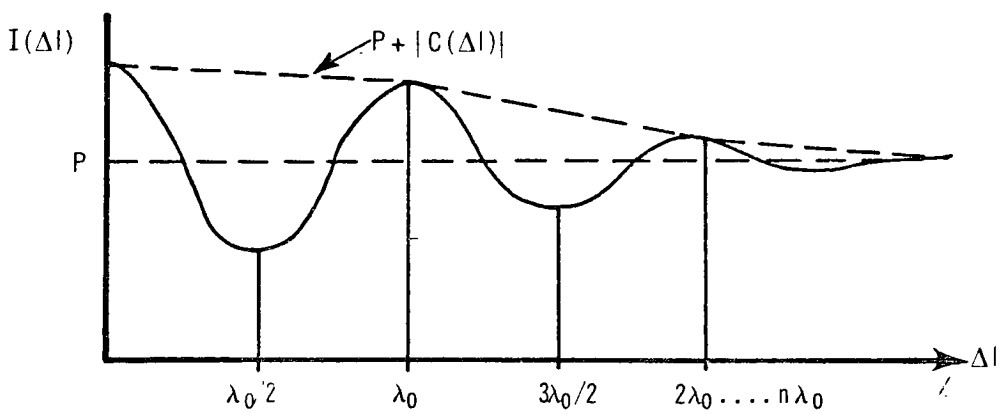

Figure 10-1. Intensity Distribution

The two extreme values of $I(\Delta\zeta)$ being given as

$$I_{max.} = P + C(n\lambda_o)\cdot\cos(\bar{k}_o\cdot n\lambda_o) \qquad 10.214$$

and

$$I_{min} = P + C[(n+1/2)\lambda_o]\cdot\cos[\bar{k}_o(n+1/2)\lambda_o] \qquad 10.215$$

leading to a visibility, as defined in equation 3.503, given by

$$V_n = \frac{C(n\lambda_o)\cdot\cos(\bar{k}_o\cdot n\lambda_o) - C[(n+1/2)\lambda_o]\cdot\cos[\bar{k}_o(n+1/2)\lambda_o]}{2P + C(n\lambda_o)\cdot\cos(\bar{k}_o\cdot n\lambda_o) + C[(n+1/2)\lambda_o]\cdot\cos[\bar{k}_o(n+1/2)\lambda_o]} \qquad 10.216$$

Since for nearly monochromatic light, $\times \ll k_o$, the variation of $C(\Delta\zeta)$ is negligible compared to that of the $\cos(k_o\cdot\Delta\zeta)$, and the visibility can be approximated by

$$V_n \approx \frac{C(n\lambda_o)}{P} \qquad 10.217$$

From equations 10.211 and 10.217, we obtain

$$\beta\cdot V_n = \int_{-\Delta k}^{\Delta k} j(X)\cdot\cos(n\lambda_o\cdot X)\,dX \qquad 10.218$$

where $\beta = P/2$ is a constant.

From Fourier theory, we can define a Fourier transform pair

$$V(\zeta) = \int_{-\infty}^{\infty} j(X)\cdot\cos(\zeta\cdot X)\,dX \qquad 10.219$$

and

$$j(X) = \int_{-\infty}^{\infty} V(\zeta)\cdot\cos(\zeta\cdot X)\,d\zeta \qquad 10.220$$

which, in terms of equations 10.218 and 10.220, become

$$j(X) = \int_{-\Delta k}^{\Delta k} \beta\cdot V(n\lambda_o)\cdot\cos(n\lambda_o\cdot X)\,d\zeta \qquad 10.221$$

or, in terms of the series expansion, become

$$j(X) = \beta\left[V(0) + 2\sum_{n=1}^{N} V(n\lambda_o)\cdot\cos(n\lambda_o\cdot X)\right] \qquad 10.222$$

for the period of $X = 2\pi/\lambda_o$.

In this particular investigation, the functions $V(\Delta\lambda)$ and $J^{\circ}(X)$ can be graphically represented as shown in Figures 10-2 and 10-3.

Rewriting equation 10.222 to account for the increments in the spectral intensity distribution, we obtain

$$J^{\circ}\left(\frac{m}{B}\cdot X\right) = \beta\left[V(0) + 2\sum_{n=1}^{N} V(5n\lambda_o)\cdot \mathrm{Cos}\left(5n\lambda_o\cdot\frac{m}{B}\cdot X\right)\right] \qquad 10.223$$

Since the experimental visibility values were normalized, the value of $V(0)$ is equal to unity and the value of β can be neglected. Thus, equation 10.223 becomes

$$J^{\circ}\left(\frac{m}{B}\cdot X\right) = 1 + 2\sum_{n=1}^{N} V(5n\lambda_o)\cdot \mathrm{Cos}\left[5n\lambda_o\left(\frac{m}{B}\cdot X\right)\right] \qquad 10.224$$

The increments of the visibility values were defined by the experimental data as $5n\lambda_o$. The increments of the spectral intensity distribution, which were not clearly defined, were selected as $2m\pi/250(5\lambda_o)$ where $B = 250$ and $m = 1, 2, 3, 4 \cdots\cdots 249$.

Thus, equation 10.224 becomes

$$J^{\circ}\left(\frac{m}{250}\cdot\frac{2\pi}{5\lambda_o}\right) = 1 + 2\sum_{n=1}^{N} V(5n\lambda_o)\cdot \mathrm{Cos}\left[2\pi\cdot\frac{mn}{250}\right] \qquad 10.225$$

The solution of equation 10.225 yields the normalized spectral intensity distribution values plotted in Figures 10-4 through 10-7. As shown, the half-power spectral widths, Δk, are given as a function of mean wavelength, $\overline{\lambda_o}$, and Table 10-VI lists these widths for each of the respective source/filter combinations.

TABLE 10-VI. SPECTRAL WIDTHS OF SOURCE/FILTER COMBINATIONS

Exposure Level	Source/Filter Number	Spectral Width $(\mu m)^{-1}$
1	4043	0.4513
1	42-47-57	0.5005
2	33-78-54	0.5824
2	33-78-55	0.7644

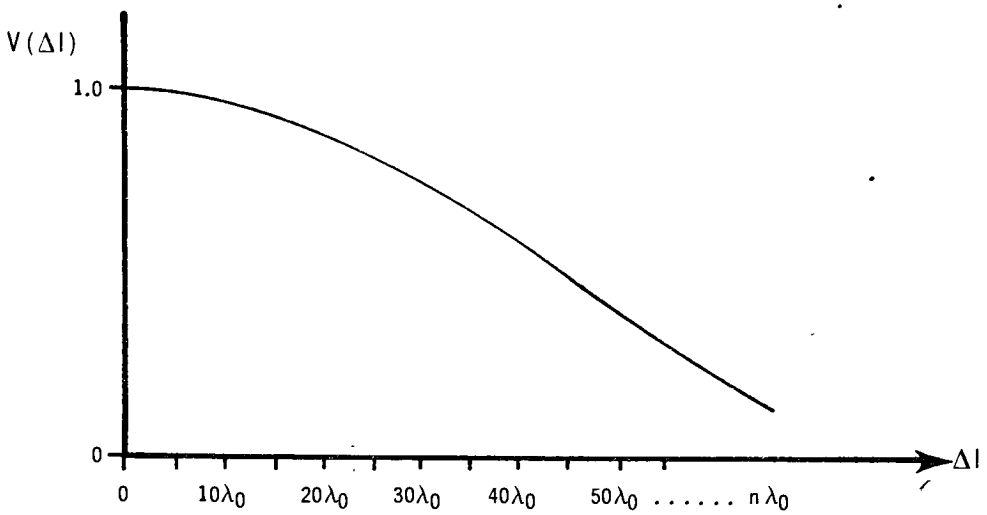

Figure 10-2. Generalized Visibility Function

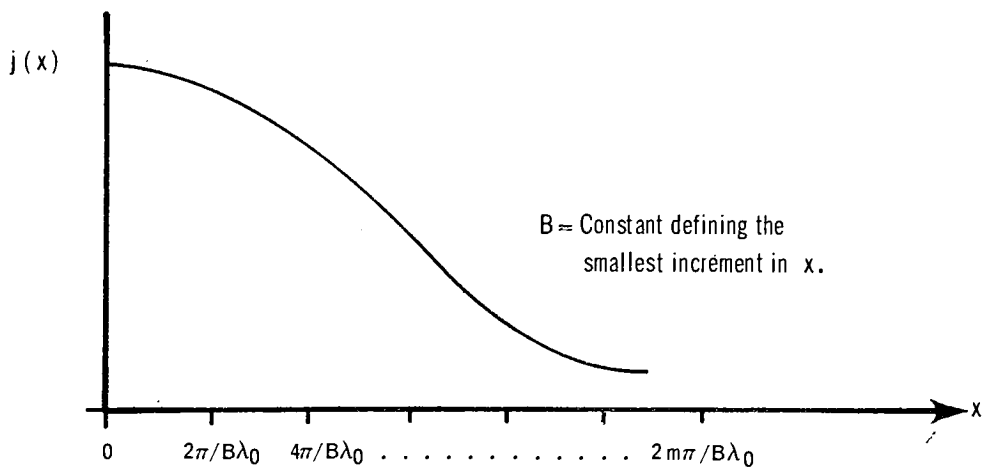

Figure 10-3. Generalized Intensity Distribution

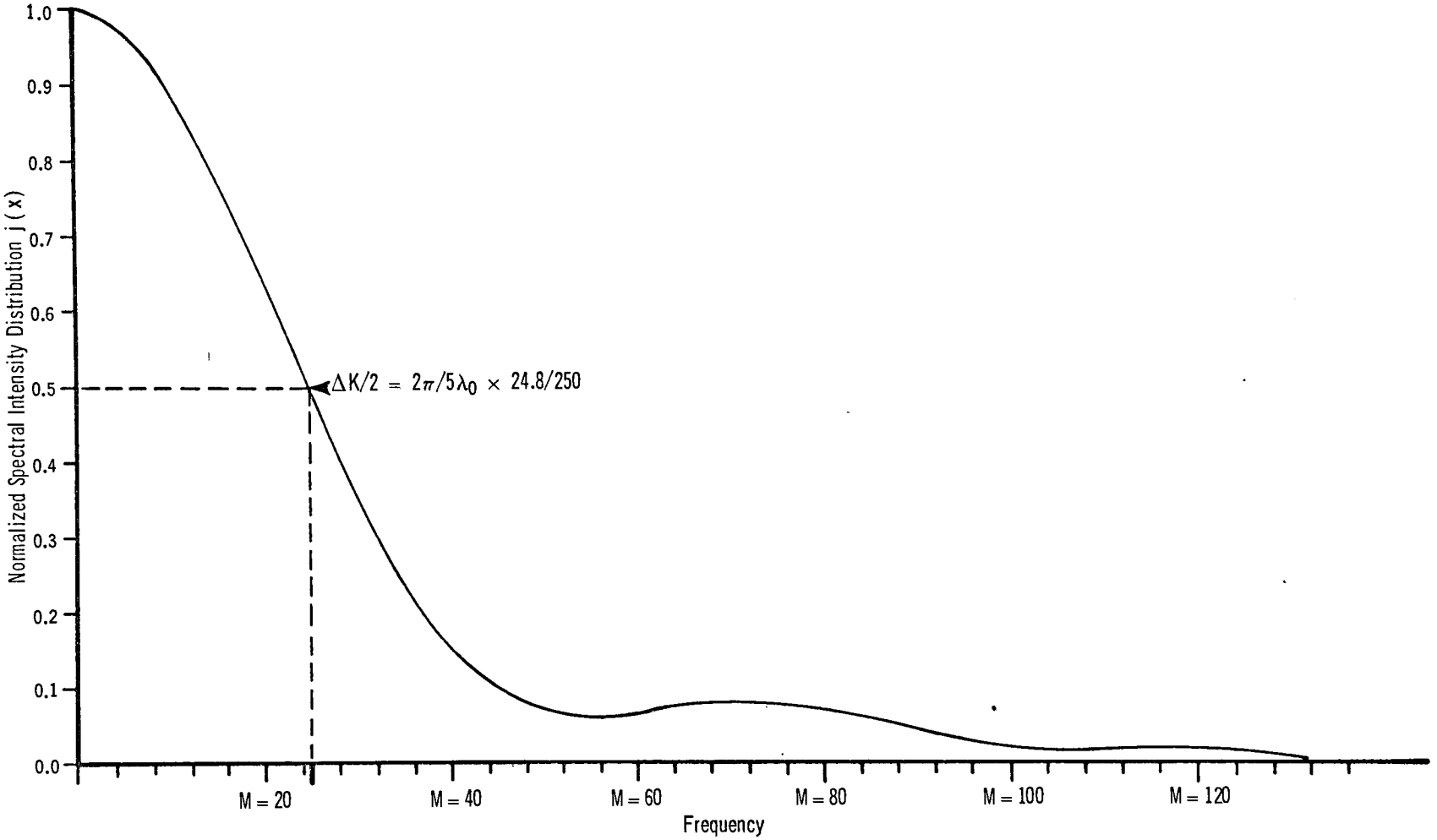

Figure 10-4. Normalized Spectral Intensity Distribution for Source/Filter No. 4043

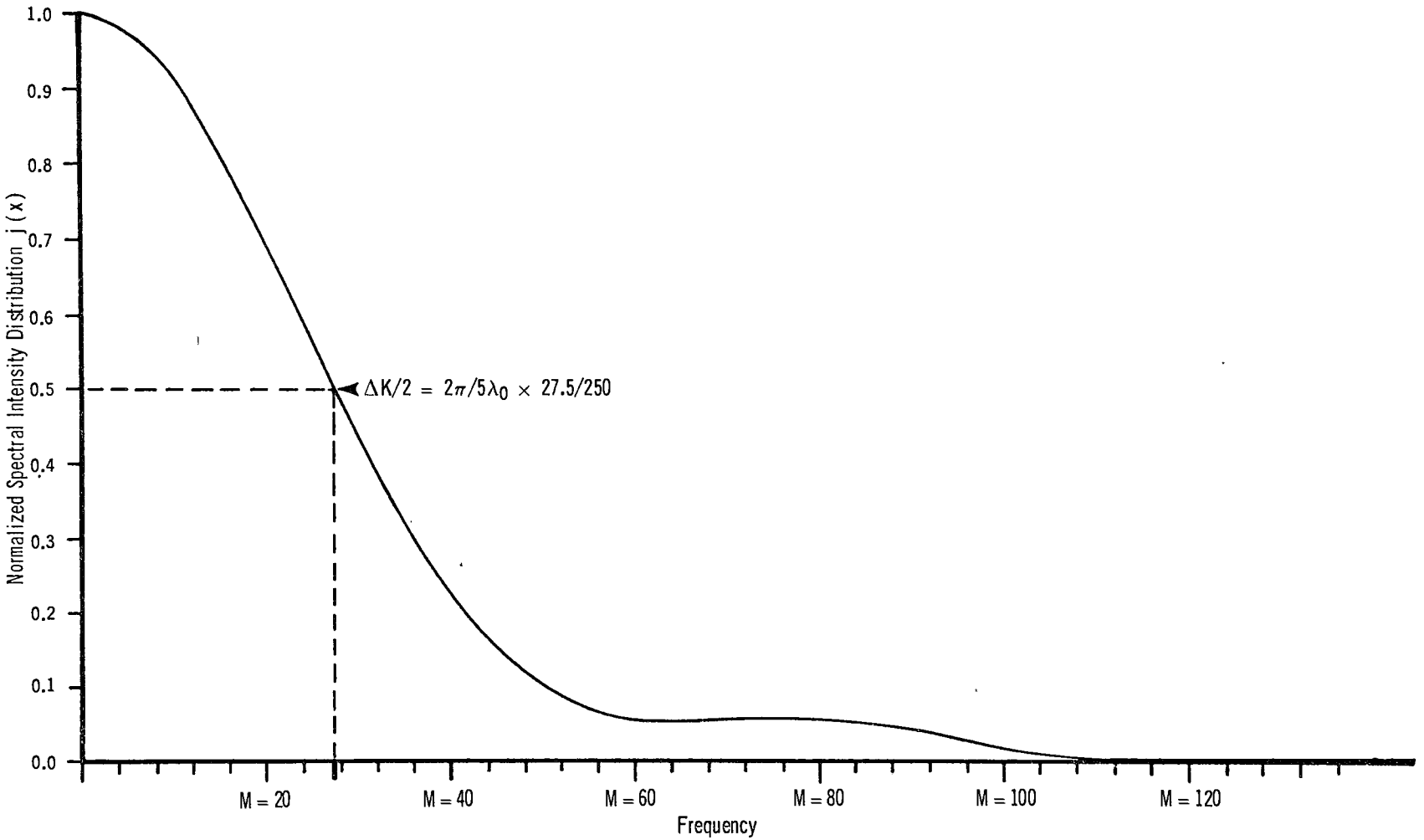

Figure 10-5. Normalized Spectral Intensity Distribution for Source/Filter No. 42-47-57

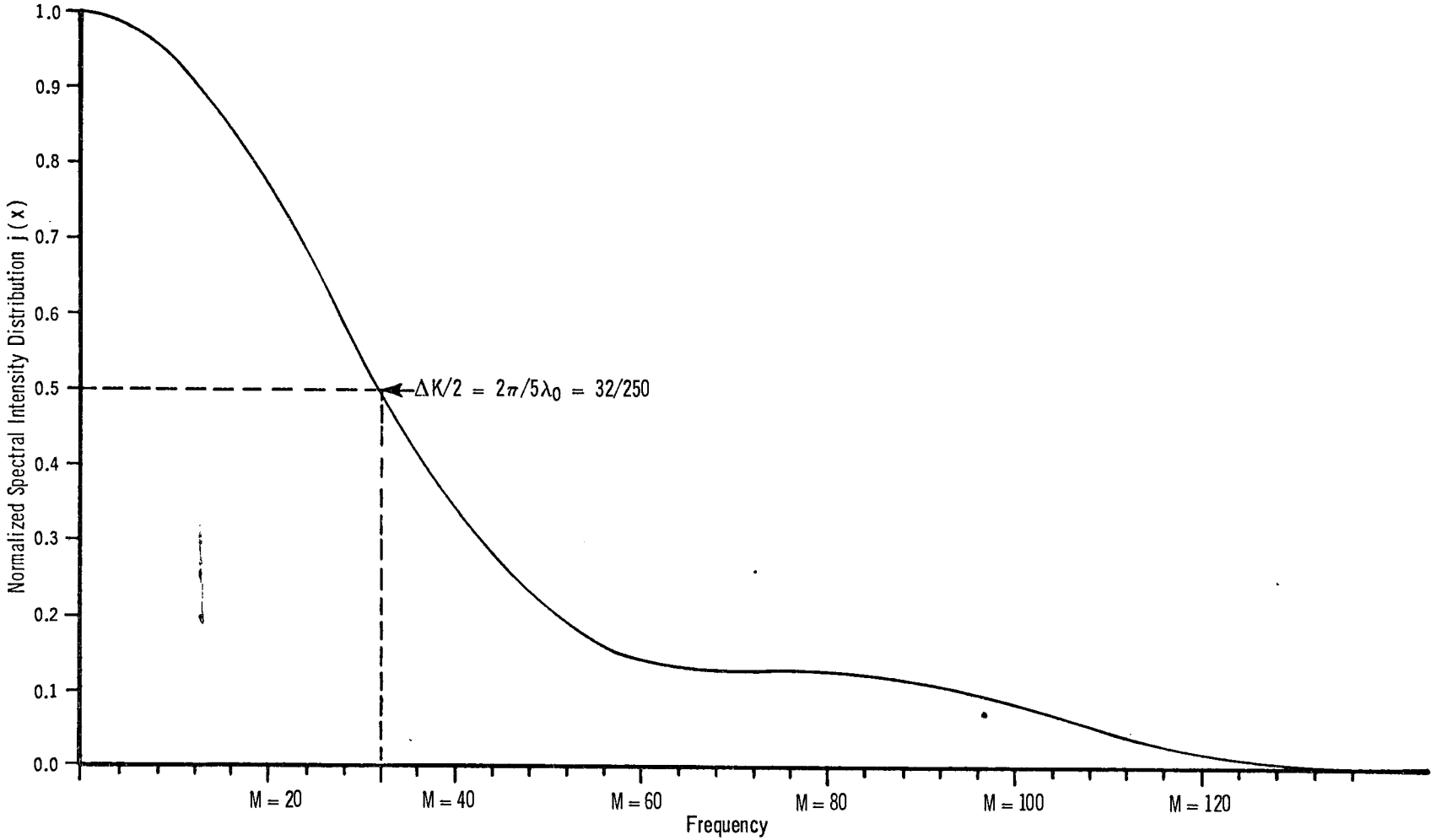

Figure 10-6. Normalized Spectral Intensity Distribution for Source/Filter No. 33-78-54

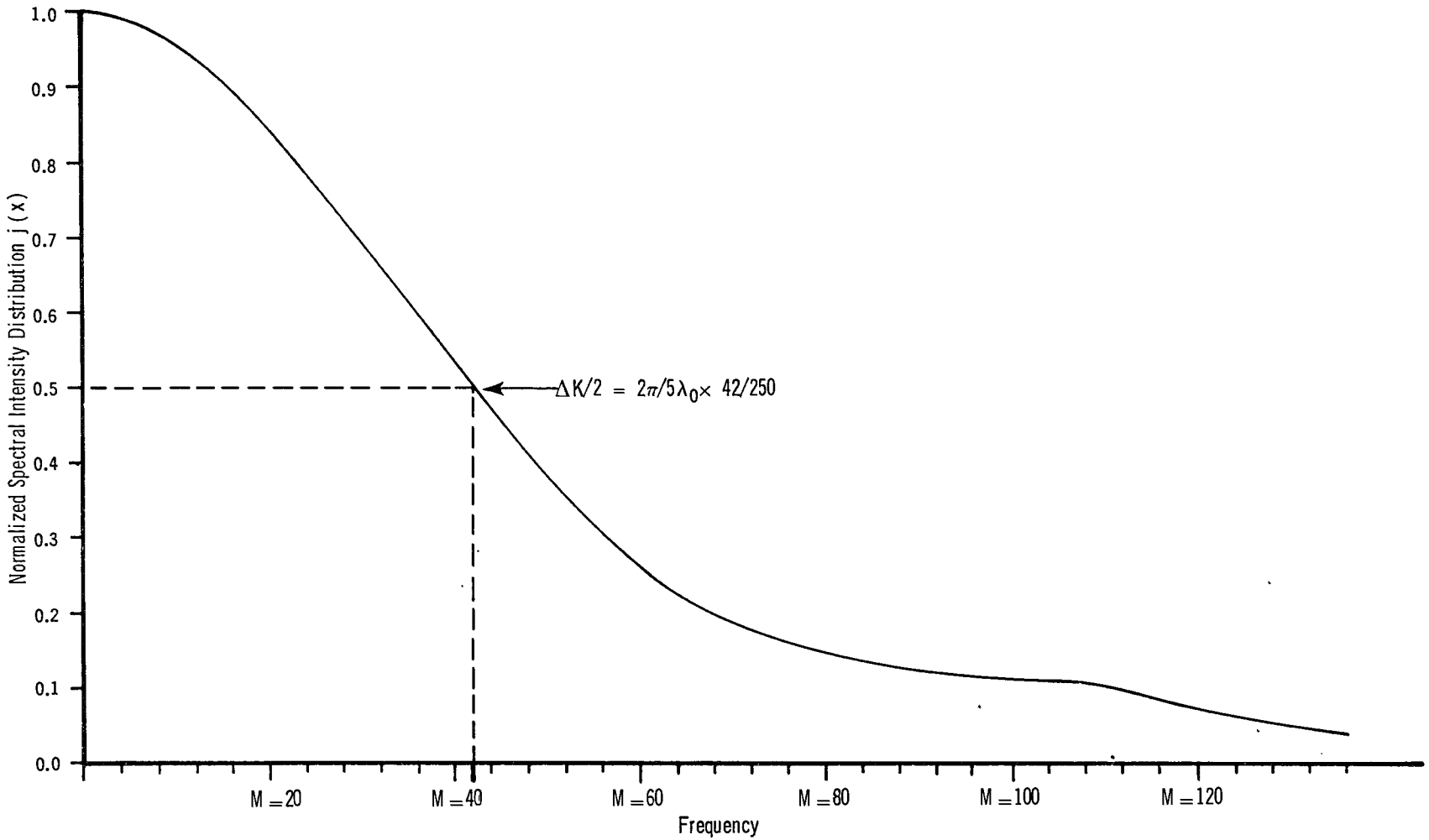

Figure 10-7. Normalized Spectral Intensity Distribution for Source/Filter No. 33-78-55

Comparing the spectral widths in Table 10-VI to the cohcrence lenghts given in Table 10-V yields experimcntal proof supporting the coherence theory described in this investigation. As expected, the source/filter combinations with the longer coherence lenghts, due primarily to temporal coherence considerations, yielded intensity distributions with the narrowest half-power spectral widths.

10.3 ANALYSIS OF DENSITY VALUES OBTAINED FROM HOLOGRAPHIC FRINGES

1. Method I: The first method of investigation considers the effects of the four source/filter combinations and the three group replicates on certain density values of the hologram itself. The density information was obtained from Micro-Analyzer traces which scanned a line perpendicular to the recorded fringes of the holograms. The traces were made using Data Corporation's Mann-Data Micro-Analyzer with a projected spot size of 20.958 microns. The traces were taken through the entire area covered by the various hologram diffraction patterns, which included the fringes of maximum contrast. Actual density values were obtained from a calibration curve made by tracing the calibrated step tablet illustrated in Figure 6-1.

The results of this set of Micro-Analyzer traces are given in Table 10-VII. Note that four density values are listed: D-max, D-min, ΔD, and D-avg. After careful consideration of the information contained within the traces, it was decided that these four density values contained the information of primary importance. This logically follows from the following observations.

a. The holograms were developed in a reversal process so that the value for minimum density, D-min, relates to the value of maximum exposure. Also, the relation must be linear, since all exposures were made on the linear portion of the characteristic curve shown in Figure 6-1.

b. The average density, D-avg, is important since it relates to the exposure level of the higher contrast fringes which contain the greater portion of the information necessary to reconstruct the holographic images.

TABLE 10-VII. DENSITY VALUES OBTAINED FROM MICRO-ANALYZER TRACES

Group No.	Exposure Number	Filter Number	D-max*	D-min*	ΔD*	D-avg*	D-max**	D-min**	ΔD**	D-avg*
I	1	33-78-55	2.60	2.11	0.49	2.36	2.52	2.10	0.42	2.31
I	2	42-47-57	2.50	1.95	0.55	2.28	2.43	1.95	0.48	2.19
I	3	33-78-54	2.57	2.12	0.45	2.35	2.49	2.11	0.38	2.30
I	4	4043	2.25	1.71	0.54	1.98	2.22	1.74	0.48	1.98
II	1	33-78-55	2.55	2.08	0.47	2.30	2.48	2.07	0.41	2.27
II	2	4043	2.29	1.76	0.53	2.03	2.25	1.77	0.48	2.01
II	3	42-47-57	2.38	1.96	0.42	2.18	2.33	1.96	0.37	2.14
II	4	33-78-54	2.57	2.15	0.42	2.36	2.49	2.13	0.36	2.31
III	1	4043	2.34	1.89	0.45	2.12	2.29	1.90	0.39	2.09
III	2	33-78-54	2.68	2.27	0.41	2.49	2.58	2.23	0.35	2.40
III	3	33-78-55	2.75	2.35	0.40	2.55	2.65	2.30	0.35	2.47
III	4	42-47-57	2.50	2.15	0.35	2.33	2.43	2.13	0.30	2.28

*Density values obtained directly from Micro-Analyzer traces.

**Actual density values obtained from Micro-Analyzer trace density values and calibration step tablet.

c. The density difference, ΔD, relates linearly to the exposure levels which created the maximum fringe contrast. It, therefore, is important to the contrast of the reconstructed image.

d. The values of the maximum density, D-max, relate linearly to the minimum exposure values at the maximum fringe contrast.

In investigating the significance of the data of Table 10-VII, the statistical method of Analysis of Variance (ANOVA) will be used.[34,35]

The purpose of the statistical test is to show whether the data imply that only one density population is being represented or that more than one density population is represented.

The null hypothesis being tested states that no significant difference exists between the various density levels. For each of the cases to be tested, this can be stated as follows:

Case I $\quad H_o: D_{1\,avg} = D_{2\,avg} = D_{3\,avg} = D_{4\,avg}$ $\quad$ 10.301

Case II $\quad H_o: \Delta D_1 = \Delta D_2 = \Delta D_3 = \Delta D_4$ $\quad$ 10.302

Case III $\quad H_o: D_{1\,min} = D_{2\,min} = D_{3\,min} = D_{4\,min}$ $\quad$ 10.303

The alternative hypothesis, which must be accepted if the null hypothesis is rejected, is that a significant difference does exist between the various density levels. This can be attributed to either source/filter effects or group effects, as will be explained in the following case investigations.

The mathematical statement for the alternative hypothesis of each case need not be stated. Since rejection can occur for a number of combinations of density differences, it will not be as simplified as above. In other words, the alternative hypothesis states that the density levels are not all equal. Thus, the null hypothesis will be rejected whenever one or more of the density levels differs from the other density levels.

Whenever the density levels differ and the null hypothesis is rejected, a small risk known as the alpha risk is assumed. In this circumstance, as in equation 10.201, the alpha risk occurs when the data indicate that this difference in density levels occurs,

when in truth, no significant difference actually existed due to changes in the factor under investigation. The consequence of rejecting the null hypothesis when it should be accepted is that false conclusions would be made concerning the entire experiment. Thus, the alpha risk, α , is set at a low value to avoid this situation. In all the following analyses, an alpha risk of 0.05 was adopted to yield a 95% level of significance to the conclusions.

The procedure to be followed in using ANOVA in this investigation is based on the testing of various levels of two factors: (1) Source/filter combinations, and (2) groups. As discussed in Chapter IX, the randomness of the exposures was purposely contained within groups. Thus, the significance of the environmental changes, as represented by each of three groups, could be tested independently as a variable factor rather than treated as a replicate for future estimation of experimental error. The actual calculations for each of the tests to be discussed are given in Appendix V.

The mathematical model assumed by this procedure is as follows:

$$D_{ij} = \bar{D} + SF_i + G_j + E_{ij} \qquad 10.304$$

which states that each density observation, D_{ij}, is based on four possible effects: (1) The general mean, $\bar{D}$, of the density observations; (2) a possible effect due to the source/filter factors, SF_i; (3) a possible effect due to the group effects, G_j; and (4) the effect of error.

The significance of the two factors is based on an F-ratio, which compares the mean squares of each of the factors against the mean square of the residual term. These values of F-ratio are then compared to standard values obtained from known statistical tables.[34] In each case, the standard F-ratio is defined by the given alpha risk and the number of degrees of freedom associated with the factor of interest.

The results of the analysis of the density values obtained from the holographic fringes will now be discussed for each of the previously described cases.

a. Case I — Average density of fringes: For the average density of the fringes, D-avg, the calculated F-ratio was 75.333, while the table value for the F-ratio was only 4.7571. Thus, the null hypothesis is rejected and the various source/filter

levels are considered to have had a significant effect on the average density level of the holographic fringes. The calculated F-ratio for the group levels is 21.89, while the table value is only 5.1433. Thus, the null hypothesis is also rejected for the group data and its various levels show a significant effect on the average density level of the fringes.

b. Case II: For the density difference, ΔD, or basic contrast of the fringes, an entirely different result is found. The calculated value of the F-ratio is 3.47 for the source/filter levels, while the table yields a value of 4.7571. Since the calculated value of the F-ratio is found to be less than the table value, it is concluded that the effect of changes in the source/filter combinations have no significant effect on the density differences. Thus, the null hypothesis is retained for the source/filter factor. However, the calculated F-ratio for the group factor is 7.25, which is greater than the table value for the F-ratio of 5.1433. Thus, for group levels, the null hypothesis is again rejected as in the first case.

c. Case III: The results for the minimum density level, D-min, are similar to those found in the first case. The calculated F-ratio for the first factor, source/filter combinations, is 66.00, which is greater than the table value of 4.7571. The calculated F-ratio for the second factor, group levels, is 19.08, which is again greater than the table ratio of 5.1433. Thus, the null hypothesis is rejected for both of the factors tested.

In summarizing the results of the analysis made in each of these three cases, the following conclusions are important.

a. The source/filter factor is significant for both the average density level and the minimum density level of the holographic fringes. Since the holograms were exposed at two different energy levels and at four different coherence levels, this was anticipated. It must be noted, however, that these results reveal only that a significant difference between source/filter levels exists. It does not reveal whether the significant difference in the holographic fringes is related either to changes in the temporal coherence level or to changes in the exposure level. This point will be investigated further in later tests.

b. The fact that the source/filter factor is considered to have no significant effect on the contrast of the fringes is also easily understood. The values of the density differences, as obtained from the Micro-Analyzer traces of the holographic fringes, represent the maximum contrast along the center line of the entire fringe pattern. Since this is, essentially, the sums and differences of the object and reference beams along with a d-c background term, it follows that the energy ratio between the beams for the various source/filter combinations is at an almost constant value. It does not yield information concerning the difference in level of energy that exists between the two sets of source/filter combinations.

c. These initial statistical tests give a definite indication that exposure differences were, in fact, present among the three groups. As previously explained, this can be attributed to two main factors which are connected, precluding individual investigation. The first and most important of these would be changes in the surrounding environment during the holographic exposures. The second factor concerns the changes that occur among the three main processing procedures. In each case, the greatest precaution was taken to guard against changes that might have affected the holographic fringes; however, it was impossible to completely control each of the factors during the experiment.

2. Method II: An alternative to the first method of analysis stems from the fact that even though four source/filter combinations existed, all of the holograms were formed through the use of only two significant energy or exposure levels — the first for source/filter combinations 4043 and 42-47-57, and the second for source/filter combinations 33-78-54 and 33-78-55.

Thus, it is perfectly acceptable to treat the data as being generated by two levels of source/filter combinations and assuming that each level consisted of two replicates, one for each of the pairs within an exposure level. Therefore, a two-factor ANOVA test can be performed using the replicate data as a basis for experimental error, and using the ratio of the mean square of a given factor to the mean square for error to perform the F-test of significance. Since replicates are available, the effects of interaction between the two main factors can also be determined.

As in the previous ANOVA, the null hypothesis states that no significant difference exists between the density values for the factors under investigation. The alternative hypothesis again states that a density difference does indeed exist for a calculated F-ratio found to be larger than that obtained from the tables.[28] The mathematical model for the following ANOVA is

$$D_{ijk} = \underline{D} + SF_i + G_j + (SF \times G)_{ij} + k(ij) \qquad 10.305$$

which is similar to equation 10.304. The added factor $(SF \times G)_{ij}$ represents the effect of interaction between the two factors.

The calculations of this two-factor, replicated ANOVA are given in Appendix V. Note that the calculations were performed for Case I only. Since the primary concern of this analysis is to investigate the effects of exposure level, the average density case becomes the most important.

For the source/filter factor, the calculated F-ratio is 18.186, while the table F-ratio is only 5.9874. Thus, the null hypothesis is rejected for the source/filter factor, and it is concluded that a significant difference in the average density level does exist for the exposures made at each level of the factor.

The calculated F-ratio for the group factor is 2.302, while the table F-ratio is 5.9874. Thus, the null hypothesis is accepted for the group levels, and it is concluded that the group factor had no significant effect on the holographic exposures.

In comparing the results found for group effects between Method I and Method II, it must be remembered that Method II yields a higher value of error, which reduces the F-ratio for the group factor and makes the factor become insignificant. Also, Method I does not have an error term based on replication. Instead, it has a value of residual which is attributed to chance causes and not, specifically, to experimental error. Since the values used as replicates, in Method II, are not true replicates in that the filters have been changed even though the energy level has remained the same, the value found for error is higher. Thus, the ratio of group-mean-square to error-mean-square decreases compared to that found in Method I.

In addition, it is interesting to note that if the analysis of Method II is twice repeated with the position of the filters shifted to obtain all other possible combinations, the F-ratio for the filter factors becomes insignificant in each case. That is, the null hypothesis is accepted for all other combinations of filters besides the one previously tested. The values for these calculations are also given in Appendix V and stand to further emphasize the significance of the fact that the density values obtained were functions of two independent exposure levels.

Also, in the analysis of the effects of temporal coherence on the variations of the reconstructed images, it is important to compare only those results obtained from holograms constructed at the same exposure level.

3. Method III: The first method of investigation considered all of the source/filter levels together, including those performed at two independent exposure levels. The results of this method showed that changes in all the levels of the source/filter factor had a significant effect on the average density values of the holographic fringes. The second method helped to clarify these effects by showing that the average density values were significantly affected by the two independent exposure levels of the source/filter factor. This third method will proceed one step further by investigating the possibility that each of the two source/filter levels, within each of the two independent exposure levels, had a significant effect on the average density values of the holographic fringes.

The null hypothesis for this ANOVA states that a significant difference in average density value does not exist for level changes within each of the factors. Mathematically, the null hypothesis is the same as that given in equation 10.304.

In the analysis, as shown in Appendix V, the source/filter factor is divided into two separate subfactors representing each of the two exposure levels. Thus, two separate ANOVA's are performed, one for the exposure subfactor containing source/filter combinations 4043 and 42-47-57 and another for the exposure subfactor containing source/filter combinations 33-78-54 and 33-78-55. The first of these subfactors will be treated as the upper exposure level and the second as the lower exposure level.

a. Upper exposure level: The calculated F-ratio for the source/filter factor was 52.000, which exceeds the table value of 18.518. The calculated F-ratio for the

group factor is 8.222, which is less than the table value of 19.000. Thus, a significant difference is found to exist between the average density levels of the holographic fringe data at this exposure level. This difference is attributed to the change in temporal coherence previously shown to exist between source/filter factors 4043 and 42-47-57.

b. Lower exposure level: The F-ratios of both the source/filter factor and the group factor are found to be much less than the table values of F-ratios. Thus, each has failed to show a significant change due to temporal coherence effects.

10.4 ANALYSIS OF DENSITY VALUES OBTAINED FROM RECONSTRUCTED HOLOGRAPHIC IMAGES

Each of the ANOVA methods used in the previous section of this chapter applies to the analysis of density data obtained from Micro-Analyzer traces of the reconstructed bar images. However, only one case, that of the average density, need be discussed to obtain information of the level of the holographic exposures. The reason for this is that the original bar target consisted of one energy level throughout its entire cross-sectional area and the average density level of the reconstructed images correlates to this rather than the other density level choices. Also, as in previous sections, the analysis is given in Appendix VI and only the significant results will be discussed here.

1. Method I: This first method analyzes the reconstructed images at four source/filter levels and at three group factor levels. The mathematical model of the analysis is given in equation 10.304. The null hypothesis states that a significant difference in density exists due to changes in the level of the factors involved.

The calculated F-ratio for the source/filter factor is found to be 9.232, which is greater than the table value of 4.7571. Thus, the null hypothesis is rejected and, with 95% confidence, it can be stated that changes in the source/filter level had significant effects on the average density of the reconstructed bars.

The calculated F-ratio for the group levels is found to be 1.117, which is less than the table value of 5.1433. Thus, the null hypothesis is accepted for the group levels.

Note that even though the holographic fringe densities were significantly affected by the group factor, the reconstructed image densities were not found to be significantly affected. In making this comparison, however, it must be emphasized that this

result is based on a single Micro-Analyzer scan through the center and parallel to the edge of the longest side of the image. This section of the bar would be the least affected by vibrations and component movements. For further insight into the effects of environment changes, a careful inspection should be made at the outer edges of the bar where slight movements would have more of an effect on the density level of the reconstructed images.

Since it is not within the scope of this investigation to consider air turbulence and environmental changes, a further interpretation of these facts is left up to the reader. In the next section, however, analysis of the shape of the reconstructed images will further clarify the above conclusion.

In summary, it can be stated that the average density levels of the reconstructed bar images varied significantly with changes in the source/filter factor, while the alternate was found to be true for the group factor.

2. Method II: The treatment of the source/filter factor as being of two levels instead of four levels, as in Method I, adds further insight to the significance that the source/filter combinations have on the reconstructions. As in the previous section, the source/filter combinations are split into two levels, one containing filters 4043 and 42-47-57, and one containing filters 33-78-55 and 33-78-54.

In the analysis, it is found that the calculated F-ratio for the source/filter factor is 6.588, which is greater than the table value of 5.9874. Thus, the two levels are again found significant, further strengthening the fact of the presence of two levels of energy. The F-ratio as calculated for the groups is found to be 0.428, which is much less than the table value of 5.1433. Again, the null hypothesis is accepted and the groups can be considered as replicates rather than as a separate factor. The interaction is also found to be insignificant.

In addition, it is interesting to note that when the positions of the source/filter levels are shifted, as shown in Appendix VI, and the analysis is repeated, in each case the filter factor is found to be insignificant. Also, the group levels and the interaction term remain insignificant.

3. Method III: When the source/filter factors are divided into two separate sub-factors representing each of the two exposure levels, as previously discussed in paragraph 10.3, it was found that the F-ratios for both the source/filter factor and the group factor were less than the respective table values of F-ratios. This occurred at both the upper and lower exposure levels.

Therefore, it can be concluded that changes in the temporal coherence showed no significant effect on the average density level of the path traced on the reconstructed bar images. This does not imply, however, that density changes did not take place around the outside edge of the bar images. This will be implicit in the following analysis.

10.5 ANALYSIS OF THE GEOMETRICAL SHAPES OF THE RECONSTRUCTED BAR IMAGES

The final analysis performed in this investigation involves a comparison of geometrical measurements made on the reconstructed bar images. All measurements were performed on a D. W. Mann Comparator with measurement precision of better than one micron.

The purpose of these measurements was to obtain accurate information concerning the geometrical shapes of the real images so that comparisons could be made between the various levels of holographic exposure. Thus, a multitude of data was desired and the problem became one of economics, requiring a compromise in the amount of necessary data to obtain the most important information required.

From this compromise, the following methods of evaluation were selected.

1. A subjective evaluation based on the overall geometrical shapes of the reconstructed real images. These shapes are derived from measurements taken at 25-micron intervals throughout the entire length of the reconstructed bars.

2. An objective evaluation using the ANOVA methods of the previous sections of this chapter. These evaluations, also based on the above measurements, consist of an investigation of the changes that occurred between the lengths, widths, and areas of the reconstructed bars due to changes in the source/filter levels and the group levels. The lengths and widths were obtained directly from the measurements, while the areas were found from sketches made of the bars using interpolation of the measurements.

The values obtained for the comparator measurements made on the reconstructed real images yield the geometrical shapes shown in Figures 10-8 through 10-19.

1. Subjective Evaluation: This portion of the evaluation is straightforward because of the enormous change that takes place between the geometrical shapes of the real images. As the figures show, some of the bars have closely maintained their original shapes while others have become quite distorted. Also, to simplify the evaluation, comparisons are made between the geometrical outline figures and the source/filter combinations. These comparisons are given in Table 10-VIII.

TABLE 10-VIII. COMPARISON OF COHERENCE LENGTHS TO IMAGE SHAPES

Exposure Level	Source/ Filter	Coherence Lengths	Previous Figure No.
1	4043	31.90	10-11, 10-13, 10-16
1	42-47-57	28.60	10-9, 10-14, 10-19
2	33-78-54	20.35	10-10, 10-12, 10-17
2	33-78-55	15.40	10-8, 10-15, 10-18

The greatest change in geometrical shape takes place between the two main energy levels. This is due to the fact that at the higher exposure levels, approaching the maximum density of the holographic film, higher order fringes appear to the sides of the primary fringe pairs. These higher order fringes on the holograms carry the higher frequency information, which appears as more detailed information on the outer edges of the reconstructed real images.

However, within each exposure level, a very significant change in geometrical shape also takes place. This change can only be due to changes in the temporal coherence of the source and, in each case, the greater the coherence length (as shown in Table 10-V), the greater the temporal coherence and the greater the detail obtained in the reconstructed images. In the cases of the longest coherence length, the geometrical shape of the reconstructed images closely approached that of the original rectangular bar target.

2. Objective Evaluation: The objective portion of this evaluation is based on the ANOVA methods used in the preceding sections of this chapter. In this section, however, the overall results are listed together, as shown in Table 10-IX, while the actual

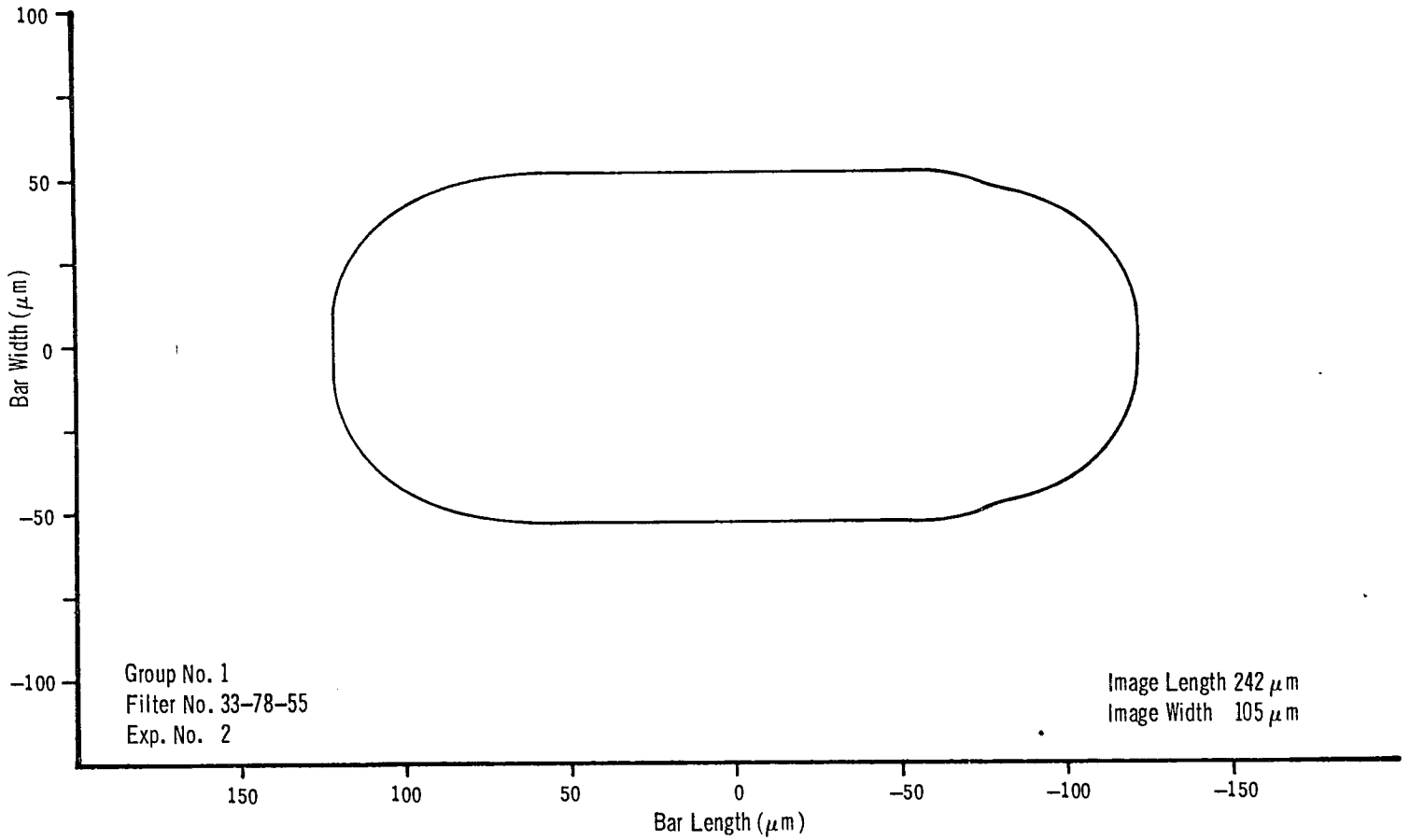

Figure 10-8. Reconstructed Image Shape from Length and Width Measurements

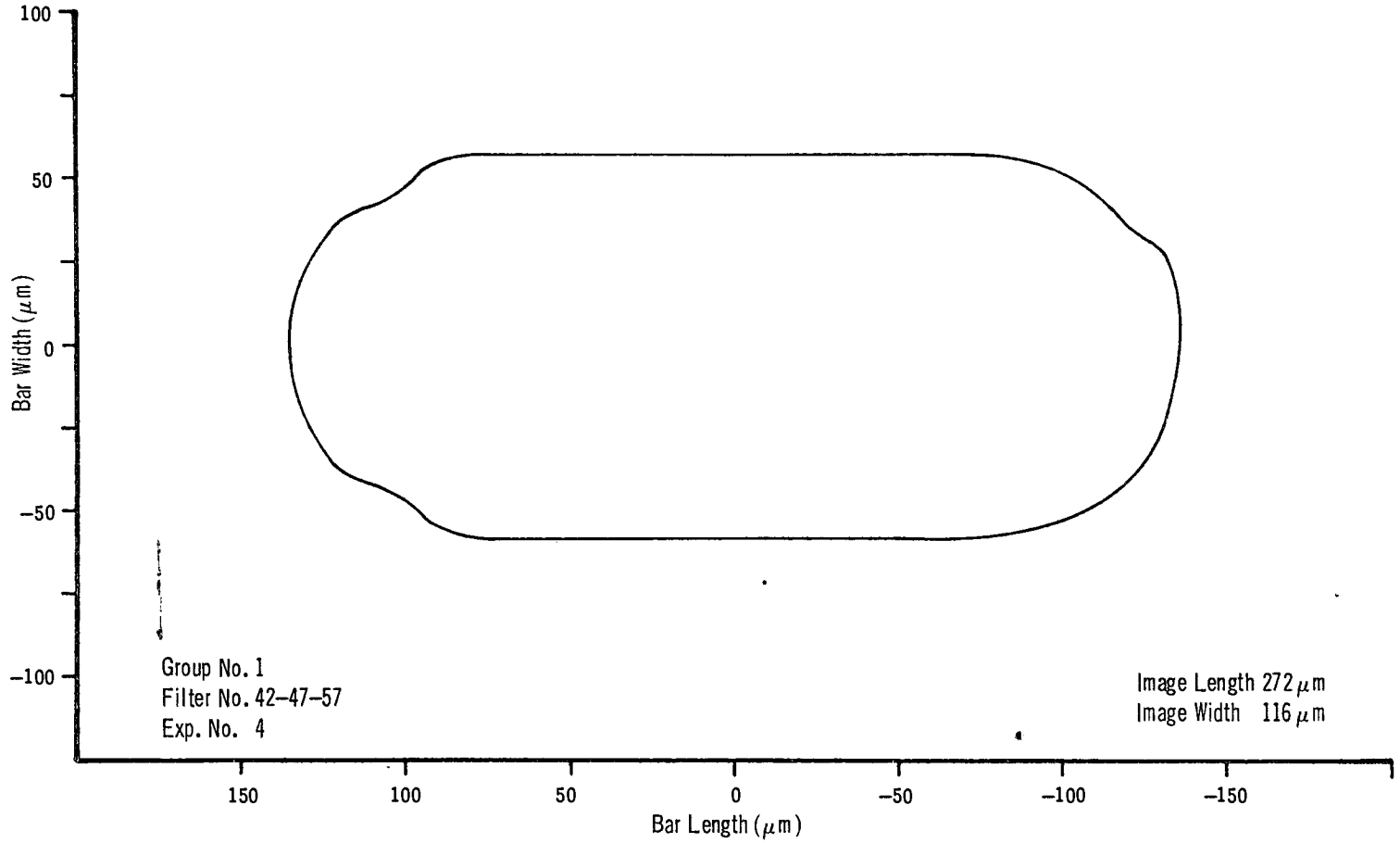

Figure 10-9. Reconstructed Image Shape from Length and Width Measurements

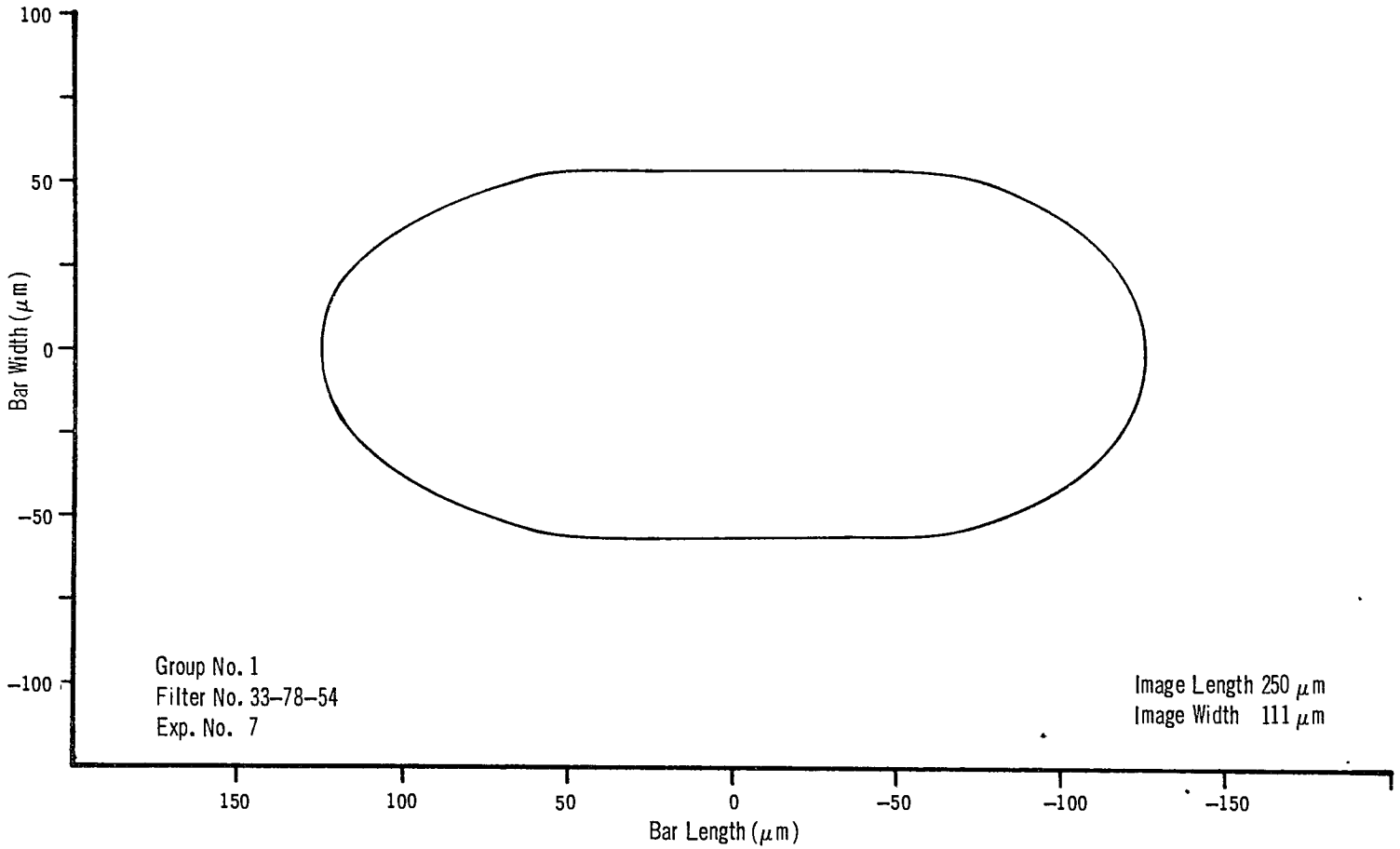

Figure 10-10. Reconstructed Image Shape from Length and Width Measurements

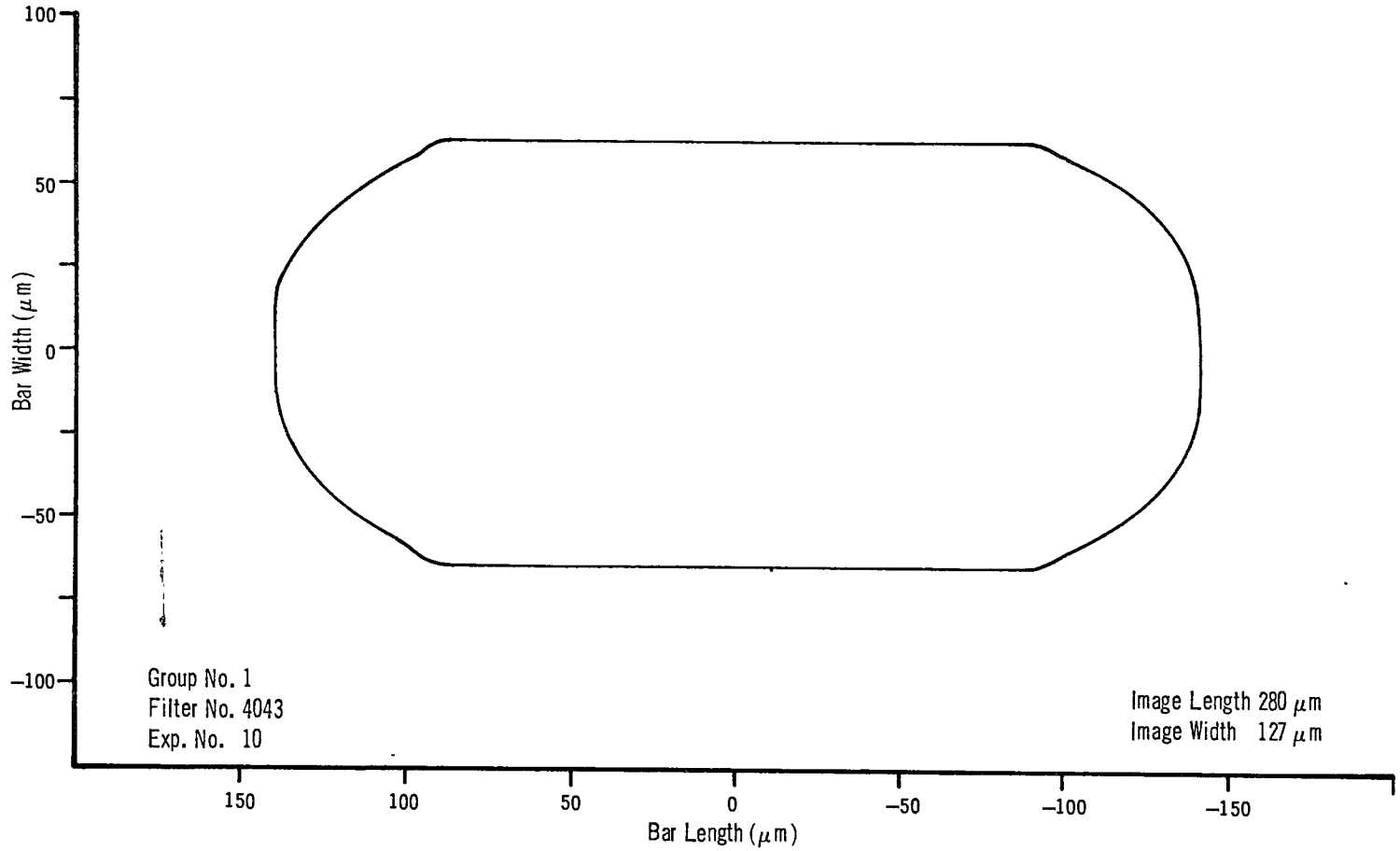

Figure 10-11. Reconstructed Image Shape from Length and Width Measurements

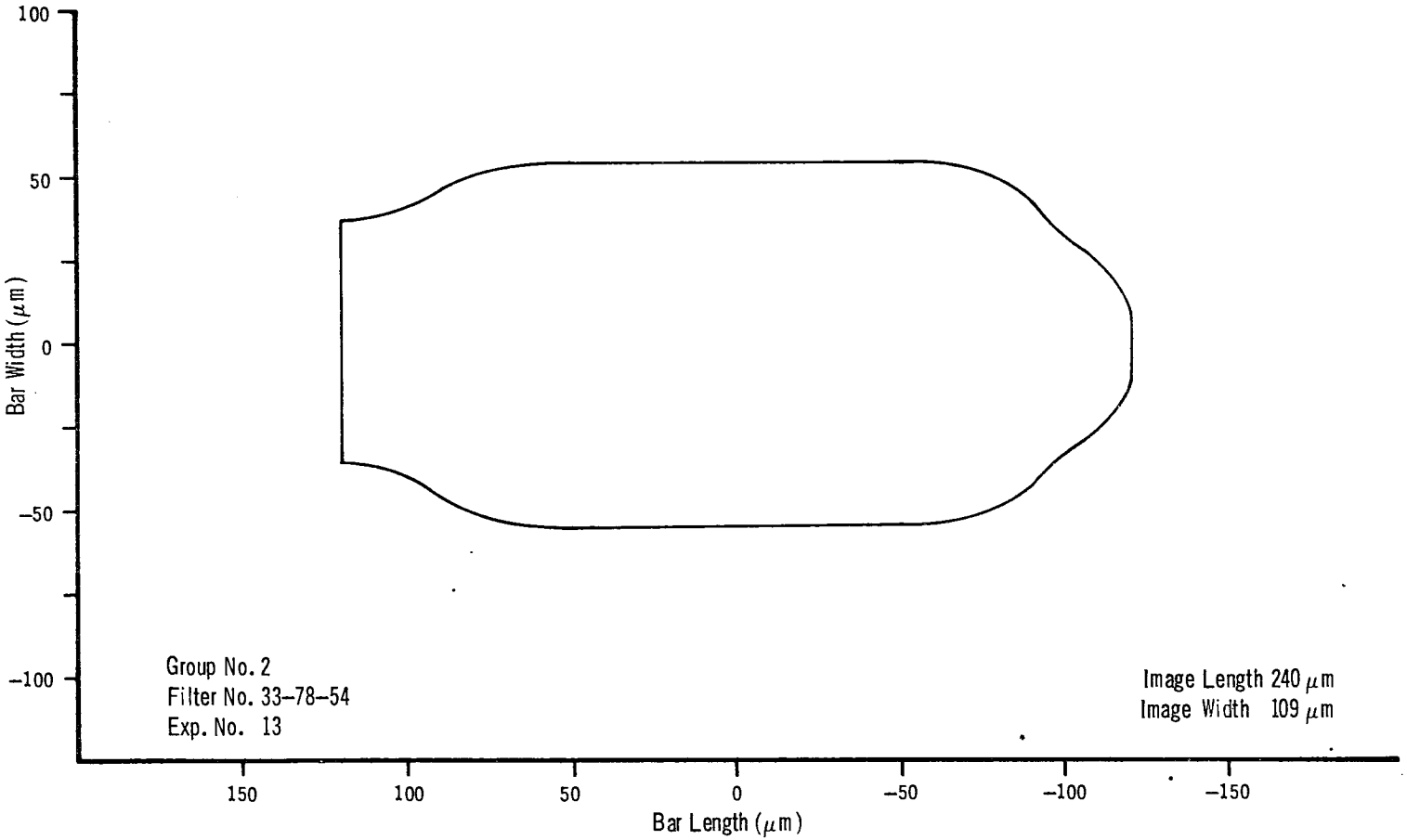

Figure 10-12. Reconstructed Image Shape from Length and Width Measurements

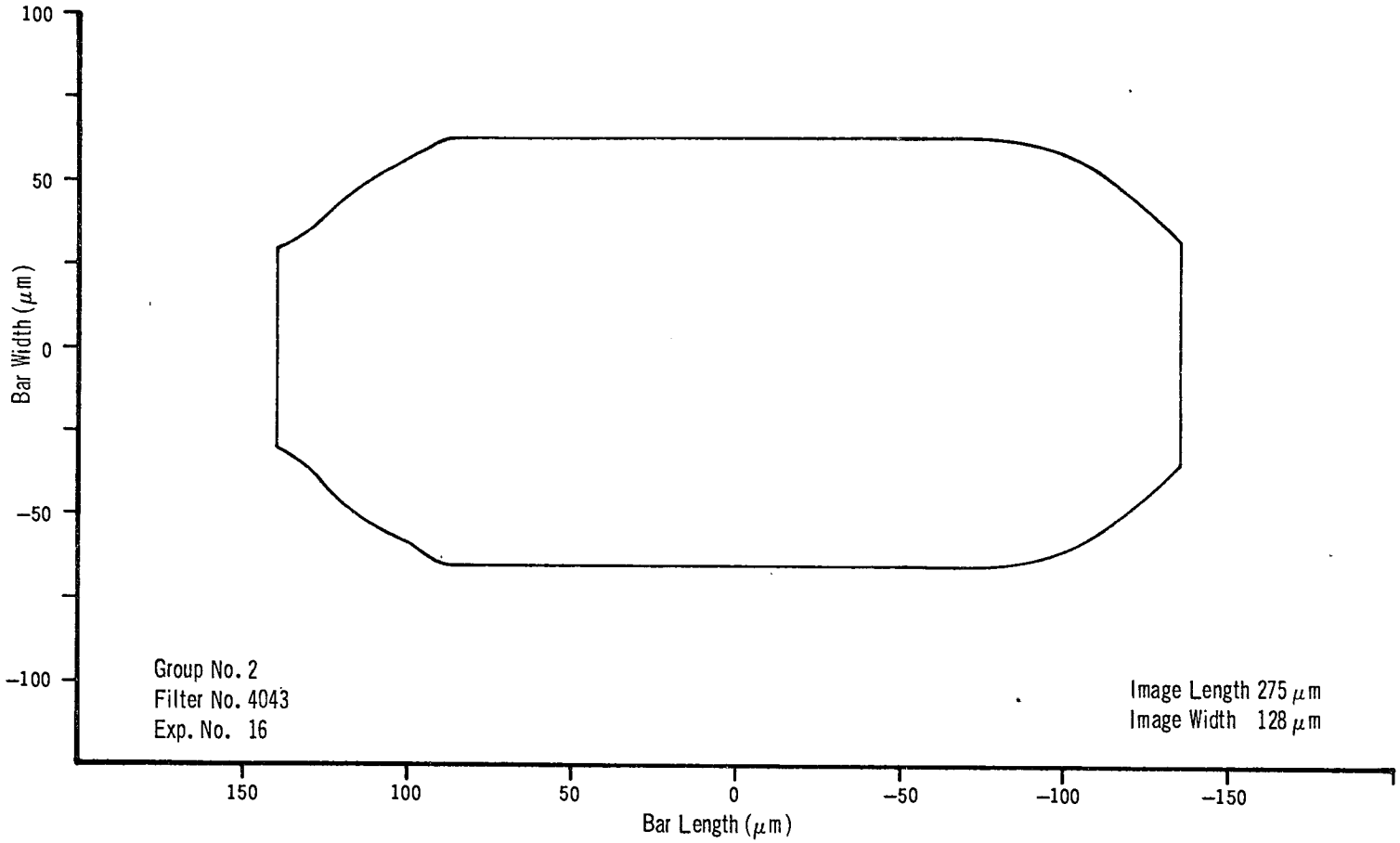

Figure 10-13. Reconstructed Image Shape from Length and Width Measurements

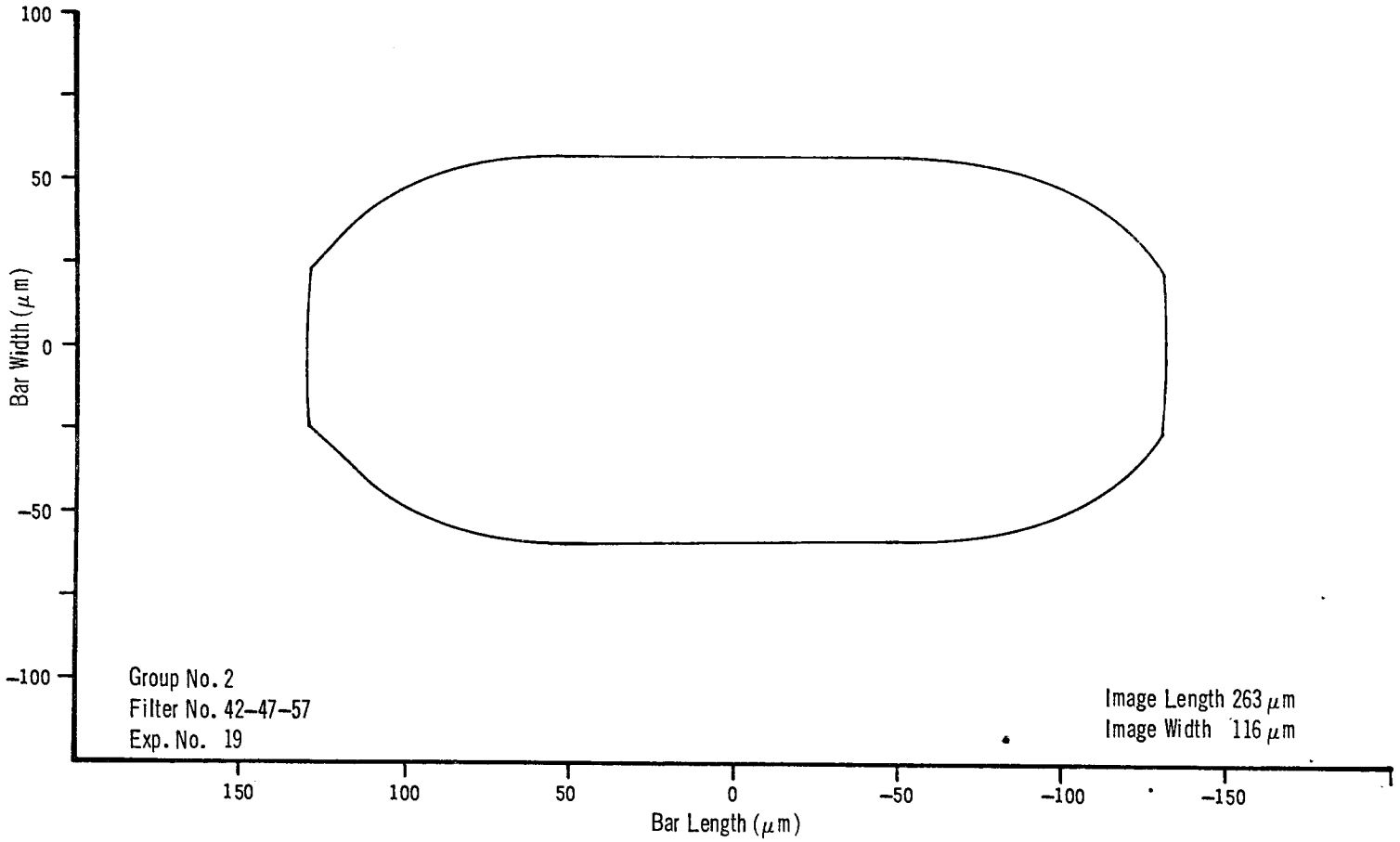

Figure 10-14. Reconstructed Image Shape from Length and Width Measurements

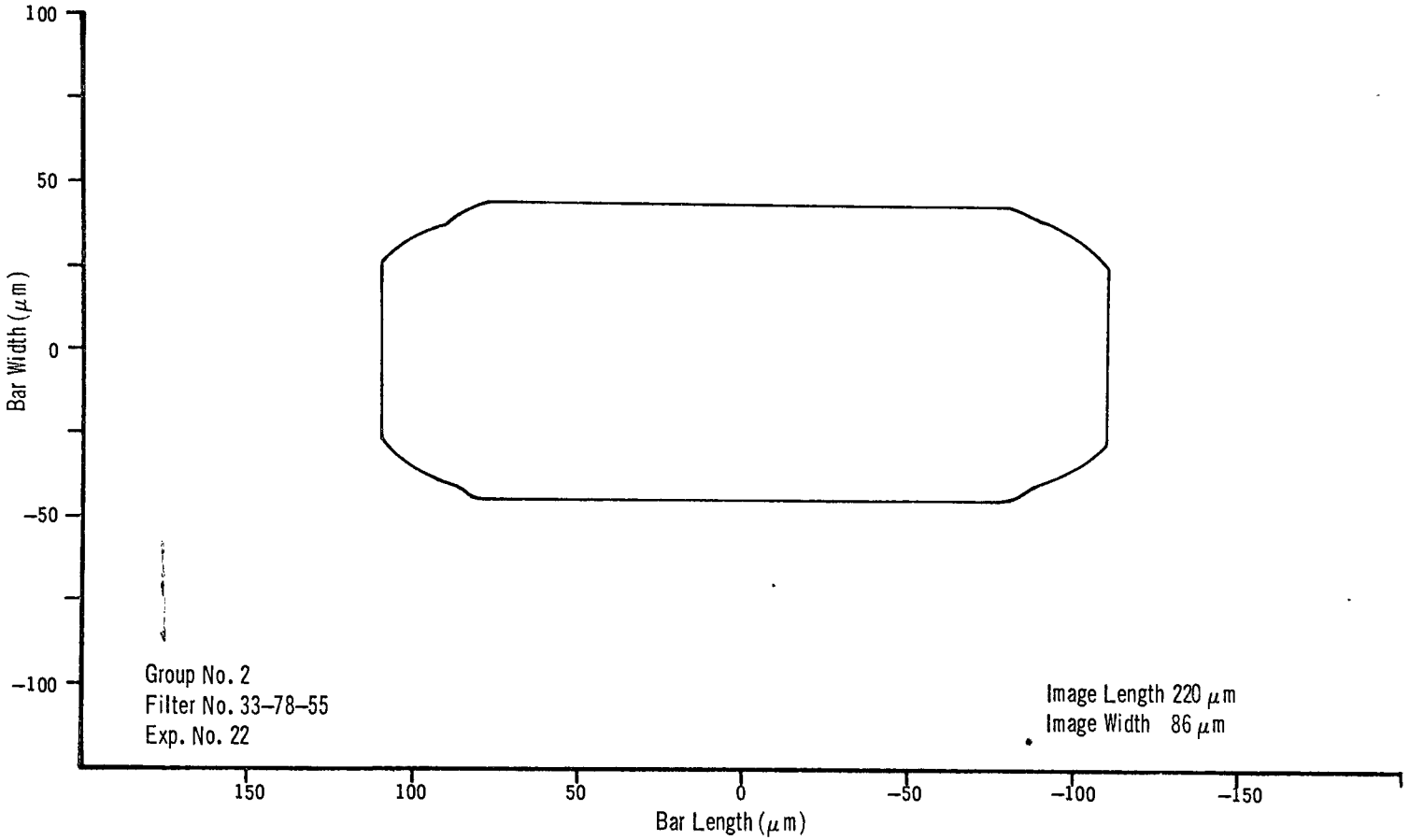

Figure 10-15. Reconstructed Image Shape from Length and Width Measurements

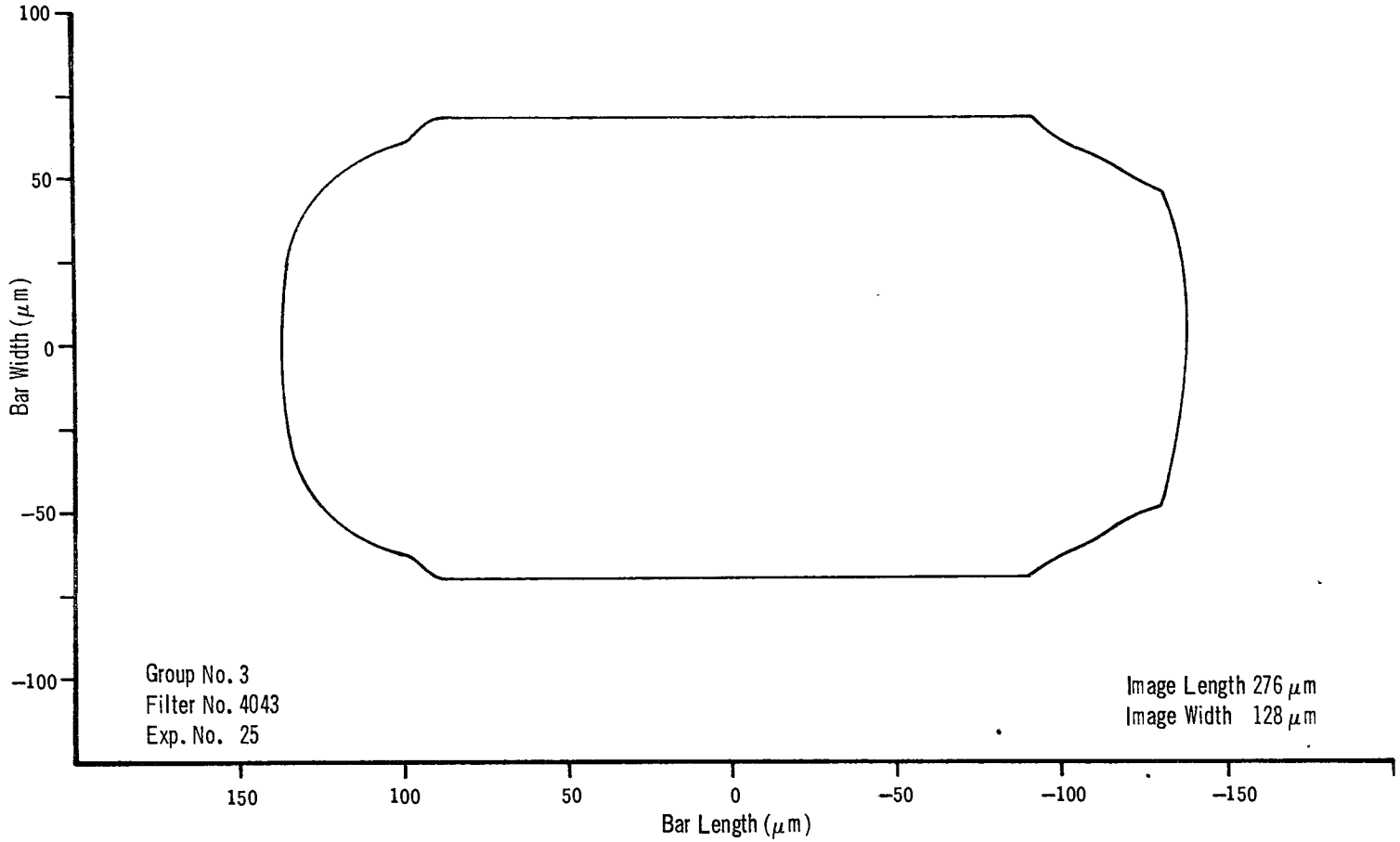

Figure 10-16. Reconstructed Image Shape from Length and Width Measurements

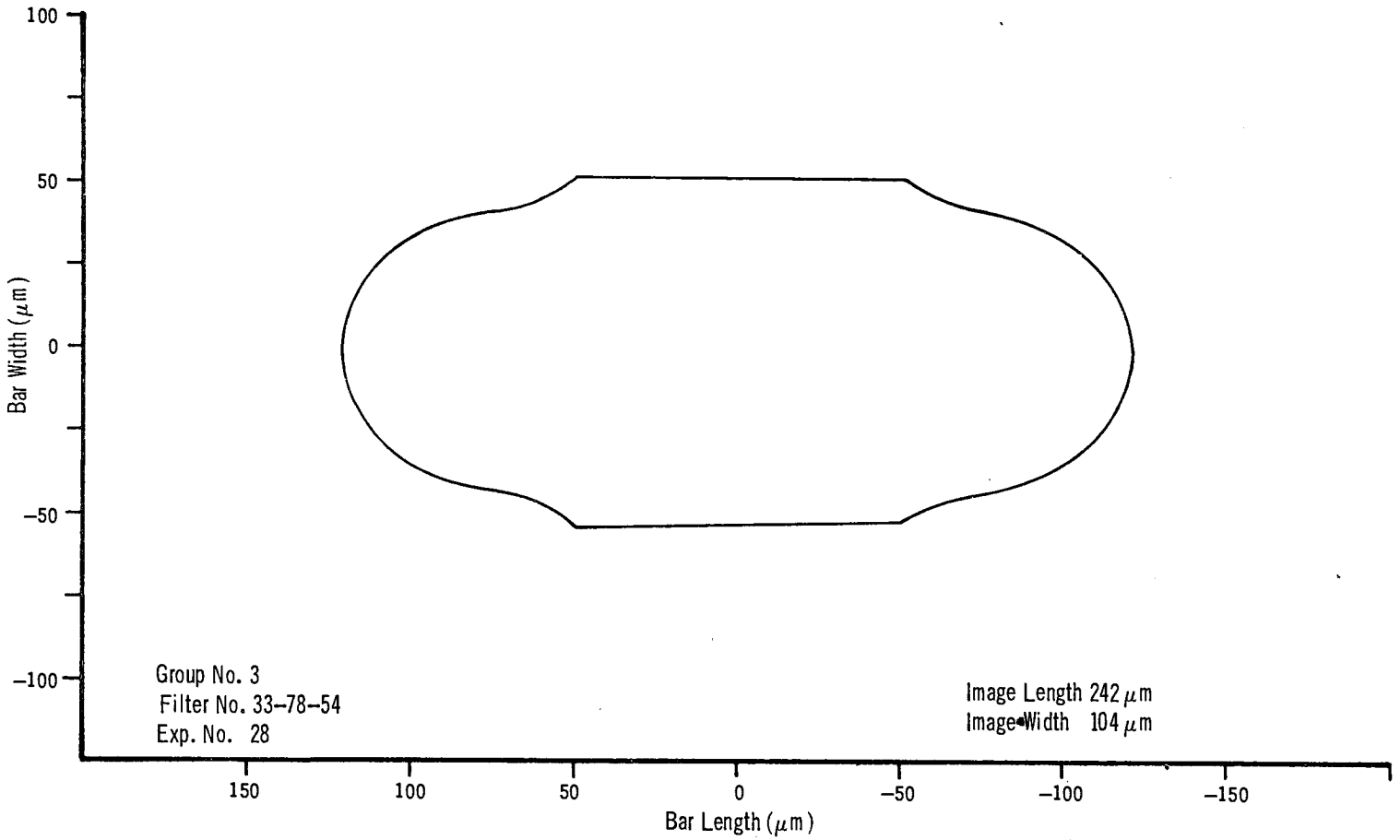

Figure 10-17. Reconstructed Image Shape from Length and Width Measurements

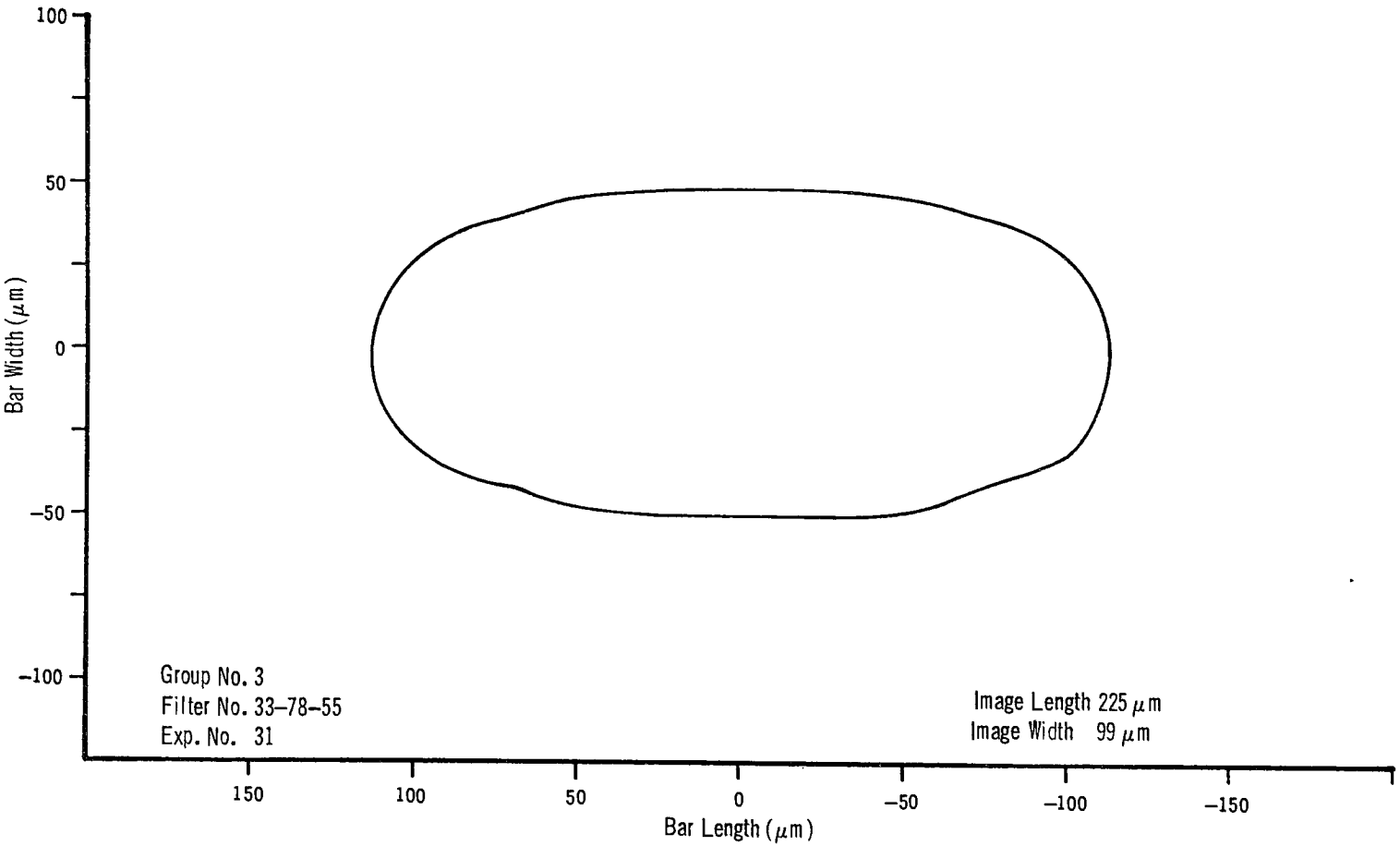

Figure 10-18. Reconstructed Image Shape from Length and Width Measurements

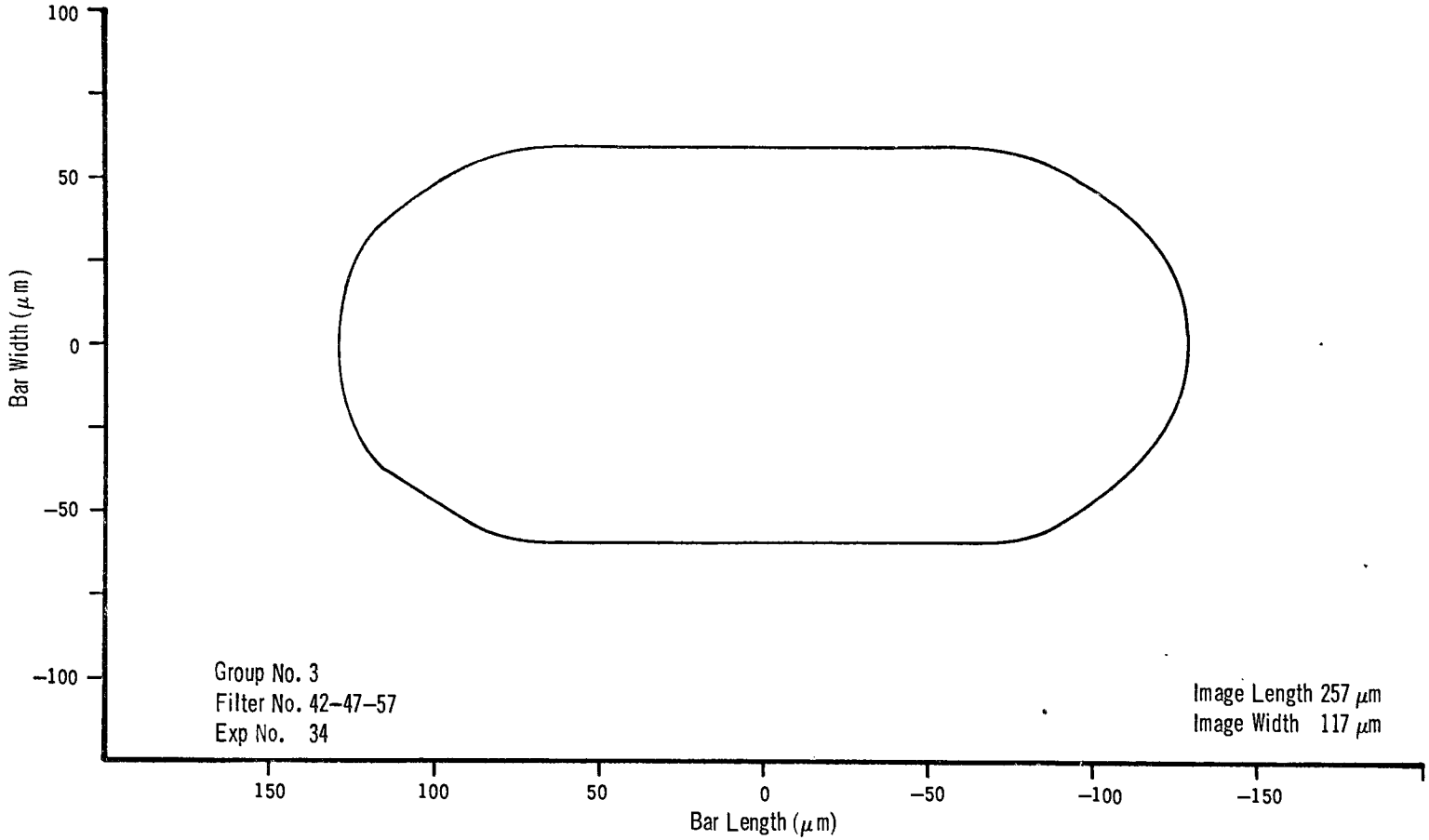

Figure 10-19. Reconstructed Image Shape from Length and Width Measurements

TABLE 10-IX. OBJECTIVE EVALUATION OF GEOMETRICAL SHAPE

Type of Geometrical Analysis	Method Of Analysis	Level Of Exposure	Factor Under Investigation	Calculated F-Ratio	Table F-Ratio	Conclusions From ANOVA
Length	I	Both	S. F. F.	72.50	4.7571	Significant
			G. F.	9.0568	5.1433	Significant
Length	III	Upper	S. F. F.	16.3548	18.5180	Not Significant
			G. F.	3.1290	19.0000	Not Significant
Length	III	Lower	S. F. F.	17.3076	18.5180	Not Significant
			G. F.	7.2564	19.0000	Not Significant
Width	I	Both	S. F. F.	19.9022	4.7571	Significant
			G. F.	0.6737	5.1433	Not Significant
Width	III	Upper	S. F. F.	90.7590	18.5180	Significant
			G. F.	0.3333	19.0000	Not Significant
	III	Lower	S. F. F.	3.9890	18.5180	Not Significant
			G. F.	0.9487	19.0000	Not Significant
Area	I	Both	S. F. F.	20.5020	4.7571	Significant
			G. F.	0.7309	5.1433	Not Significant
Area	III	Upper	S. F. F.	35.7548	18.5180	Significant
			G. F.	0.4497	19.0000	Not Significant
Area	III	Lower	S. F. F.	5.6165	18.5180	Not Significant
			G. F.	3.5105	19.0000	Not Significant

calculations are deferred to Appendix VII. The response variables that are utilized are geometrical measures consisting of lengths, widths, and total areas of the respective bar images.

Referring to Table 10-IX, it will be noted that two methods of ANOVA are used for each of the geometrical measures. Each of these methods has previously been discussed and will only be outlined in this section. Method I treats all four of the source/filter factors on an equal-level basis, whereas Method III treats the four source/filter factors as two sets of two level components — the first set at an upper exposure level (filters 4043 and 42-47-57), and the second set at a lower exposure level (filters 33-78-54 and 33-78-55). Thus, the purpose of Method I is to emphasize that significant geometrical changes take place due to exposure and temporal coherence differences between the four source/filter factors. Method III becomes more specific by emphasizing that some of these geometrical changes can be attributed directly to changes in the temporal coherence.

In each case, the importance of the results obtained for the group factor are secondary to those obtained for the source/filter factor since the primary concern of this investigation is temporal coherence effects and not environmental effects. It is interesting to note, however, that in all but one case, that of the length analysis utilizing Method I, the group factor becomes insignificant due to the F-test results. Thus, it is safe to conclude that the environmental effects on the widths and areas of the reconstructed holograms can be generally neglected, while the effects on the length should be carefully separated from the source/filter effects.

The general results of the Method I analysis show that the four source/filter levels have a significant effect on the lengths, widths, and areas of the reconstructed bars. Since these four levels encompass two significantly large exposure differences, these results were anticipated. When the exposure levels are separated, as in Method II, however, the significance of the temporal coherence effects becomes more evident.

For the upper exposure level (source/filter combinations 4043 and 42-47-57), the geometrical changes that take place between the respective bar widths and bar areas are found to be significant, while those for the bar lengths, even though the F-ratios

are relatively close, are found to be insignificant. For the lower exposure level, no significant geometrical changes are shown to exist.

Thus, for the upper exposure level, the changes in temporal coherence between the source/filter combinations 4043 and 42-47-57, as shown in Figure 7-2 and Table 10-V, significantly affect the geometrical widths and areas of the reconstructed real images.

CHAPTER XI

CONCLUSION

The primary purpose of this investigation was an experimental evaluation of the effects of slight changes in temporal coherence on Fourier transform holograms and their respective real images. After a review of some of the theoretical aspects of Fourier transform holography, partial coherence, and temporal coherence effects, the experimental holographic system was described and some of the system limitations were discussed. This was followed by a detailed description of the methods of analysis employed to obtain meaningful results from the experimental data presented.

A summarization of the results of the analysis performed on the experimental data is given in Table 11-I. Note that as the coherence length of the source increases, the spectral width becomes narrower and the real-image bar widths and areas increase to obtain the rectangular shape of the original object.

TABLE 11-I. SUMMARY OF EXPERIMENTAL RESULTS

Coherence Length (micrometers)	Spectral Width $(\text{micrometer})^{-1}$	Averaged Density of Hologram Fringes	Average Bar Widths of Real Images (micrometers)	Average Areas of of Real Images (micrometers)
31.9	0.4513	2.03	128	33,250
28.6	0.5005	2.21	117	27,327
20.4	0.5824	2.34	108	22,656
15.4	0.7644	2.35	97	19,261

Through the application of Analysis of Variance, ANOVA, a significant change was shown to exist for: (1) The average densities of the holograms, (2) the bar widths of the real images, and (3) the bar areas of the real images; these were due to changes that occurred between the first two coherence lengths and spectral widths listed in Table 1-I. These first two sets of values were considered to be at a higher exposure level than the last two sets of values, as indicated by the lower average densities of the hologram fringes obtained through the previously described photographic reversal process.

For the lower exposure level (i. e. , the last two coherence lengths and respective spectral widths listed in Table 11-I), the methods of ANOVA indicated that no significant change occurred between either the hologram densities or the respective real-image geometric parameters. This is verified by the values of 2. 34 and 2. 35 obtained for the last two hologram densities. However, for the average real-image bar widths, a change of 11 micrometers occurred between the two values at the lower exposure level, which is equivalent to the 11-micrometer change that occurred at the higher exposure level. The fact that the ANOVA did not consider this change to be significant at the lower exposure level is attributed to the value of 45. 50 calculated for the residual error term at this exposure level, in comparison to the value of 1. 99 calculated for the residual error term at the higher exposure value. Close examination of the experimental data indicates that the variability between bar-width values at the lower exposure level is much greater than the variability between these same measurements at the upper exposure level.

Thus, at the higher exposure level, where the real images have approximately reached the rectangular shape of the original object, slight changes in the source coherence length and spectral width significantly changes: (1) The average hologram fringe density, (2) the bar widths of the real images, and (3) the areas of the real images. At the lower exposure level, where the real images have blurred edges and are still approaching the rectangular shape of the original object, the changes in coherence length and spectral width of the source are not of great enough magnitude to indicate significant changes in image shape.

BIBLIOGRAPHY

1. D. Gabor, "Microscopy by Reconstructed Wave-Fronts", Proceedings of the Royal Society (London), A197, 454-487 (1949).

2. D. Gabor, "Microscopy by Reconstructed Wave-Fronts II", Proceedings of the Physical Society, B64, Part 6, 449-469 (1951).

3. E. N. Oeith and J. Upatnieks, "Reconstructed Wave-Fronts and Communication Theory", J. Opt. Soc. Am., 52, 1123-1130 (1962).

4. J. B. DeVelis and G. O. Reynolds, Theory and Applications of Holography, Addison-Wesley Publishing Co., Inc., Reading, Mass. (1967).

5. E. N. Leith and J. Upatnieks, "Holography", Lecture Notes from Introduction to Optical Data Processing, University of Michigan (1966).

6. E. N. Leith and J. Upatnieks, "Wave-Front Reconstruction with Continuous Tone Objects", J. Opt. Soc. Am., 53, 1377-1381 (1963).

7. W. E. Kock, "Fundamentals of Holography", Laser Focus, 26-34, February (1969).

8. E. B. Champagne, "A Qualitative and Quantitative Study of Holographic Imaging", Ph.D. Thesis, Ohio State University (1967).

9. J. C. Wyant and M. P. Givens, "Effect of the Photographic Gamma on the Luminance of Hologram Reconstructions", J. Opt. Soc. Am., 58, 357 (1968).

10. R. F. van Ligten, "Influence of Photographic Film on Wavefront Reconstruction. I. Plane Wavefronts", J. Opt. Soc. Am., 56, 1 (1966).

11. J. W. Goodman, "Introduction to Fourier Optics", McGraw-Hill Book Co., New York, N. Y. (1968).

12. M. Lurie, "Fourier-Transform Holograms with Partially Coherent Light: Holographic Measurement of Spatial Coherence", J. Opt. Soc. Am., 58, 614-619 (1968).

13. D. Corson and P. Lorrain, Introduction to Electromagnetic Fields and Waves, W. H. Freeman & Co., San Francisco and London (1962).

14. M. Born and E. Wolf, Principles of Optics (3rd Ed.) Pergamon Press, New York (1964).

15. M. J. Beran and G. B. Parrent, Jr., Theory of Partial Coherence, Prentice Hall, Inc., Englewood Cliffs, N. J., (1964).

16. E. L. O'Neill, Introduction to Statistical Optics, Addison-Wesley Publishing Co., Inc., Reading, Mass., (1963).

17. T. J. Skinner, "Energy Considerations, Propagation in a Random Medium and Imaging in Scalar Coherence Theory", PH. D. Thesis, Boston University (1964).

18. F. Zernike, "Diffraction and Optical Image Formation", Proc. Phys. Soc., 61, Part 2, 158-164 (1948).

19. B. Thompson, "Illustration of the Phase Change in Two-Beam Interference with Partially Coherent Light", J. Opt. Soc. Am., 48, 95-97 (1958).

20. B. Thompson and E. Wolf, "Two-Beam Interference with Partially Coherent Light", J. Opt. Soc. Am., 47, 895 (1957).

21. J. B. Develis and B. J. Thompson, "Introduction to Coherent Optics and Holography", Paper presented to the Society of Automotive Engineers, Jan. 8-12, 1968.

22. R. B. Blackman and J. W. Tukey, The Measurement of Power Spectra, Dover Publications, Inc., New York (1958).

23. E. Wolfe and E. W. Marchand, "Comparison of the Kirchoff and the Rayleigh-Sommerfield Theories of Diffraction at an Aperture", J. Opt. Soc. Am., 54, 587, (1964).

24. P. Moon, The Scientific Basis of Illuminating Engineering, Dover Publications, Inc., New York, N. Y. (1961).

25. J. W. T. Walsh, Photometry, Dover Publications, Inc., New York, N. Y. (1958).

26. H. M. Smith, Principles of Holography, John Wiley & Sons, Inc., New York, N. Y. (1969).

27. "Kodak Plates and Films for Science and Industry", Eastman Kodak Publication No. P-9, 1967.

28. Mees and James, Theory of the Photographic Process, The Macmillan Company, New York, N. Y. (1966).

29. A. Kozma, "Photographic Recording of Spatially Modulated Coherent Light", J. Opt. Soc. Am., 56, 428-432 (1966).

30. A. A. Friesem and J. S. Zelenka, "Effects of Some Photographic Characteristics on the Light Flux in a Holographic Image", J. Opt. Soc. Am., 58, 970-976 (1968).

31. J. W. Goodman and G. R. Knight, "Effects of Film Nonlinearities on Wavefront-Reconstruction Images of Diffuse Objects", J. Opt. Soc. Am., 58, 1276-1283 (1968).

32. G. R. Knight, "Effects of Film Nonlinearities in Wavefront Reconstruction Imaging", Ph. D. Thesis, Stanford University (1967).

33. A. P. Rickmers and H. N. Todd, Statistics, An Introduction, McGraw-Hill Book Company, New York, N. Y. (1967).

34. A. J. Duncan, Quality Control and Industrial Statistics, Richard D. Irwin, Inc., Homewood, Illinois (1965).

APPENDIX I

PHOTOGRAPHIC PROCESSING PROCEDURE

APPENDIX I

PHOTOGRAPHIC PROCESSING PROCEDURE

	Procedure	Temperature (°F)	Time (min.)	Total Time
1.	First Developer — Kodak DK-50, Full Strength	68 ± 1/2	6	6
2.	Wash — Running Water	65 - 70	2	8
3.	Bleach — Kodak Bleach Bath R-9	65 - 70	2	10
4.	Rinse — Running Water	65 - 70	1/2	10-1/2
5.	Clear — Kodak Clearing Bath CB-6	65 - 70	3	13-1/2
	Remaining steps can be completed in normal room light.			
6.	Wash and Reversal Exposure* — Running Water	65 - 70	4	17-1/2
7.	Second Developer — Kodak D-8, Diluted 1:1	65 - 70	2	19-1/2
8.	Fix — Kodak Rapid Fix	65 - 70	2	21-1/2
9.	Wash — Running Water	65 - 70	5	26-1/2
10.	Dry	Less than 110	As required	

*With film in wash, expose to a No. 212 or 302 enlarging lamp for 30 seconds at a distance of 2-1/2 feet (30 to 40 foot-candles).

APPENDIX II

SPECTRAL CHARACTERISTICS OF INTERFERENCE FILTERS

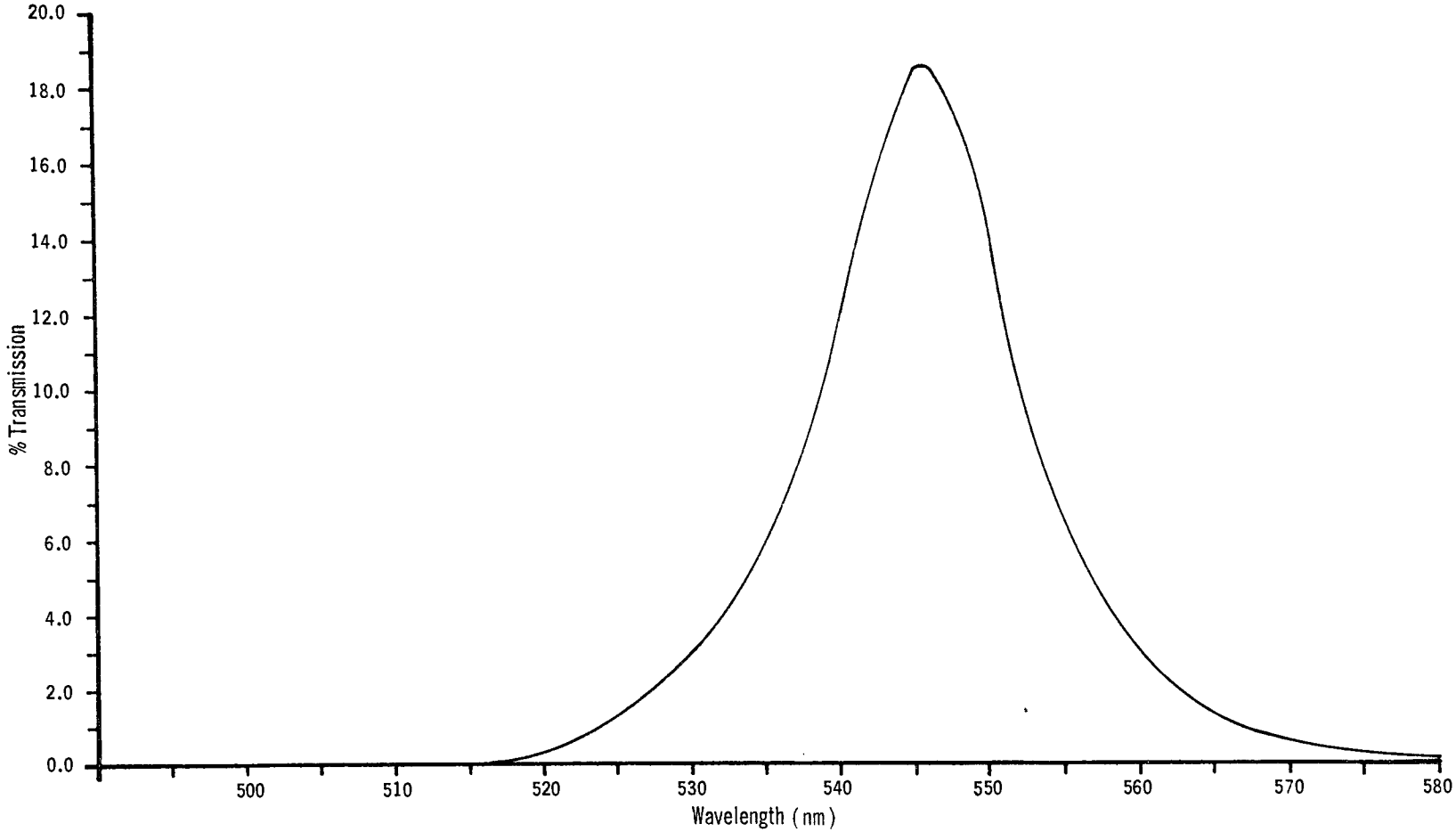

Spectrophotometric Measurements for Filter No. 4043

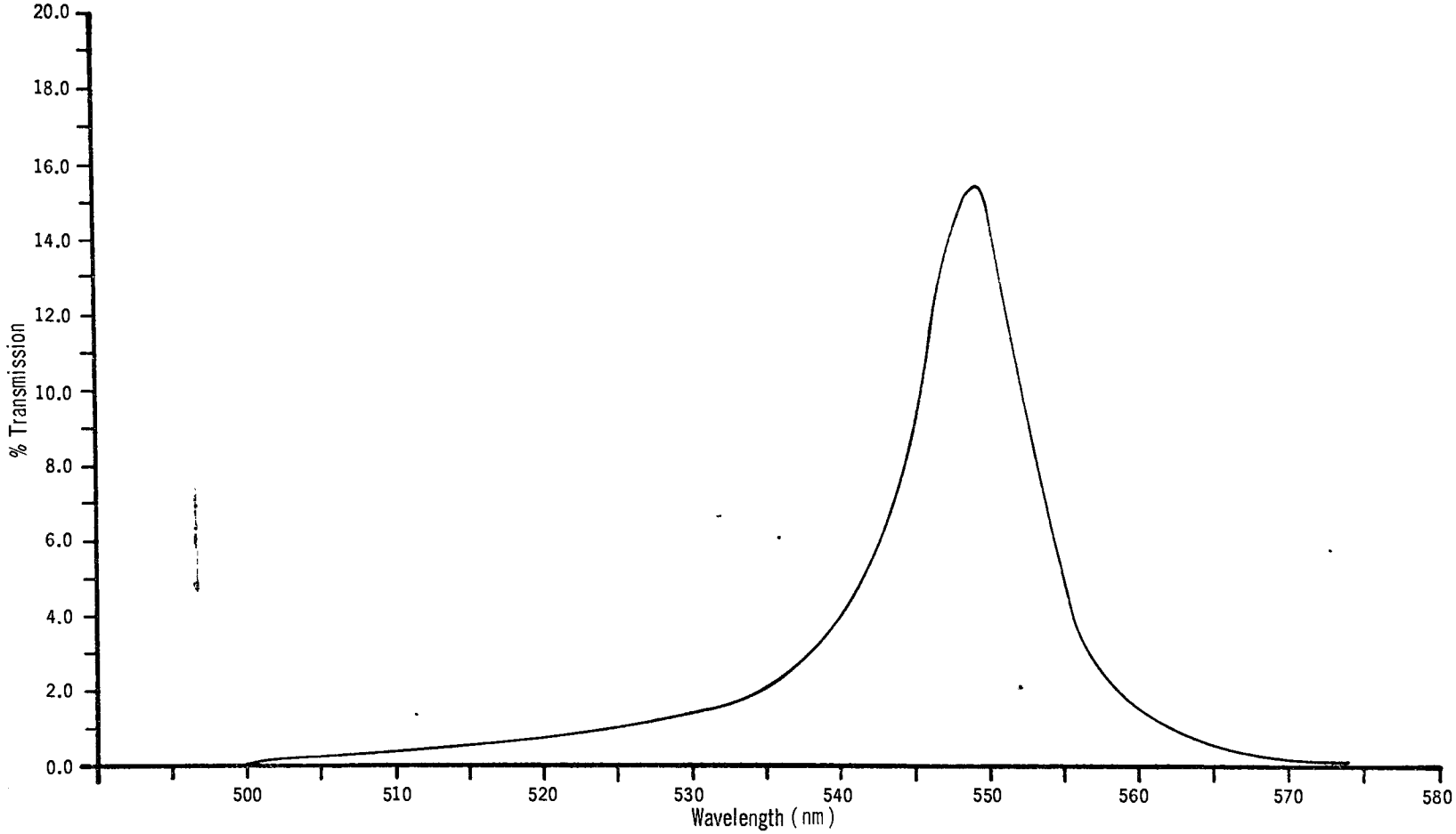

Spectrophotometric Measurements for Filter No. 42-47-57

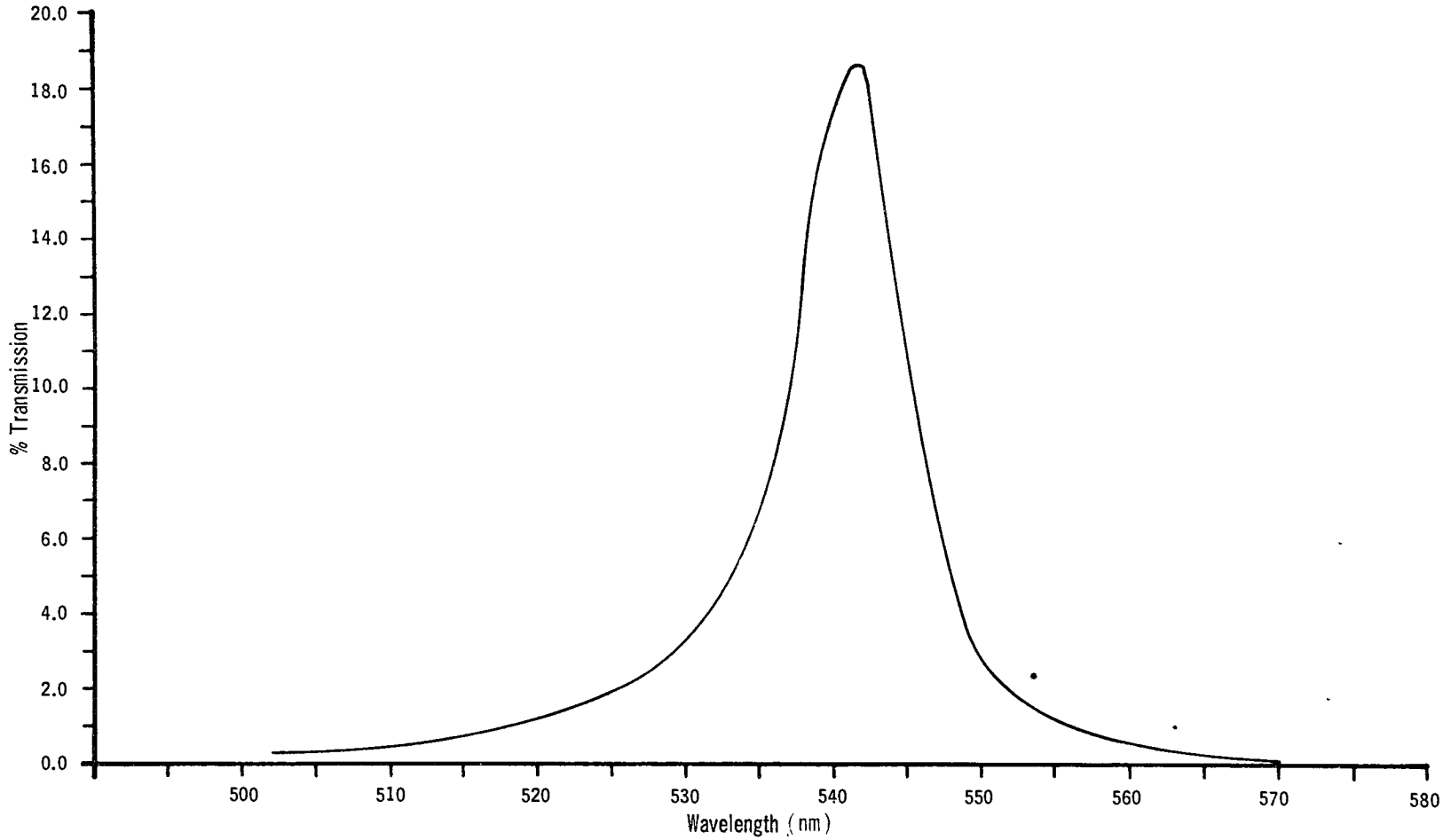

Spectrophotometric Measurements for Filter No. 33-78-54

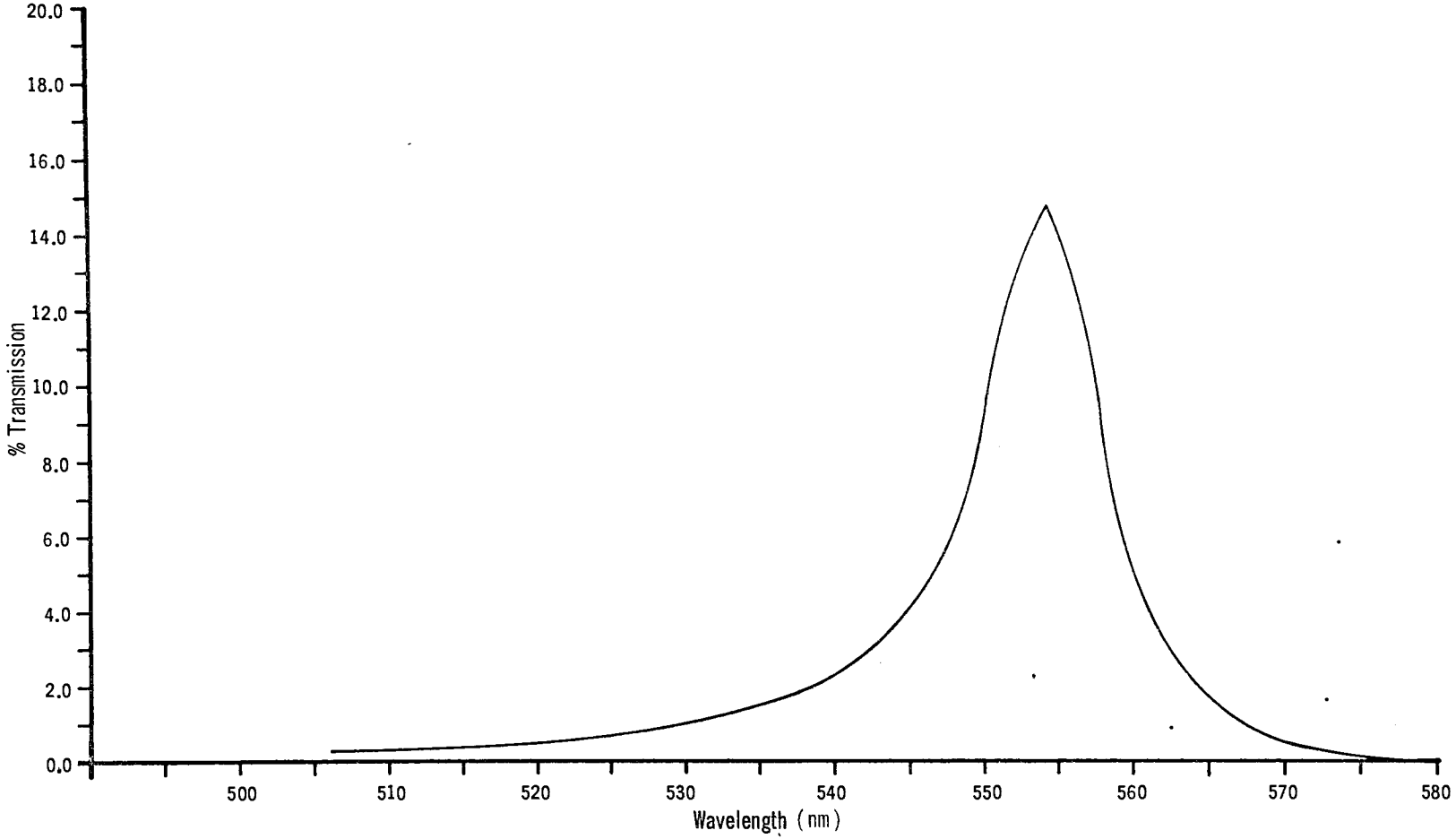

Spectrophotometric Measurements for Filter No. 33-78-55

APPENDIX III

EXPERIMENTAL APPARATUS FOR TEMPORAL COHERENCE MEASUREMENTS

APPENDIX III

EXPERIMENTAL APPARATUS

1. Michelson Interferometer — Ealing No. 25-700
2. Low-Pressure Mercury Arc Source — Tech/Ops
3. Photomultiplier Assembly — RCA
4. Power Supply — Universal No. 401
5. Photomultiplier Meter — Aminco American Instrument Corp.
6. Kodak Gelatin Filter — No. 58 Green
7. Interference Filters — Bausch & Lomb
   A. 33-78-54
   B. 33-78-55
   C. 42-47-57
8. Interference Filter — Optics Technology — Set 10A 4043
9. X-Y Mount — Tech/Ops
10. Optical Bench — 3 Meter — Tech/Ops
11. 50 mm Collimating Lens and Lens Mount
12. Micro-Optical Bench — RIT — No. 10-171

APPENDIX IV

VISIBILITY MEASUREMENTS

APPENDIX IV

VISIBILITY MEASUREMENTS

	Measurement No. 1 Filter No. 4043			Measurement No. 2 Filter No. 33-78-54		
Fringe Order	I-max	I-min	Visibility	I-max	I-min	Visibility
0	81.0	22.0	1.0000	80.0	22.0	1.0000
1	81.0	22.5	0.9832	80.0	23.0	0.9661
5	80.5	24.0	0.9339	79.0	25.5	0.8841
10	77.0	26.5	0.8487	74.0	29.0	0.7627
15	74.0	28.0	0.7931	70.0	31.5	0.6696
20	72.5	30.0	0.7265	67.0	35.0	0.5517
25	70.0	32.5	0.6410	65.5	38.5	0.4500
30	68.0	33.5	0.6000	62.5	40.0	0.3846
35	66.5	35.0	0.5478	62.0	42.0	0.3333
40	65.0	36.5	0.4956	61.0	43.5	0.2892
45	63.5	38.0	0.4435	60.0	43.0	0.2881
50	62.0	39.5	0.3913	58.0	43.5	0.2522
55	61.5	40.5	0.3621			
60	60.0	41.5	0.3217			
65	58.5	42.0	0.2020			
70	58.0	43.5	0.2522			
	Meter Multiplier — 0.03 Sensitivity — 33			Meter Multiplier — 0.01 Sensitivity — 20		

Fringe Order	Measurement No. 3 Filter No. 33-78-54 I-max	I-min	Visibility	Measurement No. 4 Filter No. 33-78-54 I-max	I-min	Visibility
0	78.5	20.0	1.0000	83.0	22.0	1.0000
1	78.5	21.0	0.9664	83.0	22.5	0.9837
5	73.5	23.5	0.8772	80.0	24.0	0.9333
10	71.5	27.0	0.7607	77.0	28.5	0.7886
15	69.0	30.0	0.6610	73.5	31.0	0.7025
20	66.0	33.0	0.5593	70.5	33.0	0.6302
25	63.5	35.5	0.4746	68.5	38.0	0.4880
30	61.5	38.0	0.3950	66.0	40.5	0.4080
35	59.0	40.0	0.3220	63.0	43.0	0.3226
40	59.0	42.5	0.2683	61.0	44.0	0.2787
45	58.0	43.0	0.2459	59.0	45.0	0.2333
50	57.0	43.0	0.2333	59.0	45.0	0.2333
	Meter Multiplier — 0.01 Sensitivity — 20			Meter Multiplier — 0.01 Sensitivity — 20		

Fringe Order	Measurement No. 5 Filter No. 4043 I-max	I-min	Visibility	Measurement No. 6 Filter No. 33-78-55 I-max	I-min	Visibility
0	82.0	23.0	1.0000	72.0	20.0	1.0000
1	80.0	24.0	0.9655	71.0	21.5	0.9428
5	78.5	26.0	0.8974	68.0	25.5	0.7944
10	76.0	28.0	0.8276	65.5	29.0	0.6697
15	73.0	30.0	0.7544	62.0	31.0	0.5849
20	70.5	33.0	0.6522	58.0	34.0	0.4615
25	68.0	35.0	0.5789	56.0	37.0	0.3585
30	66.0	37.0	0.5088	52.0	40.0	0.2307
35	64.0	37.5	0.4775			
40	62.0	38.5	0.4312			
45	60.5	40.5	0.3636			
50	60.0	42.0	0.3214			
55	58.5	43.0	0.2793			
60	56.0	43.5	0.2336			
	Meter Multiplier — 0.03 Sensitivity — 33			Meter Multiplier — 0.01 Sensitivity — 20		

Fringe Order	Measurement No. 7 Filter No. 33-78-55 I-max	I-min	Visibility	Measurement No. 8 Filter No. 4043 I-max	I-min	Visibility
0	72.0	19.0	1.0000	79.0	22.0	1.0000
1	71.5	19.5	0.9811	78.5	22.5	0.9824
5	67.0	23.0	0.8462	75.0	23.5	0.9450
10	63.0	26.0	0.7255	72.0	26.0	0.8518
15	60.0	29.0	0.6078	70.0	27.5	0.7944
20	56.0	33.0	0.4510	67.5	29.5	0.7170
25	52.0	37.5	0.2816	65.5	31.5	0.6145
30	50.0	39.0	0.2157	64.0	33.5	0.5701
35				62.0	35.0	0.5094
40				60.5	36.0	0.4666
45				60.0	37.5	0.4206
50				58.0	38.5	0.3714
55				56.5	40.0	0.3143
60				55.0	40.5	0.2816
65				53.5	41.0	0.2475

Meter Multiplier — 0.01
Sensitivity — 20

Meter Multiplier — 0.03
Sensitivity — 33

Fringe Order	Measurement No. 9 Filter No. 42-47-57 I-max	I-min	Visibility	Measurement No. 10 Filter No. 4043 I-max	I-min	Visibility
0	82.5	21.5	1.0000	73.0	20.0	1.0000
1	82.0	22.0	0.9836	72.0	21.0	0.9623
5	80.5	23.5	0.9344	69.0	21.5	0.9406
10	76.0	25.5	0.8632	67.0	24.0	0.8431
15	73.0	28.0	0.7759	65.5	26.5	0.7500
20	71.0	30.0	0.7069	63.5	28.0	0.6893
25	68.5	33.0	0.6068	62.0	29.5	0.6311
30	65.5	34.5	0.5439	60.0	31.0	0.5686
35	64.0	36.5	0.4783	58.5	32.5	0.5098
40	62.0	38.0	0.4210	57.0	33.5	0.4653
45	61.0	40.0	0.3621	55.5	34.5	0.4200
50	59.0	42.5	0.2820	54.0	35.0	0.3878
55	58.0	43.5	0.2479	53.0	36.0	0.3469
60	55.5	44.5	0.1930	52.5	37.0	0.3131
65				51.5	38.0	0.2727
	Meter Multiplier — 0.03 Sensitivity — 45			Meter Multiplier — 0.03 Sensitivity — 33		

Fringe Order	Measurement No. 11 Filter No. 33-78-54 I-max	I-min	Visibility	Measurement No. 12 Filter No. 42-47-57 I-max	I-min	Visibility
0	70.0	18.0	1.0000	76.0	21.0	1.0000
1	70.0	18.5	0.9810	76.0	21.5	0.9820
5	70.0	21.5	0.8739	71.5	22.0	0.9612
10	67.0	24.0	0.7818	70.0	24.5	0.8667
15	64.5	27.0	0.6757	68.0	25.5	0.8252
20	62.0	30.0	0.5714	66.0	27.0	0.7647
25	59.5	32.0	0.4955	64.0	29.5	0.6699
30	57.0	35.5	0.3805	61.5	31.5	0.5882
35	54.5	38.0	0.2902	59.5	33.5	0.5098
40	53.5	38.5	0.2678	57.5	34.5	0.4600
45	51.0	38.0	0.2453	55.5	36.0	0.3939
50	49.5	38.5	0.2115	54.5	37.5	0.3400
55				54.0	40.0	0.2692
60				52.0	41.0	0.2157
	Meter Multiplier — 0.01 Sensitivity — 20			Meter Multiplier — 0.03 Sensitivity — 45		

Fringe Order	Measurement No. 13 Filter No. 42-47-57 I-max	I-min	Visibility	Measurement No. 14 Filter No. 4043 I-max	I-min	Visibility
0	74.5	17.0	1.0000	89.5	31.0	1.0000
1	77.0	18.0	0.9672	90.0	32.0	0.9667
5	74.0	20.0	0.9000	87.0	33.0	0.9310
10	72.0	22.0	0.8333	84.0	36.0	0.8276
15	69.0	24.0	0.7627	82.0	38.5	0.7436
20	66.5	27.0	0.6639	80.0	41.0	0.6610
25	65.0	27.5	0.6410	78.0	42.5	0.6068
30	63.5	31.0	0.5372	74.5	45.0	0.5130
35	61.0	32.5	0.4790	73.5	45.5	0.4912
40	60.0	34.0	0.4333	71.0	47.0	0.4286
45	57.5	36.0	0.3613	69.0	48.0	0.3818
50	57.0	39.0	0.2903	67.0	48.5	0.3458
55	55.5	38.5	0.2833	66.5	50.0	0.2909
60	54.5	40.0	0.2397	65.0	51.0	0.2592
65				64.5	52.0	0.2294
	Meter Multiplier — 0.03 Sensitivity — 45			Meter Multiplier — 0.03 Sensitivity — 30		

Fringe Order	Measurement No. 15 Filter No. 42-47-57 I-max	I-min	Visibility	Measurement No. 16 Filter No. 42-47-57 I-max	I-min	Visibility
0	80.0	27.0	1.0000	84.0	28.0	1.0000
1	78.5	27.5	0.9808	84.5	29.0	0.9652
5	75.0	28.0	0.9592	82.5	30.0	0.9292
10	70.5	29.0	0.9121	78.5	32.0	0.8532
15	69.0	31.0	0.8261	76.5	34.5	0.7636
20	66.0	33.0	0.7333	75.0	36.5	0.6937
25	65.0	34.5	0.6703	73.0	39.0	0.6071
30	63.0	36.5	0.5824	72.0	40.5	0.5575
35	62.5	38.0	0.5269	69.0	42.0	0.4909
40	60.0	39.0	0.4667	66.0	44.0	0.4074
45	58.5	40.0	0.4157	65.0	44.5	0.3832
50	57.0	41.0	0.3636	63.5	46.0	0.3271
55	55.0	43.0	0.2727	61.0	48.0	0.2453
	Meter Multiplier — 0.03 Sensitivity — 40			Meter Multiplier — 0.03 Sensitivity — 40		

Fringe Order	Measurement No. 17 Filter No. 33-78-54 I-max	I-min	Visibility	Measurement No. 18 Filter No. 33-78-54 I-max	I-min	Visibility
0	83.5	27.5	1.0000	84.0	27.5	1.0000
1	83.5	28.0	0.9823	83.5	28.0	0.9823
5	83.0	31.5	0.8655	83.0	29.0	0.9474
10	80.0	34.0	0.7797	79.0	32.0	0.8393
15	76.0	38.0	0.6441	76.0	35.0	0.7321
20	73.0	41.0	0.5424	73.0	38.5	0.6106
25	70.0	44.0	0.4407	68.0	43.0	0.4464
30	67.5	46.0	0.3675	67.0	45.0	0.3860
35	66.0	48.0	0.3051	65.0	47.0	0.3158
40	65.0	48.5	0.2820	63.5	48.5	0.2632
45	64.5	49.0	0.2650	63.5	50.0	0.2308
50	63.0	50.0	0.2241	63.0	51.0	0.2034
	Meter Multiplier — 0.01 Sensitivity — 20			Meter Multiplier — 0.01 Sensitivity — 20		

Fringe Order	Measurement No. 19 Filter No. 33-78-54 I-max	I-min	Visibility	Measurement No. 20 Filter No. 33-78-54 I-max	I-min	Visibility
0	79.0	26.0	1.0000	80.5	27.0	1.0000
1	80.0	27.0	0.9636	80.0	27.5	0.9813
5	78.5	29.0	0.8919	77.0	29.0	0.9231
10	76.5	32.0	0.7876	74.0	32.0	0.8077
15	72.5	34.5	0.6909	71.5	35.0	0.6952
20	70.0	37.0	0.6000	70.0	37.0	0.6226
25	67.0	42.0	0.4386	67.0	39.5	0.5238
30	67.0	44.0	0.3898	65.0	43.0	0.4074
35	65.0	45.0	0.3445	62.5	45.0	0.3271
40	62.0	46.5	0.2743	61.0	46.0	0.2830
45	61.0	46.5	0.2613	60.0	47.0	0.2453
50	59.0	47.0	0.2222	58.5	48.0	0.2000

Meter Multiplier — 0.01
Sensitivity — 20

Meter Multiplier — 0.01
Sensitivity — 20

Fringe Order	Measurement No. 21 Filter No. 4043 I-max	I-min	Visibility	Measurement No. 22 Filter No. 42-47-57 I-max	I-min	Visibility
0	76.0	27.0	1.0000	70.0	23.5	1.0000
1	75.5	28.0	0.9596	68.5	24.5	0.9565
5	72.0	28.0	0.9565	66.5	24.5	0.9545
10	68.5	29.0	0.9080	65.0	25.0	0.9302
15	67.0	31.0	0.8182	63.0	28.0	0.7954
20	65.0	33.0	0.7273	62.0	29.0	0.7500
25	62.0	35.0	0.6279	59.5	31.0	0.6552
30	62.0	37.0	0.5556	59.0	33.0	0.5778
35	60.0	37.0	0.5349	57.0	35.0	0.4889
40	59.0	38.5	0.4713	55.0	37.0	0.4000
45	58.0	40.0	0.4091	54.0	38.0	0.3556
50	56.0	40.0	0.3810	53.0	39.0	0.3111
55	55.5	40.5	0.3571	51.0	41.0	0.2222
60	55.0	41.5	0.3176			
65	53.5	42.0	0.2771			
	Meter Multiplier — 0.03 Sensitivity — 30			Meter Multiplier — 0.03 Sensitivity — 40		

Fringe Order	Measurement No. 23 Filter No. 42-47-57 I-max	I-min	Visibility	Measurement No. 24 Filter No. 33-78-54 I-max	I-min	Visibility
0	69.0	23.5	1.0000	90.0	31.0	1.0000
1	67.0	24.0	0.9773	88.0	32.0	0.9655
5	65.0	24.5	0.9529	90.0	36.0	0.8438
10	65.0	27.0	0.8444	85.5	37.0	0.8016
15	63.0	28.5	0.7751	80.5	40.0	0.6923
20	61.0	30.0	0.7045	77.0	43.0	0.5862
25	59.0	32.0	0.6136	74.0	46.0	0.4828
30	56.5	33.0	0.5529	70.0	48.0	0.3928
35	54.0	34.5	0.4699	69.0	50.5	0.3217
40	52.5	35.0	0.4321	67.0	52.0	0.2632
45	51.5	36.0	0.3827	66.5	51.5	0.2545
50	50.5	38.0	0.3012	64.5	54.0	0.1858
	Meter Multiplier — 0.03 Sensitivity — 40			Meter Multiplier — 0.01 Sensitivity — 20		

Fringe Order	Measurement No. 25 Filter No. 33-78-55 I-max	I-min	Visibility	Measurement No. 26 Filter No. 33-78-54 I-max	I-min	Visibility
0	84.0	26.0	1.0000	84.5	29.0	1.0000
1	82.0	27.0	0.9649	84.5	29.5	0.9821
5	80.0	31.0	0.8305	83.0	31.0	0.9286
10	75.0	34.5	0.7043	79.0	34.0	0.8182
15	70.5	38.0	0.5752	76.0	37.5	0.6937
20	67.5	41.0	0.4690	72.0	42.0	0.5357
25	63.5	44.5	0.3393	71.0	45.5	0.4359
30	61.0	47.5	0.2389	67.0	48.0	0.3333
35				65.5	50.0	0.2696
40				64.5	50.5	0.2456
45				63.5	51.5	0.2105
	Meter Multiplier — 0.01 Sensitivity — 20			Meter Multiplier — 0.01 Sensitivity — 20		

Fringe Order	Measurement No. 27 Filter No. 33-78-55 I-max	I-min	Visibility	Measurement No. 28 Filter No. 4043 I-max	I-min	Visibility
0	80.0	28.0	1.0000	86.0	31.5	1.0000
1	78.5	29.0	0.9612	86.0	32.5	0.9640
5	74.5	33.0	0.8058	82.0	32.5	0.9612
10	71.0	36.5	0.6699	79.5	34.5	0.8824
15	66.0	40.5	0.5050	76.0	36.0	0.8163
20	61.5	44.0	0.3535	73.0	38.5	0.7113
25	58.0	46.0	0.2500	71.0	40.0	0.6458
30	58.0	47.5	0.2121	69.0	42.0	0.5625
35				67.5	43.0	0.5158
40				65.5	44.0	0.4624
45				65.0	45.5	0.4102
50				64.5	47.0	0.3608
55				63.0	47.0	0.3404
60				61.5	48.0	0.2903

Meter Multiplier — 0.01
Sensitivity — 20

Meter Multiplier — 0.03
Sensitivity — 33

Fringe Order	Measurement No. 29 Filter No. 33-78-55 I-max	I-min	Visibility	Measurement No. 30 Filter No. 33-78-55 I-max	I-min	Visibility
0	81.0	27.5	1.0000	76.5	25.5	1.0000
1	78.0	28.0	0.9804	75.5	26.0	0.9802
5	75.0	30.5	0.8812	71.5	29.0	0.8586
10	71.0	33.0	0.7755	69.5	33.0	0.7087
15	67.0	35.5	0.6632	65.0	35.0	0.6122
20	63.5	39.0	0.5158	63.0	37.5	0.5152
25	60.0	41.5	0.3978	59.5	42.0	0.3465
30	57.0	44.0	0.2826	57.0	44.0	0.2600
	Meter Multiplier — 0.01 Sensitivity — 20			Meter Multiplier — 0.01 Sensitivity — 20		

Fringe Order	Measurement No. 31 Filter No. 33-78-55 I-max	I-min	Visibility	Measurement No. 32 Filter No. 4043 I-max	I-min	Visibility
0	72.0	25.0	1.0000	87.0	29.0	1.0000
1	70.5	25.5	0.9785	85.0	29.5	0.9823
5	67.5	27.0	0.9101	82.5	30.5	0.9454
10	64.0	34.5	0.7528	80.0	33.0	0.8545
15	61.0	33.0	0.6364	77.5	35.0	0.7798
20	58.0	34.5	0.5516	75.5	37.0	0.7064
25	56.0	38.0	0.4091	72.5	39.5	0.6111
30	52.0	40.0	0.2857	71.0	41.0	0.5556
35				68.5	42.0	0.5048
40				67.5	43.0	0.4667
45				66.0	44.5	0.4095
50				65.0	46.0	0.3585
55				65.0	47.5	0.3211
60				63.5	48.5	0.2778
	Meter Multiplier — 0.01 Sensitivity — 20			Meter Multiplier — 0.03 Sensitivity — 33		

Fringe Order	Measurement No. 33 Filter No. 42-47-57 I-max	I-min	Visibility	Measurement No. 34 Filter No. 42-47-57 I-max	I-min	Visibility
0	85.0	27.5	1.0000	82.0	26.5	1.0000
1	83.0	28.5	0.9646	82.0	27.0	0.9821
5	80.5	29.5	0.9273	79.0	28.5	0.9266
10	78.5	31.5	0.8545	78.0	31.0	0.8393
15	75.0	33.0	0.7924	76.0	32.5	0.7838
20	74.0	35.0	0.7222	73.5	34.5	0.7091
25	72.0	37.5	0.6330	72.5	37.0	0.6283
30	70.0	39.5	0.5596	69.5	38.0	0.5780
35	69.0	41.0	0.5091	68.0	40.5	0.4955
40	67.5	42.5	0.4545	66.5	42.0	0.4414
45	66.0	44.0	0.4000	64.0	43.5	0.3761
50	63.5	45.0	0.3458	62.0	45.5	0.3028
55	62.0	46.0	0.3019	62.0	47.5	0.2566
60	61.5	47.0	0.2710	59.5	48.0	0.2110
65	60.0	48.0	0.2264			
	Meter Multiplier — 0.03 Sensitivity — 45			Meter Multiplier — 0.03 Sensitivity — 45		

Fringe Order	Measurement No. 35 Filter No. 33-78-55 I-max	I-min	Visibility	Measurement No. 36 Filter No. 4043 I-max	I-min	Visibility
0	73.0	23.5	1.0000	78.5	28.0	1.0000
1	73.0	24.5	0.9604	78.0	28.5	0.9802
5	69.0	26.0	0.8958	76.5	29.5	0.9400
10	66.5	29.5	0.7551	73.5	31.5	0.8571
15	63.0	31.5	0.6632	71.0	33.0	0.7917
20	59.5	33.5	0.5652	68.5	34.5	0.7234
25	56.5	36.0	0.4505	67.0	36.5	0.6421
30	54.5	38.0	0.3626	65.0	38.5	0.5579
35				64.0	40.0	0.5000
40				62.5	41.5	0.4375
45				61.0	43.0	0.3750
50				60.0	43.5	0.3474
55				59.5	44.0	0.3263
60				58.5	45.0	0.2842

Meter Multiplier — 0.01
Sensitivity — 20

Meter Multiplier — 0.03
Sensitivity — 33

Fringe Order	Measurement No. 37 Filter No. 4043 I-max	I-min	Visibility	Measurement No. 38 Filter No. 33-78-55 I-max	I-min	Visibility
0	74.0	27.0	1.0000	68.5	23.0	1.0000
1	74.0	28.0	0.9583	68.0	23.5	0.9780
5	71.0	29.0	0.9130	67.0	23.5	0.9775
10	69.0	30.5	0.8462	63.0	27.5	0.7978
15	67.0	32.0	0.7778	60.0	30.0	0.6818
20	65.0	33.5	0.7079	57.0	33.0	0.5454
25	63.0	35.0	0.6364	53.0	36.5	0.3793
30	61.0	36.5	0.5632	52.0	39.5	0.2747
35	60.0	37.0	0.5349			
40	58.5	38.5	0.4651			
45	57.0	39.0	0.4286			
50	57.0	41.0	0.3636			
55	56.0	41.5	0.3333			
60	55.0	42.0	0.3023			
	Meter Multiplier — 0.03 Sensitivity — 33			Meter Multiplier — 0.01 Sensitivity — 20		

Fringe Order	Measurement No. 39 Filter No. 33-78-55 I-max	I-min	Visibility	Measurement No. 40 Filter No. 42-47-57 I-max	I-min	Visibility
0	71.0	23.0	1.0000	74.0	27.0	1.0000
1	70.0	23.5	0.9789	73.5	27.5	0.9787
5	66.0	25.5	0.8901	71.0	28.0	0.9556
10	62.5	28.5	0.7556	69.5	30.0	0.8681
15	60.0	31.5	0.6264	67.0	31.5	0.7978
20	57.5	34.0	0.5165	65.0	32.5	0.7471
25	54.0	35.0	0.4419	62.5	34.0	0.6706
30	52.0	38.0	0.3182	61.0	35.5	0.6000
35				59.0	37.5	0.5059
40				57.5	39.5	0.4186
45				56.5	40.0	0.3882
50				55.5	41.0	0.3412
55				53.5	41.5	0.2927
60				52.5	43.0	0.2289
	Meter Multiplier — 0.01 Sensitivity — 20			Meter Multiplier — 0.03 Sensitivity — 45		

APPENDIX V

ANOVA OF HOLOGRAPHIC FRINGE DATA

DATA SOURCE: Holographic Fringes METHOD NO. I

RESPONSE VARIABLE: Average Density CASE NO. I

ANOVA TABLES:

Filter Number	Group Number			Totals
	I	II	III	
4043	1.98	2.01	2.09	6.08
42-47-57	2.19	2.14	2.28	6.61
33-78-54	2.30	2.31	2.40	7.01
33-78-55	2.31	2.27	2.47	7.05
Totals	8.78	8.73	9.24	26.75

Source	SS	df	MS
S. F. F.	0.2035	3	0.0678
G. F.	0.0395	2	0.0197
Error	0.0055	6	0.0009
Total	0.2485	11	

SAMPLE CALCULATIONS:

$$SS(SFF) = \frac{(6.08)^2 + (7.01)^2 + (6.61)^2 + (7.05)^2}{3} - \frac{(26.75)^2}{12} = 0.2035$$

$$SS(GF) = \frac{(8.78)^2 + (8.73)^2 + (9.24)^2}{4} - \frac{(26.75)^2}{12} = 0.0395$$

SAMPLE CALCULATIONS:

$$SS(TOT) = (1.98)^2 + (2.01)^2 + (2.09)^2 + (2.30)^2 + (2.31)^2 + (2.40)^2 + (2\ 31)^2 + (2.27)^2 + (2.47)^2 + (2.19)^2\ (2.14)^2 + (2\ 28)^2 - \frac{(26.75)^2}{12} = 0.2485$$

$$MS(SFF) = \frac{SS(SFF)}{df(SFF)} = \frac{0.2035}{3} = 0.0678$$

$$MS(GF) = \frac{SS(GF)}{df(GF)} = \frac{0.0395}{2} = 0.0197$$

F-RATIOS:

$$SFF_{calc.} = \frac{MS(SFF)}{MS(error)} = \frac{0.0678}{0.0009} = 75.3333$$

$$SFF_{table} = F(\tfrac{3}{6}) = 4.7571 \ < \ 75.3333$$

$\alpha = .05$ SFF is significant

$$GF_{calc.} = \frac{MS(GF)}{MS(error)} = \frac{0.0197}{0.0009} = 21.8888$$

$$GF_{table} = F(\tfrac{2}{6}) = 5.1433 \ < \ 21.8888$$

GF is significant

DATA SOURCE: Holographic Fringes METHOD NO. I

RESPONSE VARIABLE: Density Difference CASE NO. II

ANOVA TABLES:

Filter Number	Group Number			Totals
	I	II	III	
4043	0.48	0.48	0.39	1.35
42-47-57	0.48	0.37	0.30	1.15
33-78-54	0.38	0.36	0.35	1.09
33-78-55	0.42	0.41	0.35	1.18
Totals	1.76	1.62	1.39	4.77

Source	SS	df	MS
S. F. F.	0.0125	3	0.0041
G. F.	0.0175	2	0.0087
Error	0.0077	6	0.0012
Total	0.0377	11	

F-RATIOS:

$$SFF_{calc.} = \frac{0.0041}{0.0012} = 3.4166$$

$$SFF_{table} = F(\tfrac{3}{6}) = 4.7571 > 3.4166$$

SSF is not significant

$$GF_{calc.} = \frac{0.0087}{0.0012} = 7.25$$

$$GF_{table} = F(\tfrac{2}{6}) = 5.1433 < 7.25$$

GF is significant

DATA SOURCE: Holographic Fringes METHOD NO. I

RESPONSE VARIABLE: Minimum Density CASE NO. III

ANOVA TABLES:

Filter Number	Group Number			Totals
	I	II	III	
4043	1.74	1.77	1.90	5.41
42-47-57	1.95	1.96	2.03	5.94
33-78-54	2.11	2.13	2.23	6.47
33-78-55	2.10	2.07	2.30	6.47
Totals	7.90	7.93	8.46	24.29

Source	SS	df	MS
S. F. F.	0.2575	3	0.0858
G. F.	0.0496	2	0.0248
Error	0.0082	6	0.0013
Total	0.3151	11	

F-RATIOS:

$$SFF_{calc.} = \frac{0.0858}{0.0013} = 66.0$$

$$SFF_{table} = F(\tfrac{3}{6}) = 4.7571 < 66.0$$

SFF is significant

$$GF_{calc.} = \frac{0.0248}{0.0013} = 19.0769$$

$$GF_{table} = F(\tfrac{2}{6}) = 5.1433 < 19.0769$$

GF is significant

DATA SOURCE: Holographic Fringes METHOD NO. II

RESPONSE VARIABLE: Average Density CASE NO. I

ANOVA TABLES:

Filter Number	Group Number			Totals
	I	II	III	
4043 & 42-47-57	1.98 2.19 4.17	2.01 2.14 4.15	2.09 2.28 4.37	12.69
33-78-54 & 33-78-55	2.30 2.31 4.61	2.31 2.27 4.58	2.40 2.47 4.87	14.06
Totals	8.78	8.73	9.24	26.75

Source	SS	df	MS
EI-EII	0.1564	1	0.1564
G. F.	0.0395	2	0.0198
Inter.	0.0007	2	0.00035
Error	0.0519	6	0.0086
Total	0.2485	11	

SAMPLE CALCULATIONS:

$$SS(SFF) = \frac{(12.69)^2 + (14.06)^2}{3} - \frac{(26.75)^2}{12} = 0.1564$$

$$SS(GF) = \frac{(8.78)^2 + (8.73)^2 + (9.24)^2}{2} - \frac{26.75^2}{12} = 0.0395$$

SAMPLE CALCULATIONS:

$$SS(TOT) = (1.98)^2 + (2.19)^2 + (2.01)^2 + (2.14)^2 + (2.09)^2 + (2.28) + (2.30)^2 + (2.31)^2 + (2.31)^2 + (2.27)^2 + (2.40)^2 + (2.47)^2 - \frac{(26.75)^2}{12} = 0.2485$$

$$SS(INTER) = \frac{(4.17)^2 + (4.15)^2 + (4.37)^2 + (4.61)^2 + (4.58)^2 + (4.87)^2}{2} - \frac{(26.75)^2}{12}$$

$$- 0.1564 - 0.0395 = 0.0007$$

F-RATIOS:

$$SFF_{calc.} = \frac{0.1564}{0.0086} = 18.1860$$

$$SFF_{table} = F(\tfrac{1}{6}) = 5.9874 < 18.1860$$

SFF is significant

$$GF_{calc.} = \frac{0.0198}{0.0086} = 2.3023$$

$$GF_{table} = F(\tfrac{2}{6}) = 5.1433 < 2.3023$$

GF is not significant

DATA SOURCE: Holographic Fringes METHOD NO. II

RESPONSE VARIABLE: Average Density CASE NO. I

ANOVA TABLES:

Filter Number	Group Number			Totals
	I	II	III	
4043 & 33-78-55	1.98 2.31 4.29	2.01 2.23 4.24	2.09 2.47 4.56	13.09
33-78-54 & 42-47-57	2.30 2.19 4.49	2.31 2.14 4.45	2.40 2.28 4.68	13.62
Totals	8.78	8.69	9.24	26.71

Source	SS	df	MS
EI-EII	0.0234	1	0.0234
G. F.	0.0435	2	0.0218
Inter.	0.0012	2	0.0006
Error	0.1864	6	0.0310
Total	0.2485	11	

F-RATIOS:

$SFF_{calc.} = \frac{0.0234}{0.0310} = 0.7800$

$SFF_{table} = F(\frac{1}{6}) = 5.9874 > 0.7800$

SFF is not significant

$GF_{calc.} = \frac{0.0218}{0.0310} = 0.7266$

$GF_{table} = F(\frac{2}{6}) = 5.1433 > 0.7266$

GF is not significant

DATA SOURCE: Holographic Fringes METHOD NO. II

RESPONSE VARIABLE: Average Density CASE NO. I

ANOVA TABLES:

Filter Number	Group Number I	II	III	Totals
4043 & 33-78-54	1.98	2.01	2.09	
	2.30	2.31	2.04	
	4.28	4.32	4.49	13.09
33-78-55 & 42-47-57	2.31	2.23	2.47	
	2.19	2.14	2.28	
	4.50	4.37	4.75	13.62
Totals	8.78	8.69	9.24	26.71

Source	SS	df	MS
EI-EII	0.0234	1	0.0234
G. F.	0.0435	2	0.0218
Inter.	0.0062	2	0.0031
Error	0.1754	6	0.0292
Total	0.2485	11	

SAMPLE CALCULATIONS:

$$SFF_{calc.} = \frac{0.0234}{0.0292} = 0.8013$$

$$SFF_{table} = F(\tfrac{1}{6}) = 5.9874 > 0.8013$$

SFF is not significant

$$GF_{calc.} = \frac{0.0218}{0.0292} = 0.7465$$

$$GF_{table} = F(\tfrac{2}{6}) = 5.1433 > 0.7465$$

GF is not significant

DATA SOURCE: Holographic Fringes METHOD NO. III

RESPONSE VARIABLE: Average Density CASE NO. I

ANOVA TABLES:

Filter Number	Group Number			Totals
	I	II	III	
4043	1.98	2.01	2.09	6.08
42-47-57	2.19	2.14	2.28	6.61
Totals	4.17	4.15	4.37	12.69

Source	SS	df	MS
S. F. F.	0.0468	1	0.0468
G. F.	0.0148	2	0.0074
Residual	0.0018	2	0.0009
Total	0.0634	5	

SAMPLE CALCULATIONS:

$$SFF_{calc.} = \frac{0.0468}{0.0009} = 52.0000$$

$$SFF_{table} = F(\tfrac{1}{2}) = 18.518$$

SFF is significant

$$GF_{calc.} = \frac{0.0074}{0.0009} = 8.2222$$

$$GF_{table} = F(\tfrac{2}{2}) = 19.0000 > 8.2222$$

GF is not significant

DATA SOURCE: Holographic Fringes METHOD NO. III

RESPONSE VARIABLE: Average Density CASE NO. I

ANOVA TABLES:

Filter Number	Group Number			Totals
	I	II	III	
33-78-54	2.30	2.31	2.40	7.01
33-78-55	2.31	2.27	2.47	7.05
Totals	4.61	4.58	4.87	14.06

Source	SS	df	MS
S. F. F.	0.0003	1	0.0003
G. F.	0.0255	2	0.0127
Residual	0.0030	2	0.0015
Total	0.0288	5	

SAMPLE CALCULATIONS:

$$SFF_{calc.} = \frac{0.0003}{0.0015} = 0.2000$$

$$SFF_{table} = F(\tfrac{1}{2}) = 18.518 > 0.2000$$

SFF is not significant

$$GF_{calc.} = \frac{0.0127}{0.0015} = 8.4666$$

$$SFF_{table} = F(\tfrac{2}{2}) = 19.0000 > 8.4666$$

GF is not significant

APPENDIX VI

ANOVA OF REAL-IMAGE DENSITY DATA

DATA SOURCE: Real Images METHOD NO. I

RESPONSE VARIABLE: Average Density CASE NO. I

ANOVA TABLES:

Filter Number	Group Number			Totals.
	I	II	III	
4043	2.96	2.82	2.98	8.76
42-47-57	2.23	2.50	2.82	7.55
33-78-54	2.09	2.33	2.71	7.13
33-78-55	1.75	2.14	1.58	5.47
Totals	9.03	9.79	10.09	28.91

Source	SS	df	MS
S. F. F.	1.8503	3	0.6167
G. F.	0.1492	2	0.0746
Error	0.4008	6	0.0668
Total	2.4003	11	

F-RATIOS:

$SFF_{calc.} = \frac{0.6167}{0.0668} = 9.2320$

$SFF_{table} = F(\frac{3}{6}) = 4.7571 < 9.2320$

SFF is significant

$GF_{calc.} = \frac{0.0746}{0.0668} = 1.1167$

$GF_{table} = F(\frac{2}{6}) = 5.1433 > 1.1167$

GF is not significant

DATA SOURCE: Real Images METHOD NO. II

RESPONSE VARIABLE: Average Density CASE NO. I

ANOVA TABLES:

Filter Number	Group Number I	II	III	Totals
4043 & 42-47-57	2.96 2.23 5.19	2.82 2.50 5.32	2.98 2.82 5.80	16.31
33-78-54 & 33-78-55	2.09 1.75 3.84	2.33 2.14 4.47	2.71 1.58 4.29	12.60
Totals	9.03	9.79	10.09	28.91

Source	SS	df	MS
EI-EII	1.1470	1	1.1470
G. F.	0.1492	2	0.0746
Inter.	0.0593	2	0.0297
Error	1.0448	6	0.1741
Total	2.4003	11	

F-RATIOS:

$SFF_{calc.} = \frac{1.1470}{0.1741} = 6.5881$

$SFF_{table} = F(\frac{1}{6}) = 5.9874 < 6.5881$

SFF is significant

$GF_{calc.} = \frac{0.0746}{0.1741} = 0.4284$

$GF_{table} = F(\frac{2}{6}) = 5.1433 > 0.4284$

GF is not significant

DATA SOURCE: Real Images METHOD NO. II

RESPONSE VARIABLE: Average Density CASE NO. I

ANOVA TABLES:

Filter Number	Group Number I	II	III	Totals
4043 & 33-78-54	2.96 2.09 5.05	2.92 2.33 5.15	2.98 2.71 5.69	15.89
42-47-57 & 33-78-55	2.23 1.75 3.98	2.50 2.14 4.64	2.82 1.58 4.40	13.02
Totals	9.03	9.79	10.09	28.91

Source	SS	df	MS
EI-EII	0.6864	1	0.6864
G. F.	0.1492	2	0.0746
Inter.	0.0809	2	0.0405
Error	1.4838	6	0.2473
Total	2.4003	11	

F-RATIOS:

$SFF_{calc.} = \frac{0.6864}{0.2473} = 2.7755$

$SFF_{table} = F(\frac{1}{6}) = 5.9874 > 2.7755$

SFF is not significant

$GF_{calc.} = \frac{0.0746}{0.2473} = 0.3016$

$GF_{table} = F(\frac{2}{6}) = 5.1433 > 0.3016$

GF is not significant

DATA SOURCE: Real Images METHOD NO. II

RESPONSE VARIABLE: Average Density CASE NO. I

ANOVA TABLES:

Filter Number	Group Number			Totals
	I	II	III	
4043 & 33-78-55	2.96 1.75 4.71	2.82 2.14 4.96	2.98 1.58 4.56	14.23
33-78-54 & 42-47-57	2.09 2.23 4.32	2.33 2.50 4.83	2.71 2.82 5.53	14.68
Totals	9.03	9.79	10.09	28.91

Source	SS	df	MS
EI-EII	0.0168	1	0.0168
G. F.	0.1492	2	0.0746
Inter.	0.2607	2	0.1304
Error	1.9736	6	0.3289
Total	2.4003	11	

F-RATIOS:

$SFF_{calc.} = \frac{0.0168}{0.3289} = 0.0510$

$SFF_{table} = F(\frac{1}{6}) = 5.9874 > 0.0510$

SFF is not significant

$GF_{calc.} = \frac{0.0746}{0.3289} = 0.2268$

$GF_{table} = F(\frac{2}{6}) = 5.1433 > 0.2268$

GF is not significant

DATA SOURCE: Real Images METHOD NO. III

RESPONSE VARIABLE: Average Density CASE NO. I

ANOVA TABLES:

Filter Number	Group Number			Totals
	I	II	III	
4043	2.96	2.82	2.98	8.76
42-47-57	2.23	2.50	2.82	7.55
Totals	5.19	5.32	5.80	16.31

Source	SS	df	MS
S. F. F.	0.2449	1	0.2449
G. F.	0.1032	2	0.0516
Residual	0.0856	2	0.0428
Total	0.4337	5	

F-RATIOS:

$$SFF_{calc.} = \frac{0.2449}{0.0428} = 5.7219$$

$$SFF_{table} = F(\tfrac{1}{2}) = 18.518 > 5.7219$$

SFF is not significant

$$GF_{calc.} = \frac{0.0516}{0.0428} = 1.2056$$

$$GF_{table} = F(\tfrac{2}{2}) = 19.0000 > 1.2056$$

GF is not significant

DATA SOURCE: Real Images METHOD NO. III

RESPONSE VARIABLE: Average Density CASE NO. I

ANOVA TABLES:

Filter Number	Group Number			Totals
	I	II	III	
33-78-54	2.09	2.33	2.71	7.13
33-78-55	1.75	2.14	1.58	5.47
Totals	3.84	4.47	4.29	12.60

Source	SS	df	MS
S. F. F.	0.4592	1	0.4592
G. F.	0.1053	2	0.0526
Residual	0.2551	2	0.1275
Total	0.8196	5	

F-RATIOS:

$SFF_{calc.} = \frac{0.4592}{0.1275} = 3.6015$

$SFF_{table} = F(\frac{1}{2}) = 18.518 > 3.6015$

SFF is not significant

$GF_{calc.} = \frac{0.0526}{0.1275} = 0.4125$

$GF_{table} = F(\frac{2}{2}) = 19.0000 > 0.4124$

GF is not significant

APPENDIX VII

ANOVA OF REAL-IMAGE GEOMETRICAL DATA

DATA SOURCE: Real Images METHOD NO. I

RESPONSE VARIABLE: Image Length CASE NO. _____

ANOVA TABLES:

Filter Number	Group Number			Totals
	I	II	III	
4043	280	275	276	831
42-47-57	250	240	242	732
33-78-54	242	220	225	687
33-78-55	272	263	257	792
Totals	1044	998	1000	3042

Source	SS	df	MS
S. F. F.	4059	3	1353.00
G. F.	338	2	169.00
Error	112	6	18.66
Total	4509	11	

F-RATIOS:

$SFF_{calc.} = \frac{1353.00}{18.66} = 72.5000$

$SFF_{table} = F(\frac{3}{6}) = 4.7571 < 72.5000$

SFF is significant

$GF_{calc.} = \frac{169.00}{18.66} = 9.0568$

$SGG_{table} = F(\frac{2}{6}) = 5.1433 < 9.0568$

GF is significant

DATA SOURCE: Real Images METHOD NO. I

RESPONSE VARIABLE: Image Width CASE NO. _____

ANOVA TABLES:

Filter Number	Group Number			Totals
	I	II	III	
4043	127	129	127	383
42-47-57	111	110	104	325
33-78-54	105	88	99	292
33-78-55	116	116	118	350
Totals	459	443	448	1350

Source	SS	df	MS
S. F. F.	1484.33	3	494.77
G. F.	33.50	2	16.75
Error	149.17	6	24.86
Total	1667.00	11	

F-RATIOS:

$SFF_{calc.} = \frac{494.77}{24.86} = 19.9022$

$SFF_{table} = F(\frac{3}{6}) = 4.7571 < 19.9022$

SFF is significant

$GF_{calc.} = \frac{16.75}{24.86} = 0.6737$

$GF_{table} = F(\frac{2}{6}) = 5.1433 > 0.6737$

GF is not significant

DATA SOURCE: Real Images METHOD NO. I

RESPONSE VARIABLE: Image Area CASE NO. _____

ANOVA TABLES:

Filter Number	Group Number			Totals
	I	II	III	
4043	32,344	32,569	34,838	99,751
42-47-57	23,606	23,444	20,919	67,969
33-78-54	23,050	18,285	16,388	57,723
33-78-55	27,881	27,075	27,025	81,981
Totals	106,881	101,373	99,170	307,424

Source	SS	df	MS
S. F. F.	331,832,369	3	110,610,789
G. F.	7,887,566	2	3,943,783
Error	32,370,604	6	5,395,101
Total	364,202,973	11	

F-RATIOS:

$$SFF_{calc.} = \frac{110,610,789}{5,395,101} = 20.5020$$

$$SFF_{table} = F(\tfrac{3}{6}) = 4.7571 < 20.5020$$

SFF is significant

$$GF_{calc.} = \frac{3,943,783}{5,395,101} = 0.7309$$

$$GF_{table} = F(\tfrac{2}{6}) = 5.1433 > 0.7309$$

GF is not significant

DATA SOURCE: Real Images METHOD NO. III

RESPONSE VARIABLE: Image Lengths CASE NO. _____

ANOVA TABLES:

Filter Number	Group Number			Totals
	I	II	III	
4043	280	275	276	831
42-47-57	272	263	257	792
Totals	552	538	533	1623

Source	SS	df	MS
S. F. F.	253.5	1	253.5
G. F.	97.0	2	48.5
Residual	31.0	2	15.5
Total	381.5	5	

F-RATIOS:

$SFF_{calc.} = \frac{253.5}{15.5} = 16.3548$

$SFF_{table} = F(\frac{1}{2}) = 18.5180 > 16.3548$

SFF is not significant

$GF_{calc.} = \frac{48.5}{15.5} = 3.1290$

$GF_{table} = F(\frac{2}{2}) = 19.0000 > 3.1290$

GF is not significant

DATA SOURCE: Real Images METHOD NO. III

RESPONSE VARIABLE: Length CASE NO. _____

ANOVA TABLES:

Filter Number	Group Number			Totals
	I	II	III	
33-78-54	250	240	242	732
33-78-55	242	220	225	687
Totals	492	460	467	1419

Source	SS	df	MS
S. F. F.	337.5	1	337.5
G. F.	283.0	2	141.5
Residual	39.0	2	19.5
Total	659.5	5	

F-RATIOS:

$SFF_{calc.} = \frac{337.5}{19.5} = 17.3076$

$SFF_{table} = F(\frac{1}{2}) = 18.5180 > 17.3076$

SFF is not significant

$GF_{calc.} = \frac{141.5}{19.5} = 7.2564$

$GF_{table} = F(\frac{2}{2}) = 19.0000 > 7.2564$

GF is not significant

DATA SOURCE: Real Images METHOD NO. III

RESPONSE VARIABLE: Image Widths CASE NO. _____

ANOVA TABLES:

Filter Number	Group Number			Totals
	I	II	III	
4043	127	129	127	383
42-47-57	116	116	118	350
Totals	243	245	245	733

Source	SS	df	MS
S. F. F.	181.50	1	181.50
G. F.	1.33	2	0.67
Residual	3.99	2	1.99
Total	186.82	5	

F-RATIOS:

$SFF_{calc.} = \frac{181.50}{1.99} = 90.7590$

$SFF_{table} = F(\frac{1}{2}) = 18.5180 < 90.7590$

SFF is significant

$GF_{calc.} = \frac{0.67}{1.99} = 0.3333$

$GF_{table} = F(\frac{2}{2}) = 19.0000 > 0.3333$

GF is not significant

DATA SOURCE: Real Images METHOD NO. III

RESPONSE VARIABLE: Image Width CASE NO. _____

ANOVA TABLES:

Filter Number	Group Number			Totals
	I	II	III	
33-78-54	111	110	104	325
33-78-55	105	88	99	292
Totals	216	198	203	617

Source	SS	df	MS
S. F. F.	181.50	1	181.50
G. F.	86.33	2	43.16
Residual	91.00	2	45.50
Total	358.83	5	

F-RATIOS:

$SFF = \frac{181.50}{45.50} = 3.9890$

$SFF_{table} = F(\frac{1}{2}) = 18.5180 > 3.9890$

SFF is not significant

$GF = \frac{43.16}{45.50} = 0.9487$

$GF_{table} = F(\frac{2}{2}) = 19.0000 > 0.9487$

GF is not significant

DATA SOURCE: Real Images METHOD NO. III

RESPONSE VARIABLE: Image Area CASE NO. _____

ANOVA TABLES:

Filter Number	Group Number			Totals
	I	II	III	
4043	32,344	32,569	34,838	99,751
42-47-57	27,881	27,075	27,025	81,981
Totals	60,225	59,644	61,863	181,732

Source	SS	df	MS
S. F. F.	52,628,816	1	52,628,816
G. F.	1,324,094	2	662,047
Residual	2,943,871	2	1,471,935
Total	56,896,781	5	

F-RATIOS:

$$SFF_{calc.} = \frac{52,628,816}{1,471,935} = 35.7548$$

$$SFF_{table} = F(\tfrac{2}{2}) = 18.5180 < 35.7548$$

SFF is significant

$$GF_{calc.} = \frac{662,047}{1,471,935} = 0.4497$$

$$GF_{table} = F(\tfrac{2}{2}) = 19.0000 > 0.4497$$

GF is not significant

DATA SOURCE: Real Image METHOD NO. III

RESPONSE VARIABLE: Image Area CASE NO. _____

ANOVA TABLES:

Filter Number	Group Number			Totals
	I	II	III	
33-78-54	23,606	23,444	20,919	67,969
33-78-55	23,050	18,285	16,388	57,723
Totals	46,656	41,729	37,307	125,692

Source	SS	df	MS
S. F. F.	17,496,752	1	17,496,752
G. F.	21,872,202	2	10,936,101
Residual	6,230,436	2	3,115,218
Total	45,599,390	5	

F-RATIOS:

$SFF_{calc.} = \frac{17,496,752}{3,115,218} = 5.6165$

$SFF_{table} = F(\frac{1}{2}) = 18.5180 > 5.6165$

SFF is not significant

$GF_{calc.} = \frac{10,936,101}{3,115,218} = 3.5105$

$GF_{table} = F(\frac{2}{2}) = 19.0000 > 3.5105$

GF is not significant